Lawrence Berkeley National Laboratory
Lawrence Berkeley National Laboratory

Title

I. A COMPARATIVE STUDY OF RIBO-, DEOXYRIBO-, AND HYBRID OLIGONUCLEOTIDE HELICES BY NUCLEAR MAGNETIC RESONANCE. II. OPTICAL STUDIES OF ETHIDIUM BINDING TO OLIGONUCLEOTIDES.

Permalink

https://escholarship.org/uc/item/9958477f

Author

Pardi, Arthur

Publication Date

1980-11-01

Lawrence Berkeley Laboratory
UNIVERSITY OF CALIFORNIA

CHEMICAL BIODYNAMICS DIVISION

I. A COMPARATIVE STUDY OF RIBO-, DEOXYRIBO-, AND
HYBRID OLIGONUCLEOTIDE HELICES BY NUCLEAR MAGNETIC
RESONANCE. II. OPTICAL STUDIES OF ETHIDIUM
BINDING TO OLIGONUCLEOTIDES

Arthur Pardi
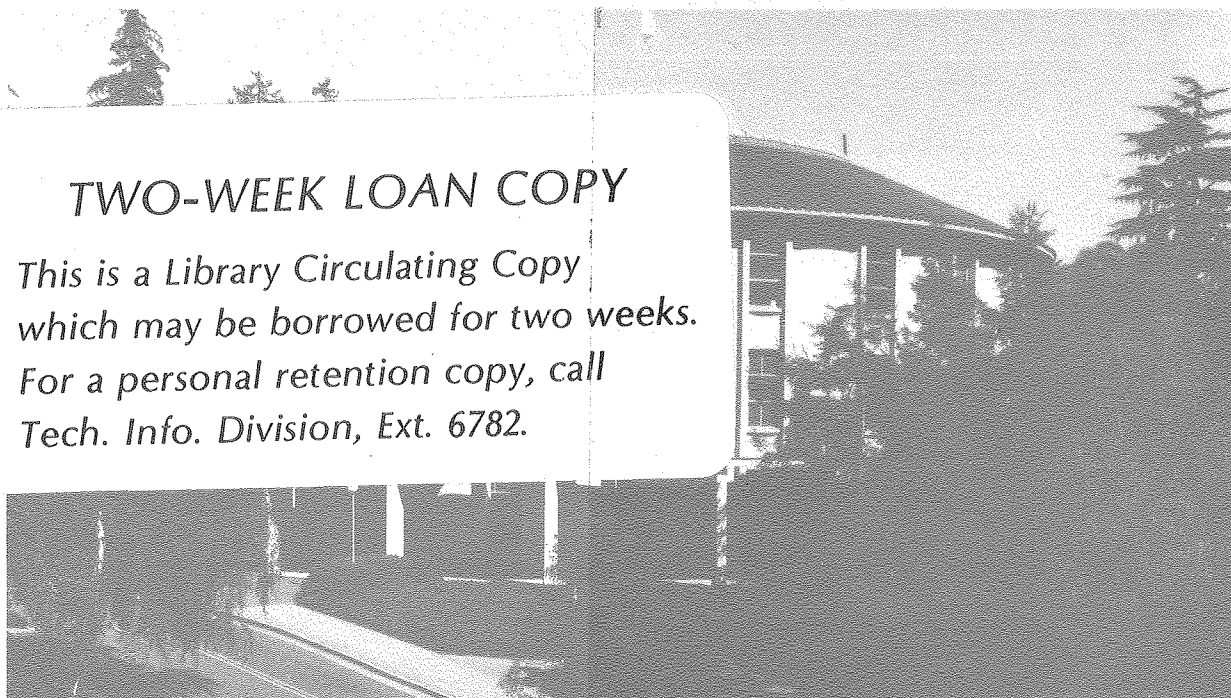(Ph.D. thesis)

November 1980

DISCLAIMER

I. A COMPARATIVE STUDY OF RIBO-, DEOXYRIBO-, AND HYBRID OLIGONUCLEOTIDE HELICES BY NUCLEAR MAGNETIC RESONANCE
II. OPTICAL STUDIES OF ETHIDIUM BINDING TO OLIGONUCLEOTIDES

by

Arthur Pardi
Lawrence Berkeley Laboratory, University of California
Berkeley, CA 94720

ABSTRACT

The nonexchangeable base protons and the hydrogen bonding N-H-N imino protons were used to study the conformations and the helix-to-coil transitions in the following oligonucleotides: (I) a DNA duplex dCT_5G + dCA_5G; (II) an RNA duplex rCU_5G + rCA_5G; (III) a DNA-RNA hybrid duplex dCT_5G + rCA_5G; and (IV) a DNA-RNA hybrid triplex rCU_5G + dCA_5G. The first three mixtures all form stable double helical structures at 5°C, whereas IV forms a triple strand with a ratio of 2:1 $rCU_5G:dCA_5G$. The chemical shifts of the imino protons in the double strands indicate that I, II, and III have different conformations in solution. For example, the hydrogen bonded proton on one of the C·G base pairs is more shielded (a 0.4 ppm upfield shift) in helix I than in helix II or III. This implies a significant change in helical parameters, such as the winding angle, the distance between base pairs, or overlap of the bases. The coupling constants of the H1' sugar protons show that helix I has 90% 2' endo sugar conformation, whereas helix III has greater than 85% 3' endo conformation for the observed sugar rings. The chemical shift and sugar pucker data are consistent with helix I having

to my parents, for their support through the
years, and for having the confidence in me
to let me make my own decisions.

ACKNOWLEDGEMENTS

The members of Mel Klein's research group provided much help and friendship while I was using their instrument. Greg Karczmar and Alan Koretsky were especially valuable in their help with instrumental problems and discussions on NMR.

Steve Winkle provided useful comments and advice, even though we did not always see eye-to-eye. Jeff Nelson took a lot of grief from me (some of it undeserved), and was still a willing source of valuable advice. David Keller helped with computer programming and more importantly helped improve my tennis game to its present (still pitiful) state. Joe Kao provided useful advice and critique. I wish to thank Carlos Bustamante for his willingness to help in whatever way he could and for his refreshing attitude on life.

Frank Martin provided innumerable invaluable discussions on the physical chemistry of nucleic acids, and was also the source of many of the oligonucleotides used in this work.

Kathy Morden took a lot of kidding that she didn't deserve, but always kept on smiling. I wish to thank her for countless hours in help on data collection on the NMR's. She also provided cookies and goodies for us to eat during the wee hours of the morning at Stanford, where the only way to keep awake is to keep eating (A. Pardi, unpublished result). Her collaboration provided a valuable source of ideas and help in sample preparation and data interpretation.

Ken Dahl was always willing to think about and work on any problem which I asked him to. He also provided valuable critiques of my work (and most other subjects) as well as numerous discussions.

The most valuable contribution all these people made was their friendship, which made this work enjoyable.

TABLE OF CONTENTS

CHAPTER I

INTRODUCTION

DNA carries all the genetic information in an organism.
The structure of DNA was first proposed by Watson and Crick
from X-ray diffraction studies.[1] Later X-ray fiber studies
on RNA and hybrid polynucleotides showed there were large
differences in the conformations of various types of nucleic
acids.[2,3] In order to understand their structure and
function in solution, nucleic acids have been studied by
many techniques including absorbance, CD, NMR, and fluorescence.[4]
Most of the early work concentrated on polymers, but as more
detailed questions about structure and function were asked,
shorter oligonucleotide systems were studied.

In this work we have used model oligonucleotides to
study the properties of nucleic acids in solution. The
oligonucleotides include a DNA duplex, an RNA duplex, a
DNA-RNA hybrid duplex, and a DNA-RNA hybrid triplex, all
of the same sequence. This gives us an opportunity to
study the differences in these nucleic acid helices without
having to worry about sequence effects. The main tool used
was proton nuclear magnetic resonance. Figure 1.1 shows an
A·T and C·G base pair, and the numbering of the base protons.
Figure 1.2 shows a proton NMR spectrum for a typical oligo-
nucleotide, and indicates the chemical shifts of protons

Figure 1.1. Watson-Crick base pairs in DNA.

WATSON – CRICK BASE PAIRS
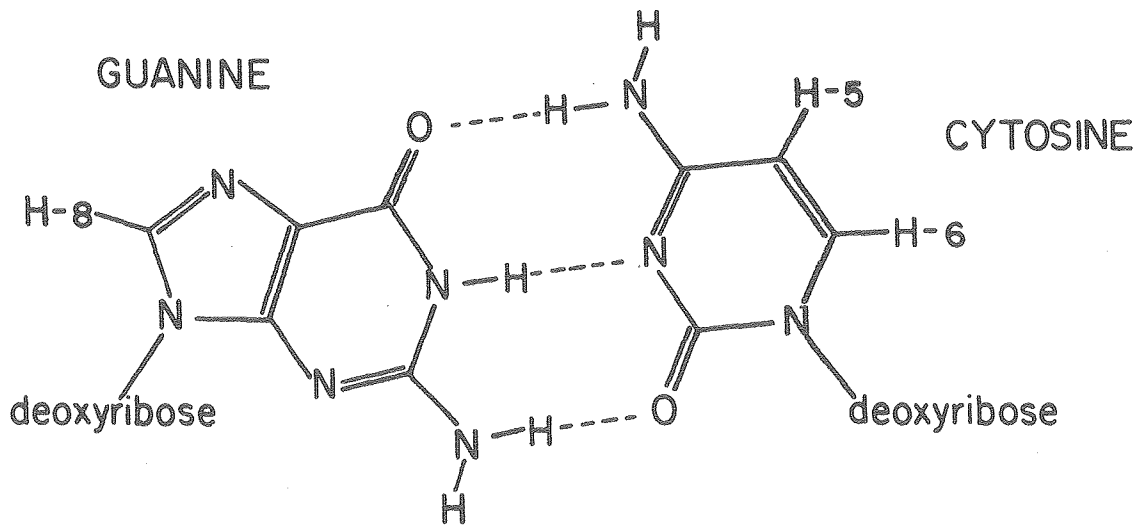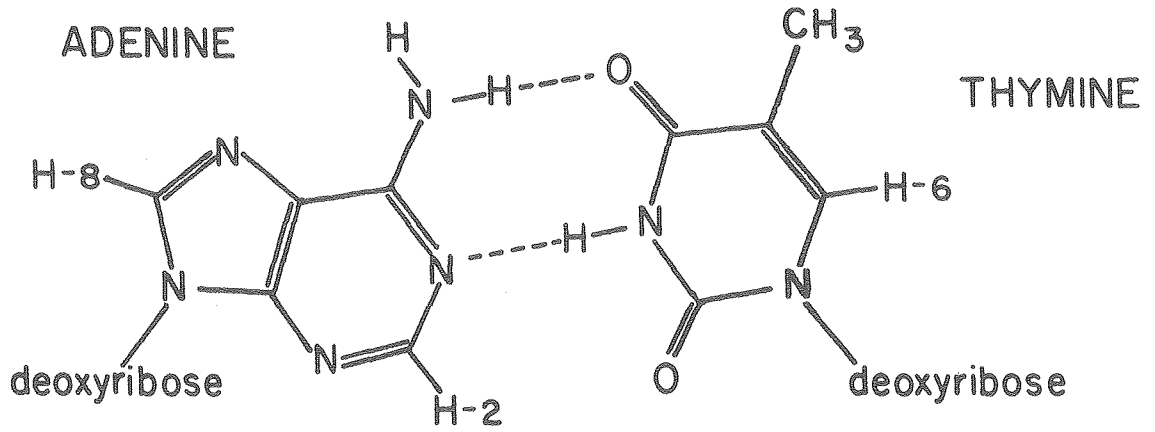
Figure 1.2. ^{1}H NMR spectrum of dCA$_5$G + dCT$_5$G.

360 MHz Proton Spectrum of dCA₅G + dCT₅G at 65°C
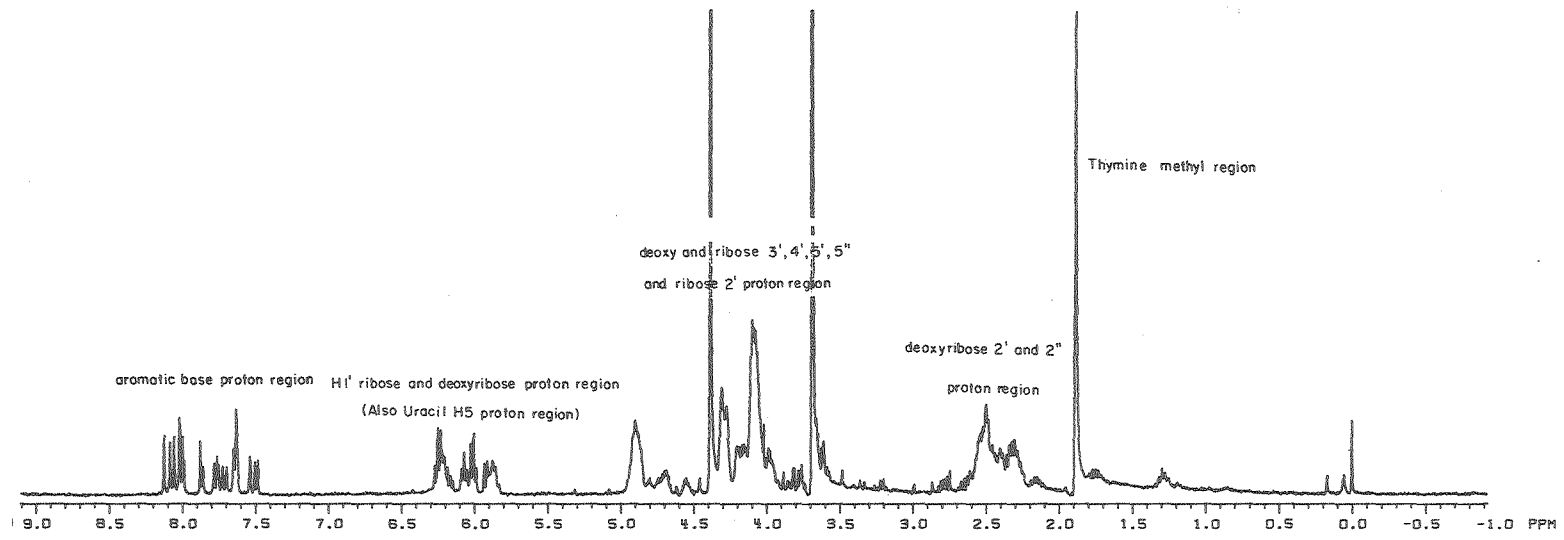
on different parts of the nucleic acid. The chemical
shifts and coupling constants of these protons were used
to obtain information on the oligomers.

The aromatic bases in nucleic acides give rise to ring
currents which affect the chemical shifts of nearby protons.[5]
The calculated shapes and magnitudes of these ring currents
for the four normal bases in DNA and RNA are shown in Figures
1.3a and 1.3b (thymine and uracil are assumed to have the
same ring current in this work). The chemical shift of a
particular proton will change with different conformations of
the neighboring bases. Thus structural information can
be obtained from the chemical shifts of protons in different
parts of the helix. This method has been used in the past
few years to obtain a much better understanding of the
solution structures of tRNA's.[6,7]

The coupling constants of protons on the ribose or
deoxyribose sugars of nucleic acids have been used by many
workers to investigate the structures of small oligonucleo-
tides.[8,9] The coupling constants are related to the dihedral
angle between two protons by the Karplus equation.[10] We
have used this empirical relation to obtain information on the
sugar pucker of several oligonucleotides.

The second part of this work involves an investigation
of the binding of ethidium to nucleic acids. Ethidium
bromide is an aromatic dye which is known to cause frameshift

Figure 1.3.

    a) Shape of ring currents due to bases in
       nucleic acids.

    b) Magnitude of ring currents due to four
       bases.

$$\frac{3\cos^2\theta - 1}{r^3}$$
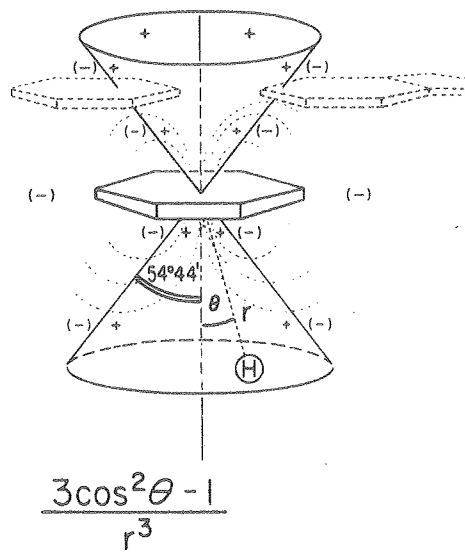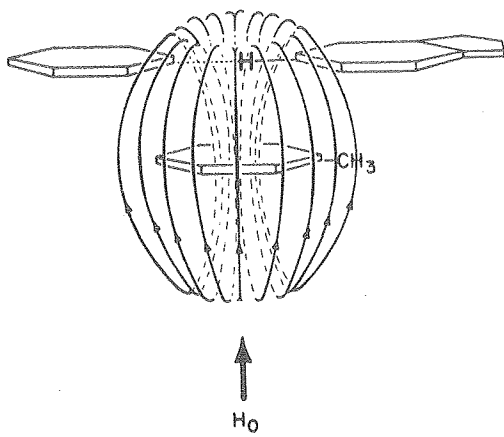
XBL 805-9519

b)

SHIELDING VALUES DUE TO RING CURRENT OF BASE
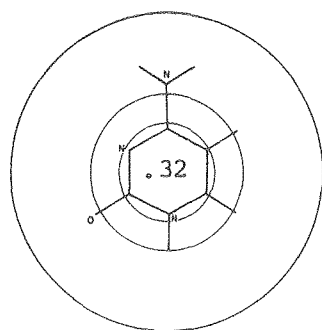
CYTOSINE
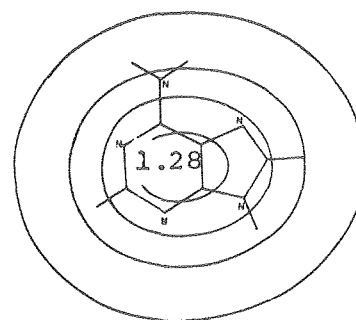
ADENINE
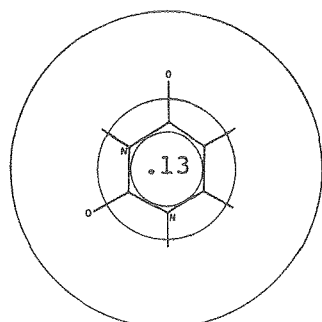
URACIL
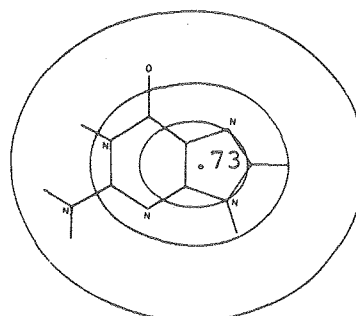
GUANINE

Numbers are for a plane 3.4 Å above or below the base.

XBL 805-9527

mutations in DNA.[11] By studying the physical properties
of ethidium binding, we may be able to understand its muta-
genic action. A model for frameshift mutagenesis has been
proposed by Streisinger where the stabilization of a bulge
in one strand causes the addition or deletion of a few
base pairs during repair or replication of the DNA.[12] This
mechanism is schematically shown in Figure 1.4; chemical
mutagens are thought to stabilize these structures thus
making frameshift mutations more likely.

Ethidium binding to three types of oligonucleotides
was studied a) perfect helices (rCpG, or dCpG), b) complexes
with a bulge on one strand (rGpUpG + rCpC), and c) complexes
with bulged bases on both strands (rCpUpG). These repre-
sent possible structures involved in the Streisinger
frameshift mechanism. The thermodynamic and spectroscopic
properties of these complexes were compared.

Figure 1.4   A representation of the Streisinger model
of frameshift mutagenesis.

FRAMESHIFT MUTATIONS

ADDITION DELETION
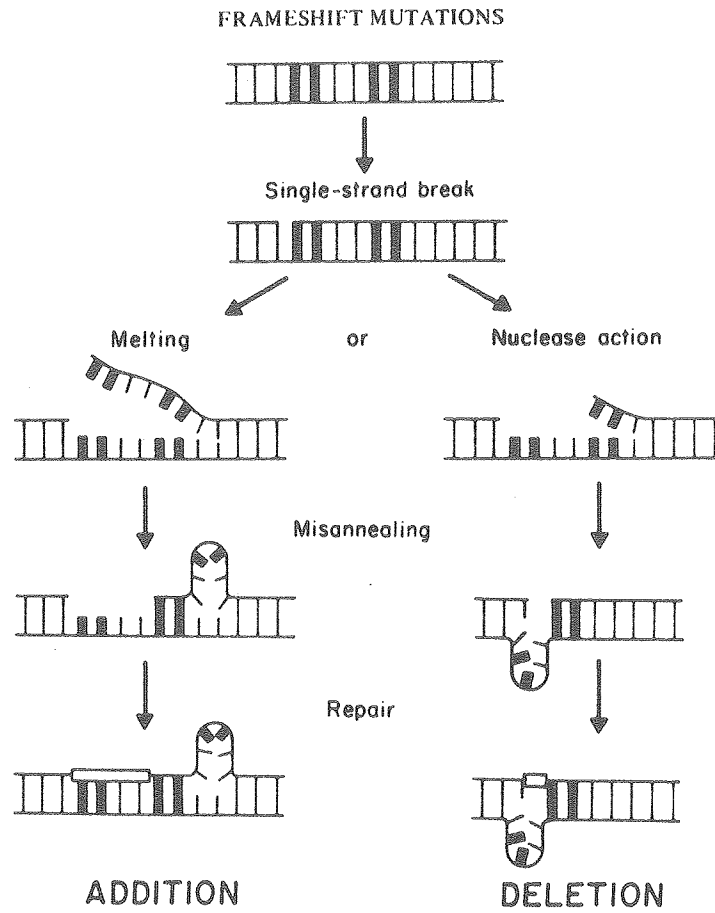
XBL 782-7420A

CHAPTER II

1.   INTRODUCTION

Proton nuclear magnetic resonance studies of oligo-
nucleotides have greatly increased our understanding of the
conformations and physical properties of nucleic acids in
solution. The chemical shifts of the NH-N imino resonances,
base proton resonances, and the H1' ribose or deoxyribose
resonances have been used separately or in combination,
to deduce RNA A or A'[3] type conformations for double helical
ribo-oligonucleotides.[13-16] Double stranded deoxyribo-
oligonucleotides have shown spectra consistent with a B
form geometry in solution. [17-20] These conclusions are
based mainly upon comparison of the experimental chemical
shifts with those computed from ring current effects for
an assumed geometry, as well as the sugar pucker deduced
from the H1' proton coupling constants.

X-ray studies of RNA-DNA hybrid duplexes have shown
them to adopt A type geometries.[3,21] The only ^{1}H NMR study
of an RNA-DNA duplex shows the structure of the hybrid to
be different than the DNA-DNA duplex of the same sequence,
and consistent with an A form in solution.[22]

Triple stranded structures are not uncommon in polynu-
cleotide or oligonucleotide solutions.[4] Under conditions
where triplexes were formed, Geerdes and Hilbers observed

the low field imino proton region of [oligo A-(oligo U)$_2$].[2,3]
They saw separate resonances for the Watson-Crick and reverse
Hoogsteen base pairs. Kallenbach et al. observed similar
results for the other triplexes including [AMP-(oligo U$_{15}$)$_2$].[19]

In this work we report the ^{1}H NMR of oligonucleotides in
a DNA duplex, an RNA duplex, a DNA-RNA hybrid duplex, and a
DNA-RNA hybrid triplex, of the same sequence. The molecules
are (I) dCT$_5$G + dCA$_5$G, (II) rCU$_5$G + rCA$_5$G, (III) dCT$_5$G +
rCA$_5$G, and (IV) rCU$_5$G + dCA$_5$G. The first three molecules
form duplexes which all have different conformations in
solution; IV forms a triple strand which is much less stable
than the other structures. These results are consistent
with optical studies previously reported on these molecules,
which pointed out the importance of the instability of the
DNA-RNA hybrid present at termination of transcription.[24]

The thermodynamics of oligonucleotides have been studied
by optical methods as well as by proton NMR.[25] The melting
temperatures, T$_m$'s, of the helix-to-coil transition from
both methods have agreed fairly well.[15,19,26] Melting of
the end base pairs before the rest of the helix has been seen
in several of the systems with A·U or A·T base pairs on the
ends of the helix.[15,19,27] In helices with C·G base pairs
on the ends there seems to be no[16] or little[27] differential
melting of the ends of the helix before the rest of the
oligonucleotide. However, most of the systems studied thus

far have been self-complementary oligonucleotides (except
Hughes et al.[16]); this precludes the measurement of the
temperature dependence of the single strands. Ignorance of
the temperature dependence of the single strands throughout
the melting transition can lead to errors in the apparent
T_m's; these errors will usually be larger for the interior
base pairs than for the terminal ones. The oligonucleotides
studied here are not self-complementary, so the single
strand dependences have been observed. The measured T_m
for each base proton is thus a more accurate representation
of the melting of that part of the helix.

2.   MATERIALS AND METHODS.

A)   Oligonucleotides

The deoxyribo-oligonucleotides were synthesized by
the diester method of Khorana.[28]   The ribo-oligonucleotides
were enzymatically prepared with polynucleotide phosphorylase.[25]
The oligonucleotides were synthesized and kindly provided by
Dr. Frank Martin and Mr. David Koh. Separation and purification
of the oligomers were performed by RPC-5 column chromatography.
Desalting of the samples was performed on Biogel P-2 columns
(Bio-Rad). All samples were run in 8.0 mM Na_2HPO_4, 20 mM
NaH_2PO_4, 0.18 M NaCl, 0.1 mM Na_2EDTA, pH = 7.0, unless
otherwise noted. Concentrations of the oligonucleotides were
calculated from the absorbance of the solutions at 260 nm.
The extinction coefficients were calculated from extinction
coefficients of dinucleoside monophosphates and mononucleotides

with the assumption of only nearest neighbor interaction.[29]
The values obtained in this way are 79×10^3, 58×10^3,
79×10^3, and 66×10^3 for dCA_5G, dCT_5G, rCA_5G and rCU_5G,
respectively, at 25°C.

B)   Experimental NMR

NMR spectra were taken on the HXS-360 MHz instrument at
Stanford Magnetic Resonance Laboratory.   Temperature was
controlled to ± 1°C by a B-ST 100/700 Bruker temperature
controller.   Spectra of the non-exchangeable protons were
measured in D_2O in the normal Fourier transform mode using
5 mm NMR tubes (Wilmad).   Spectra of the exchangeable protons
were measured in H_2O using the Redfield 214 pulse sequence
to minimize the water signal.[30]   For these samples 5 mm
microtubes which hold 160 µl of solution (508 CP Wilmad)
were used.   All solutions were measured at concentrations
of either 1.0 mM or 0.5 mM per strand.   Spectra measured in
D_2O were all referenced to the internal standard TSP, while
the spectra in H_2O were referenced to the H_2O peak.   The
chemical shifts obtained in this way are accurate to ± 0.005
ppm for the D_2O and ± 0.05 ppm for the H_2O studies.

The temperature dependence of the chemical shift of
H_2O relative to TSP was calibrated in our buffer.   The
sample   used for calibration was our standard buffer
in pure H_2O plus 20 mM TSP as reference.   A normal Fourier
transform spectrum was taken with a short pulse length and

Figure 2.1. Chemical shift of H_2O with temperature
for 8 mM Na_2HPO_4, 20 mM NaH_2PO_4, 0.18 M NaCl,
0.1 mM EDTA, pH = 7.0.
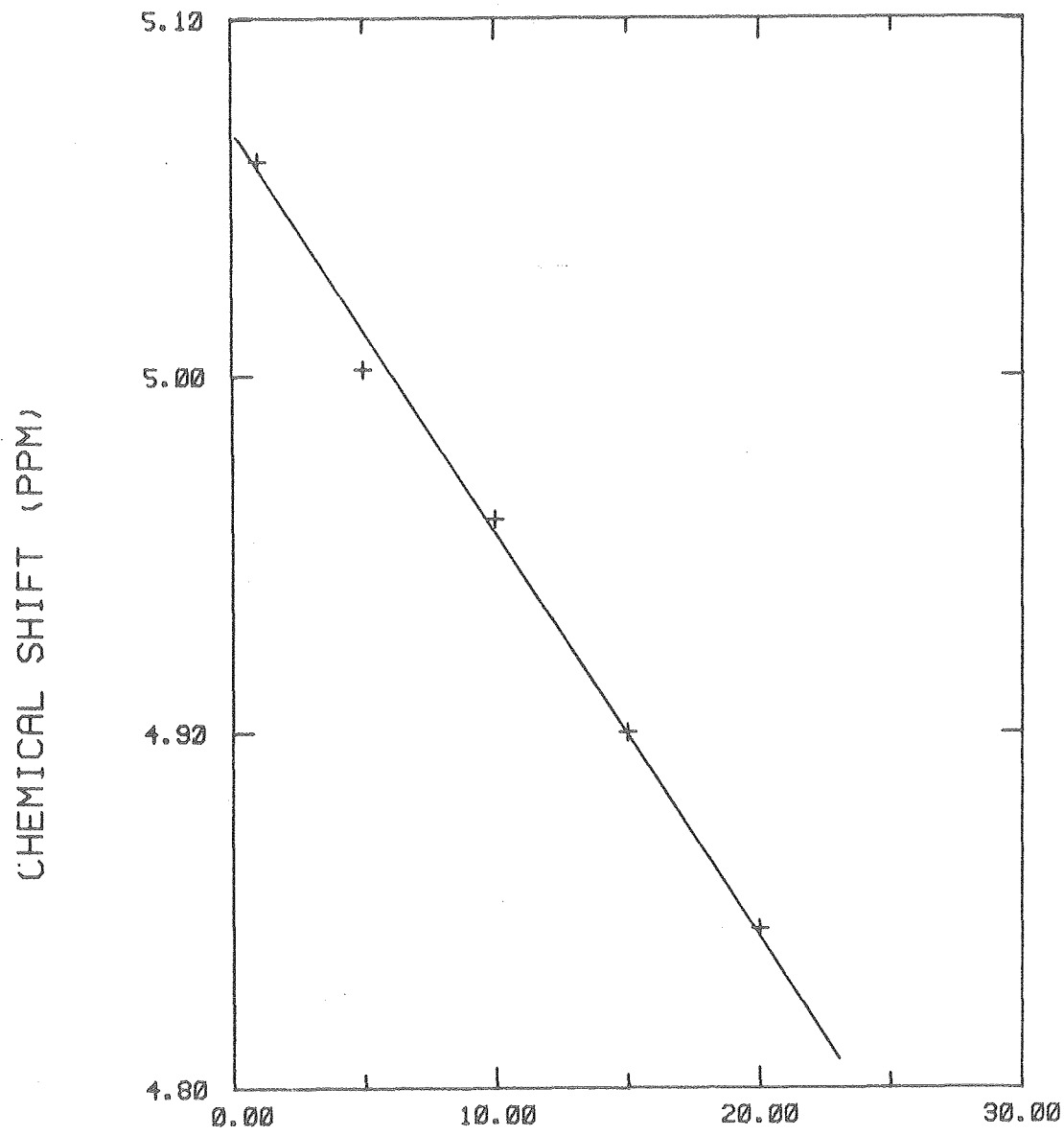
XBL 8011-7473

low power. The chemical shift of H_2O is linear with temperature over this temperature range, and is shown in Figure 2.1. The chemical shift of H_2O was used as a reference in the Redfield experiments where it was usually impossible to see the TSP peak. Since there is a large distortion around the H_2O peak in the Redfield pulse sequence, it was difficult to get accurate values for the chemical shift of H_2O in the spectrum. This problem was eliminated by also taking a short pulse, low power spectrum of the sample under conditions identical to those used in the Redfield experiment. In the short pulse experiment there are no distortions of the H_2O peak, so its position in the Redfield spectrum was taken as the same as that observed in the short pulse experiment. This method was tested and found to obtain the chemical shift of the H_2O peak to better than ± 0.05 ppm in the Redfield pulse sequence spectra.

All data were collected on a Nicolet 1180 computer with 16K data points and a sweep width of ± 1800 Hz for the D_2O work, and 8K data points and a sweep width of ± 5000 Hz for the H_2O spectra. Spectra were taken every 10° from 35 to 65°C and every 5° from 5 to 35°C, for the spectra in D_2O. In H_2O measurements were made every 5° from 5 to 25°C or until peaks were no longer observed.

Samples in D_2O were prepared by lyophilizing three times

in 99.8% D_2O (Bio-Rad) and then dissolved in 100% D_2O (Bio-

Rad). The internal reference TSP was added to the sample

after the addition of the 100% D_2O, since it had a tendency

to remain insoluble after lyophilization with the oligo-

nucleotides. Samples of the component oligomers titrated

with Mn^{2+} were measured in D_2O with no buffer added at pD = 7.0.

The pD was calculated by adding 0.4 to the measured pH, with

the pD adjusted by the addition of aqueous NaOD or DCl.

3. RESULTS

A) Assignments of Nonexchangeable Protons

The assignments of the chemical shifts of the base

protons were accomplished on the single strands. The method

of incremental assignment was used at 65°C where there is

less stacking of the bases in the single strands.[15] The

chemical shifts at other temperatures were obtained from the

change in peak position with temperature. Chemical shifts

of the single strand oligomers at 65°C are given in Table I.

The aromatic region (6.6-8.5 ppm) of rCU_5G was poorly

resolved due to the H6 doublets on the uracil residues, so no

assignments were made in solutions which contained this

oligomer. In the other solutions, the cytosine resonances

were the only doublets in the aromatic region and easily

identified. The adenine H8 protons were differentiated from

the adenine H2 protons because of the longer T_1 of the H2

TABLE I

CHEMICAL SHIFTS OF SINGLE STRANDS AT 65°C*

dCA$_5$G		C#1	A#2	A#3	A#4	A#5	A#6	G#7
	AH2	---	7.985	(7.752	7.725	7.696)	7.854	---
	CH6	7.489	---	---	---	---	---	---
A or GH8		---	8.120	(8.081	8.052	8.016	8.012)	7.872

rCA$_5$G		C#1	A#2	A#3	A#4	A#5	A#6	G#7
	AH2	---	8.091	(7.982	7.971	7.953)	8.034	---
	CH6	7.632	---	---	---	---	---	---
A or GH8		---	8.265	(8.175	8.165	8.152)	8.190	7.878

dCT$_5$G		C#7	T#6	T#5	T#4	T#3	T#2	G#1
C or TH6		7.770	7.532	(7.627	7.627	7.627)	7.645	---
	CCH$_3$	---	(1.878	1.878	1.878	1.878	1.878)	---
	GH8	---	---	---	---	---	---	7.993

*Values in parenthesis indicate that we were unable to assign these peaks to particular bases in the sequence.

protons.[31]   The H8 on guanine was distinguished from H8 of

adenine by the fact that it exchanges much faster upon

heating in D_2O at 80°C. (In one hour at 80°C the guanine

H8 intensity was decreased over 50% while the adenine H2

was decreased by about 10%.)

In the oligonucleotide dCA_5G, we unambiguously assigned

all the base protons on the cytosine, the guanine, and the

#2 adenine. Figure 2.2 shows the base proton spectrum of

dCA_5G + dCT_5G in the single strands at 65°C, and also

defines the numbering scheme. For the other penultimate

adenine (#6), we were able to specifically assign the H2,

but not the H8 proton. The four H8 adenine resonances which

belong to the three internal adenines (#3-5) and the #6

adenine were identified, but not assigned to specific bases.

The H2 protons on the three internal adenines all have very

similar chemical shifts and we were unable to assign resonances

to particular adenines in the sequence.

In order to make assignments of the penultimate adenine

resonances (#2 and #6) it was necessary to study the smaller

components of dCA_5G. The following compounds at 65°C were

used for comparison with dCA_5G: dCpA, dCpApA, $dC(pA)_6$,

dpApA, $d(pA)_4$, dpApG, and dpApApG. The assignments of the

dCpA and dpApG were made by inspection. Tentative assignment

of the base protons on dApA has previously been made by

Chang and Sarma.[32]   The assignment of the base protons in

Figure 2.2. Assignments of base protons in

single strands of dCA_5G + dCT_5G at 65°C.

360 MHz ^{1}H NMR of
dCA$_5$G + dCT$_5$G, 1 mM/strand, 65°C
D$_2$O, 0.22 M Na$^+$, pH = 7.0

SINGLE STRANDS
5'CAAAAAG3' + 5'CTTTTTG3'
1234567   7654321

3TH6's

AH8

AH8

A(2)H8

A   H8

AH8

G(1)H8

G(7)H8

A(2)H2

A(6)H2

C(7)
H6

AH2

AH2   AH2

T(6)H6

T(2)H6

C(1)H6

8.15   8.10   8.05   8.00   7.95   7.90   7.85   7.80   7.75   7.70   7.65   7.60   7.55   7.50   7.45   7.40
PPM

XBL 801-7675

24
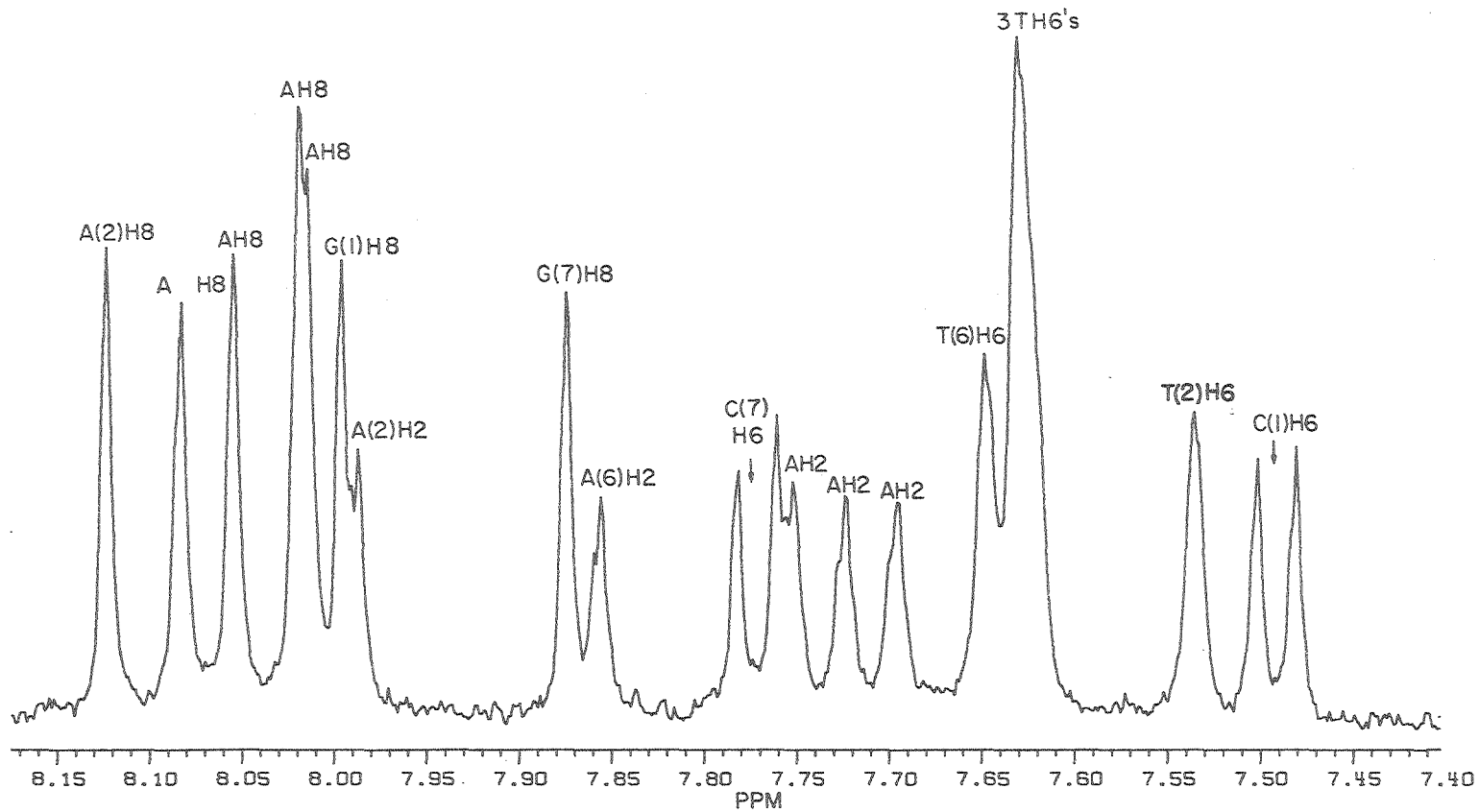
dpApA required titration with Mn^{2+}, which preferentially binds to the terminal phosphate at pD = 7 and thus broadens the 5' adenine resonances relative to those of the 3' adenine.[33] The broadening of the NMR signal from the paramagnetic Mn^{2+} ion is due to the electron-spin, nuclear-spin, dipole-dipole interaction.[34,35] This interaction goes as $1/r^6$ so only protons located very close to the phosphate binding site are broadened.[36]

The linewidths of the dpApA base protons during the titration are given in Table II. The H8 proton at 8.33 ppm clearly broadens before the H8 proton at 8.28 ppm thereby assuring the assignment of the 8.33 ppm resonance to the 5' residue, and the 8.28 ppm peak to the 3' residue. The H2 resonances were more difficult to assign because both adenine H2 protons are fairly far from the 5' phosphate. (See the single stranded right handed stack, shown in Figure 2.3, for an estimate of the distance between the 5' phosphate and the two adenine H2 protons.) At 50 μM Mn^{2+} the H2 proton at 8.03 ppm broadened to 12 Hz whereas the H2 resonance at 8.10 ppm only broadened to 6 Hz. This is indicative that the 8.03 peak belongs to the 5' adenine.

The assignment of the dpApA helped in the assignment of the oligomers dpApA and dCpApA. Only partial assignment of the oligomers $dC(pA)_6$, and $d(pA)_4$ were possible. The chemical shifts of all the components at 65°C are given in Tables III - V.

TABLE II

LINEWIDTHS OF THE BASE PROTONS OF dpApA

WHEN TITRATED WITH Mn^{2+} AT pD = 7.0

	H8 protons		H2 protons	
Chemical shift (ppm)	8.333	8.281	8.094	8.029
$[Mn^{2+}]$				
0.0	3.0	3.0	3.0	3.0
3.0 μM	12.0	6.0	3.0	3.8
10 μM	24	15	2.2	3.0
50 μM	a	a	6	12

[a] Linewidth too broad to measure.

TABLE III

CHEMICAL SHIFTS OF THE COMPONENTS OF dCA$_5$G AT 65°C[a]

```
 1 2
dCpA

    C(1)          A(2)
 H6    H5    H8    H2
7.58  5.98  8.38  8.24


 1 2 3
dCpApA
    C(1)          A(2)        A(3)
 H6    H5    H8    H2    H8    H2
7.52  5.94  8.31  8.10  8.20  8.05


 1 2 I I I I 7
dCpApApApApApA
C(1)              A(2)                A(I or 6)
 H6              H8    H2                 H8
7.5             8.12* 7.97*  (8.12,8.09,8.06,8.05,8.01)
                                         H2
                            (7.97,7.81,7.78,7.73,7.73)
 1 2
dpApA

    A(1)          A(2)
 H8    H2      H8    H2
8.33  8.03*   8.24  8.10*


 1 2 3 4
dpApApApA

    A(1)          A(2 and 3)        A(4)
 H8    H2      H8     H2       H8     H2
8.25* 7.98    8.10   7.80     8.20* 7.98

 1 2
dpApG

   A(1)          G(2)
 H8    H2         H8
8.20  8.20       7.99

 1 2 3
dpApApG

    A(1)           A(2)          G(3)
 H8    H2       H8     H2         H8
8.22  8.07     8.18   7.97       7.90
```

TABLE III

(continued)

*Indicates only tentative assignments.

aParentheses indicates that we were unable to make assignments to particular bases in the sequence.

TABLE III

(continued)

TABLE IV

CHEMICAL SHIFTS OF THE COMPONENTS OF dCT_5G at 65°C

1 2
dCpT

	C(1)		T(2)
H6	H5		H6
7.80	6.02		7.68

1 2 3
dCpTpT

	C(1)		T(2 or 3)
H6	H5		H6
7.77	6.02		7.65

1 2 3 4 5
dCpTpTpTpT

	C(1)		T(2)	T(3-5)
H6	H5		H6	H6
7.78	--		7.66	7.65

$dC(pT)_6$

	C(1)		T(all)
H6	H5		H6
7.77	--		7.63

dpTpG

T(1)			G(2)
H6	H5		H8
7.59	--		8.01

1 2 3
dpTpTpG

T(1)		T(2)	G(3)
H6		H6	H8
7.69		7.55	8.00

TABLE V

COMPONENTS OF rCA_5G AT $65°C^a$

```
 1 2
rCpA

    C(1)        A(2)
 H6    H5    H8    H2
7.76  6.00  8.41  8.29

 1 2 3
rCpApA

    C(1)          A(2)          A(3)
 H6    H5        H8    H2      H8    H2
7.66  5.83      8.32  8.20*    8.32  8.14

 1 2 3 4 5 6
rCpApApApApA

    C(1)         A(2)      A(3-5)
 H6    H5     H8    H2      H8                H2
7.63  5.82   8.29  8.16   (8.23)   (8.07,8.06,8.03)
```

*Indicates only tentative assignments.

[a]Parentheses indicates that we were unable to make assignments to particular bases in the sequence.

Figure 2.3 Solution conformations of dinucleotides proposed by Lee and Tinoco.[37] Figure (I) shows the conformation for a right handed stack of rApA.
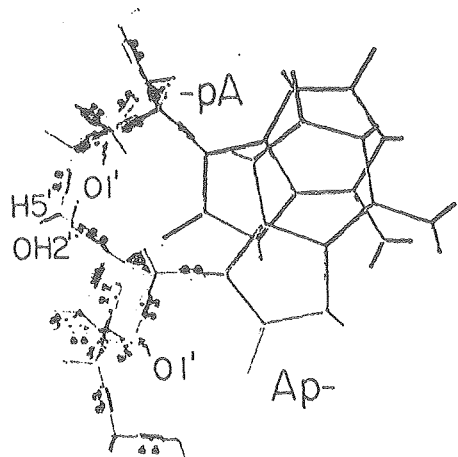
(I)
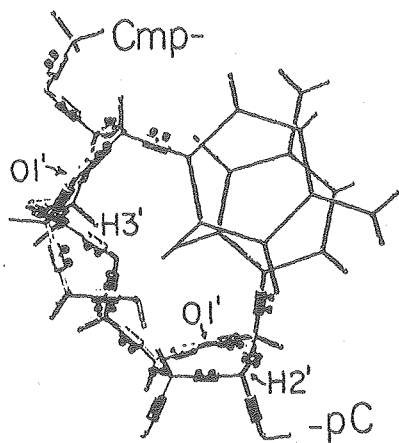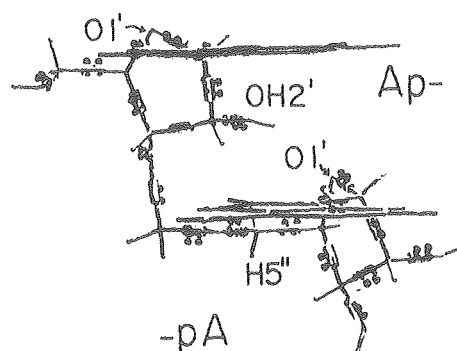
(II)
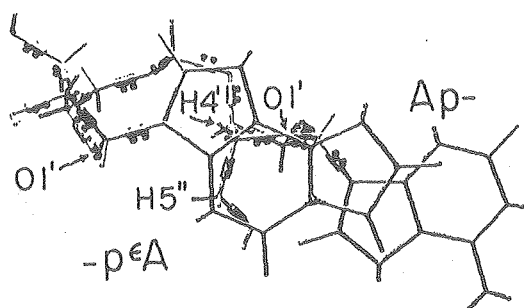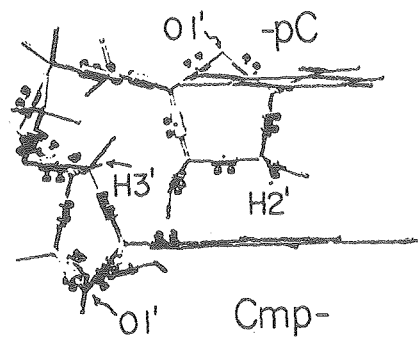
(III)
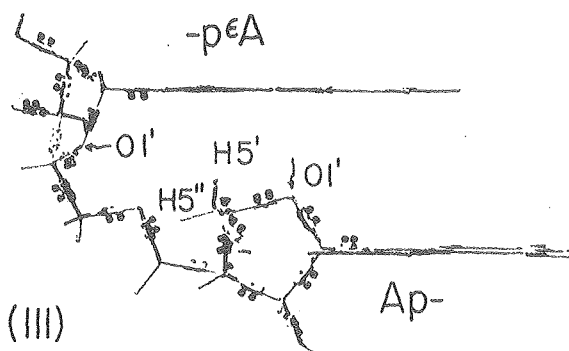
The assignments of the base protons in dCT_5G were made in a manner similar to that for dCA_5G. The components used were dCpT, dCpTpT, $dC(pT)_4$, $dC(pT)_6$, and dpTpTpG. Unambiguous assignments of the cytosine and guanine base protons as well as the H6 protons on the penultimate thymines were made. The three internal thymine H6 protons all had the same chemical shifts at 65°C. The assignments of the thymine methyl peaks to specific bases in the sequence were not made at any temperature. Chemical shifts of thes oligomers at 65°C are given in Table IV.

For the ribo-oligonucleotides no attempt was made to assign the uracil H5 and H6 base protons to particular uracils on the oligomers. Assignments of rCA_5G were made by comparison with the series $r(Ap)_nApG$ assigned by Shum,[51] as well as our analysis of the oligomers rCpA, rCpApA, and rCpApApApA (see Table V). From this work we were able to assign the cytosine and guanine base protons as well as the H8 and H2 on the penultimate adenines. Again, the assignments of the three internal H8 protons or the three internal H2 protons to specific bases were not attempted.

The assignment of the base protons at other temperatures was made by following each peak's shift with temperature; this is illustrated in Figures 2.4 and 2.5. Spectra were taken every ten degrees at higher temperatures where there are small changes in chemical shifts with temperature, and every 5°C in the range from 5 to 35°C, where the peaks shift

Figure 2.4. Helix-to-coil transition of dCA$_5$G
+ dCT$_5$G.

360 MHz ^{1}H NMR of
dCA$_5$G + dCT$_5$G, I mM/strand
D$_2$O, 0.22 M Na$^+$, pH = 7.0

45°

35°

25°

5°
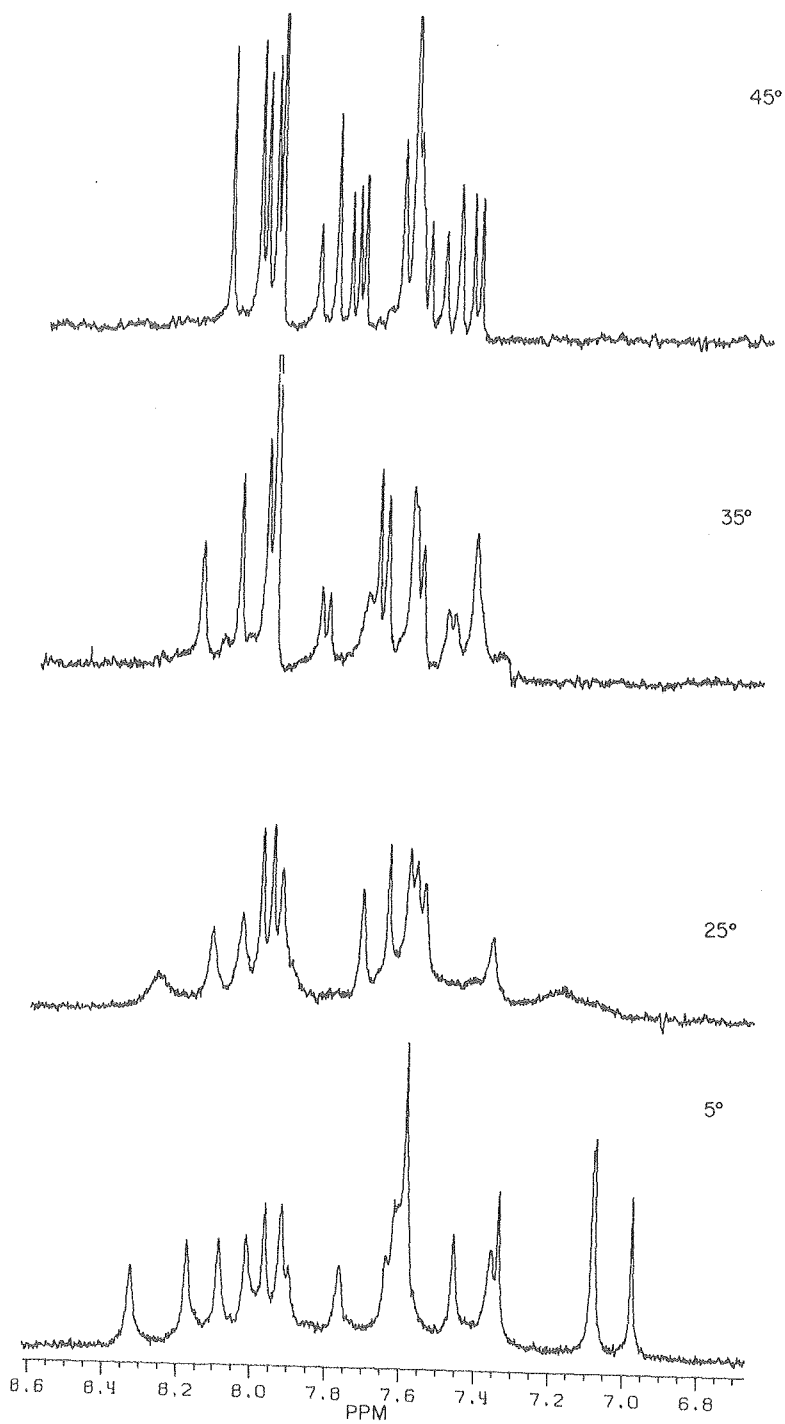
XBL 801-7673

Figure 2.5.   Melting curves for nonexchangeable

base protons in dCA_5G + dCT_5G.

NMR MELTING CURVES: CHEMICAL SHIFT VS. TEMPERATURE

5' CAAAAAG 3'
3' GTTTTTC 5'
  1234567

C(I) H-6
$T_m = 30.5°C$

A(3,4 or 5) H-2
$T_m = 29°C$

G(7) H-8
$T_m = 29.5°C$

● — double strand melt (dCA$_5$G + dCT$_5$G)

× — dCA$_5$G single strand melt

Chemical Shifts from 360 MHz ^{1}H NMR of
dCA$_5$G+dCT$_5$G, I mM/strand D$_2$O, 0.22 M Na$^+$, pH=7
and
dCA$_5$G, I mM/strand D$_2$O, 0.22 M Na$^+$, pH=7

CHEMICAL SHIFT (PPM)

TEMPERATURE (°C)

37
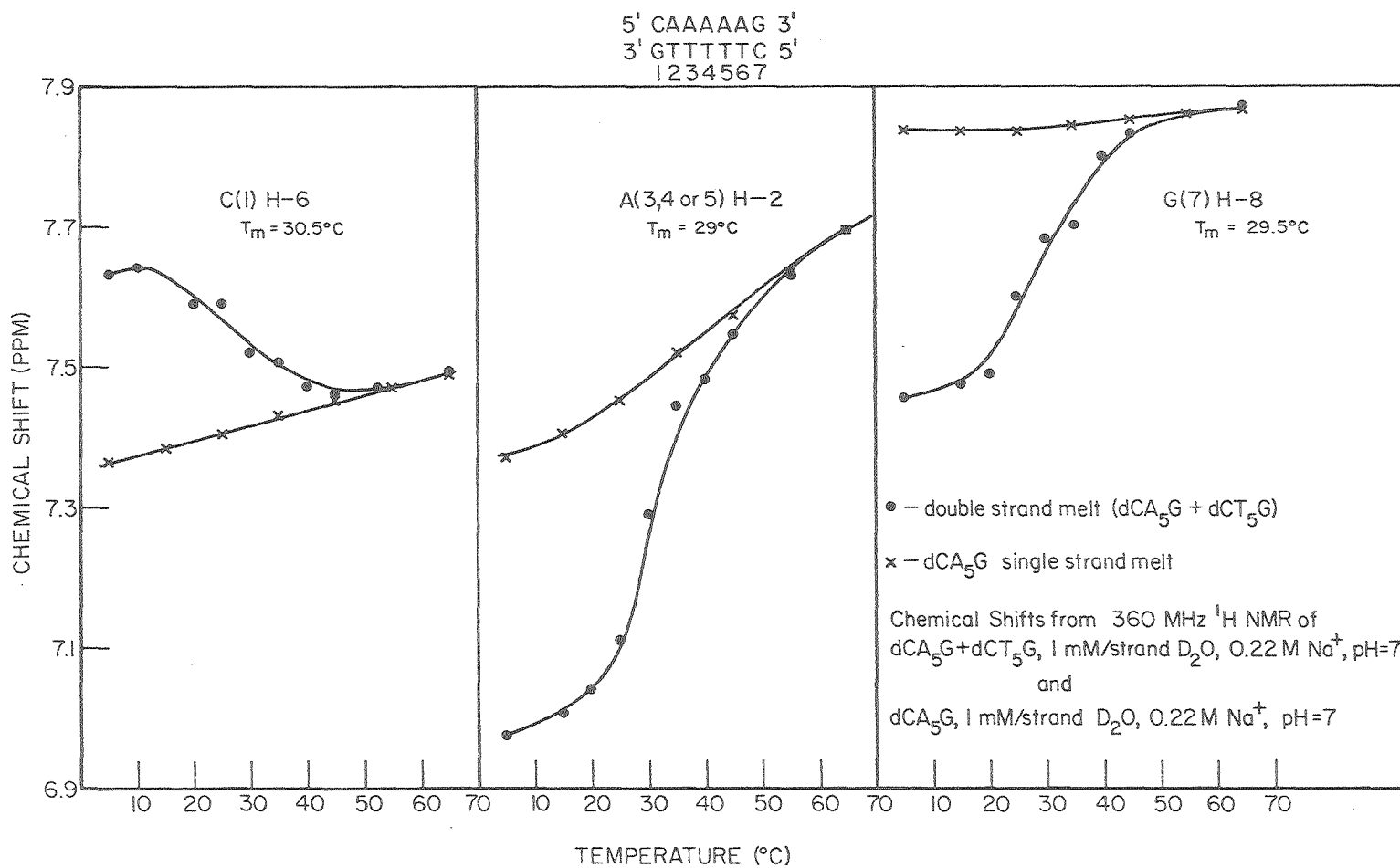
XBL 801-7671

dramatically with temperature and exchange broadening is evident. The assignment of the chemical shifts at 5°C for the double strand $dCA_5G + dCT_5G$ was aided by comparison of spectra taken before and after the guanine H8 protons were exchanged in D_2O by heating at 75°C for one hour. Chemical shifts of this double strand are given in Table VI. A small four bond coupling of the thymine methyl protons with the H6 protons helps in the identification of the H6 resonances. Assignment of the adenine H2 protons was aided by the fact that these peaks were sharper than the rest of the resonances in the double strand, presumably because of their longer T_2 compared to the T_2 of the other protons. The base proton spectrum of $dCT_5G + dCA_5G$ in the double strand at 5°C is shown in Figure 2.6.

The chemical shifts for the protons in the double strand hybrid helix ($dCT_5G + rCA_5G$) which could be unambiguously followed are given in Table VI. In the complexes $rCA_5G + rCU_5G$ and $rCU_5G + dCA_5G$ the spectra were so poorly resolved in the aromatic region because of the uracil doublets that we were unable to see individual peaks in the aromatic region at temperatures lower than 35°C, even at 360 MHz.

The H1' protons in deoxyribose and ribose sugars resonate at 5.5-6.5 ppm. The H1' proton in deoxyribose sugars is coupled to the H2' and H2" protons while the ribose H1' is only coupled to the H2' proton. Thus the H1' protons on

TABLE VI

EXPERIMENTAL AND CALCULATED CHEMICAL SHIFTS OF THE

NONEXCHANGEABLE BASE PROTONS IN THE DOUBLE HELIX[a]

	#1 C G	#2 A T	#3 A T	#4 A T	#5 A T	#6 A T	#7 G C
dCA$_5$G + dCT$_5$G helix							
AH2	--	7.337(	7.084	7.082	6.976)	7.590	--
C or T H6	7.630	7.356(	7.640	7.617	7.590)	7.760	7.910
G or A H8	7.964	8.324(	8.173	8.085	8.012	7.920)	7.870
rCA$_5$G + dCT$_5$G helix							
AH2	--	7.766(	7.229	7.229	6.876)	7.317	--
C or T H6	b	7.860(	7.676	7.621	7.574)	7.502	∿8.0
G or A H8	b	8.163	b	b	b	b	b
Calculation for DNA B form							
AH2	--	6.78	6.92	6.99	7.07	7.73	--
C or T H6	7.93	7.83	7.84	7.84	7.85	7.83	7.94
G or A H8	8.14	8.40	8.32	8.29	8.30	8.30	7.96
Calculation for RNA A form							
AH2	--	6.89	7.12	7.15	7.17	7.61	--
C or T H6	8.13	7.72	7.73	7.72	7.77	7.77	8.10
G or A H8	8.05	8.46	7.89	7.83	7.83	7.80	7.98
Calculation for RNA A' form							
AH2	--	6.80	7.06	6.82	6.89	7.57	--
C or T H6	8.13	7.71	7.72	7.71	7.76	7.76	8.10
G or A H8	8.04	8.42	7.79	7.72	7.72	7.69	7.45

TABLE VI

(continued)

[a]The calculations were done using numbers dervied by Arter and Schmidt,[41] and we assumed thymine has the same ring current as uracil. Values in parenthesis indicate that we were unable to assign these peaks to particular bases in the sequence.
[b]Poor resolution made assignment of this proton impossible.

Figure 2.6. Assignments of nonexchangeable base protons in double strand of dCA_5G + dCT_5G.

DOUBLE STRAND

5'CAAAAAG3'
3'GTTTTTC5'
 1234567

360 MHz ^{1}H NMR of
dCA$_5$G + dCT$_5$G, 1 mM/strand, 5°C
D$_2$O, 0.22 M Na$^+$, pH = 7.0

the two different rings are easily differentiated. We were
not able to assign the H1' protons to particular sugars in
the sequence, but only to either deoxyribose or ribose
sugars.

B)   Assignment of the Base Paired Imino Protons

        The base paired imino protons for the duplex dCT_5G +
dCA_5G are shown in Figure 2.7a. Partial assignment of these
resonances was made by the temperature dependences of the
protons, as well as comparison with calculations of chemical
shifts for the double strand. The guanine H1 proton involved
in a hypothetical isolated base pair has been found to resonate
1 ppm upfield from the uracil or thymine H3 in the isolated
base pair.[6,38] The numbers for these isolated base pairs
derived from tRNA data are 14.4 ppm for the A·U base pair
and 13.6 ppm for the C·G base pair.[6] Since there is only a
limited amount of work done on the imino protons in deoxyribo-
oligonucleotides of known sequence,[39] the number for isolated
base pairs derived from the tRNA work have been applied to the
DNA helices.

        For the dCA_5G + dCT_5G helix there are clearly seven
resonances in the imino region, as seen from the integration
shown in Figure 2.8. The two resonances found at 12.93
and 13.55 ppm broaden before the other peaks. Figure 2.9
shows that at 20°C these two peaks are extremely broad

Figure 2.7.

    a) dCA_5G + dCT_5G double strand at 5°C.

    b) rCA_5G + rCU_5G double strand at 5°C.

    c) rCA_5G + dCT_5G double strand at 5°C.

    d) dCA_5G + rCU_5G in triple strand at 1°C and in 1.0 M NaCl instead of 0.18 M NaCl.
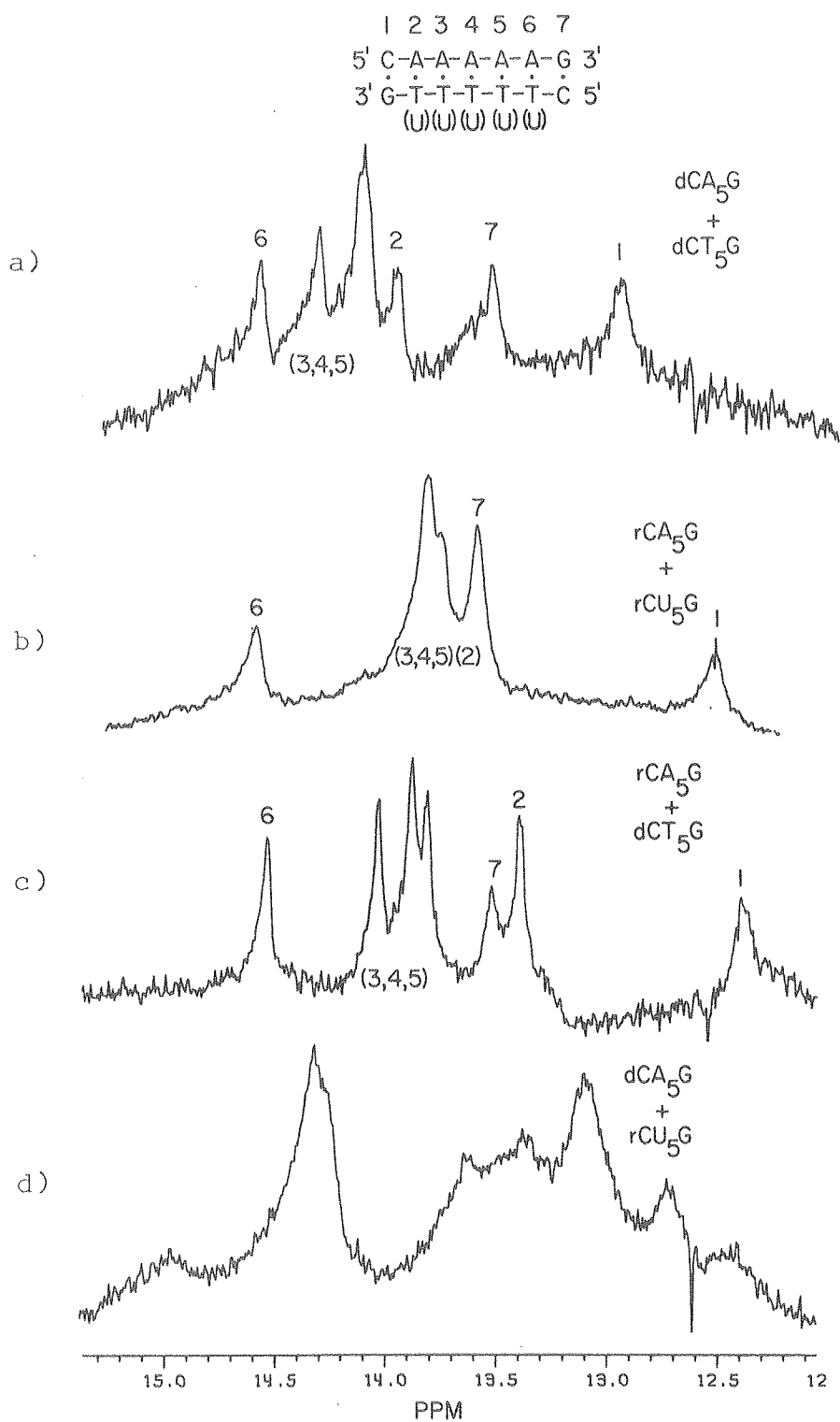
Figure 2.8. Integration of imino proton region

of dCA_5G + dCT_5G helix.
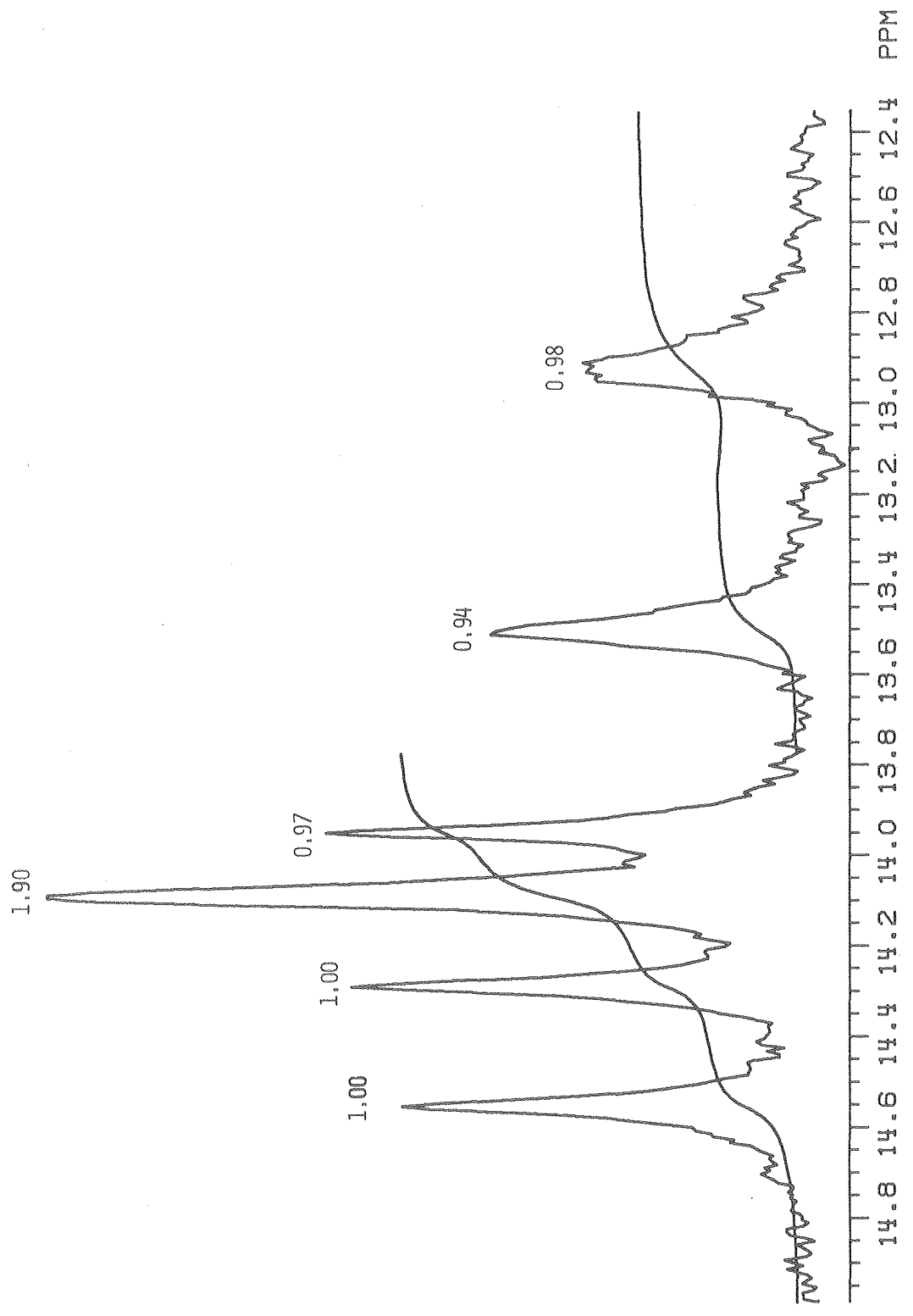
Figure 2.9.   Melting of imino proton region of

dCA$_5$G + dCT$_5$G helix.

5' CAAAAAG 3'
3' GTTTTTC 5'
1234567

25°

20°

15°

5°

6

7

1

(3,4,5,2)

15.0   14.5   14.0   13.5   13.0   12.5
PPM

XBL 8011-7471
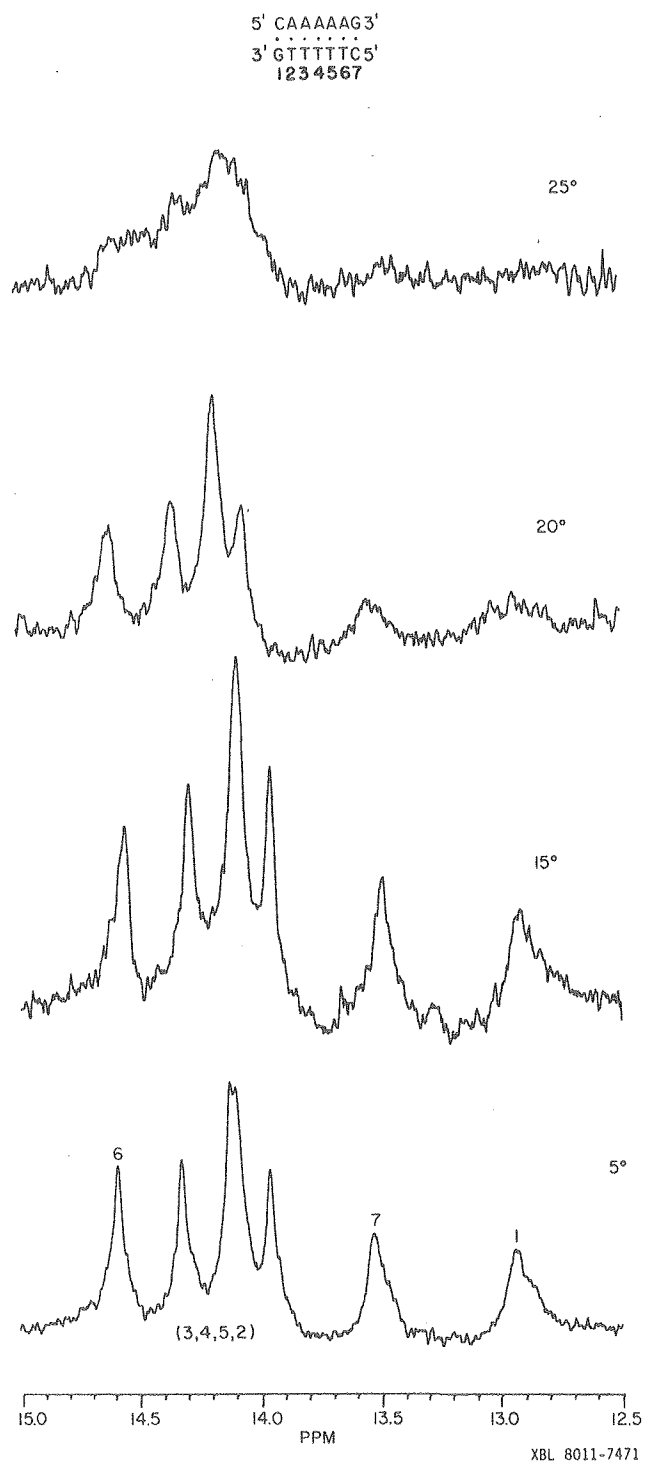
relative to the rest of the molecule, and by 25°C they have
disappeared. The differential broadening observed is due
to the faster exchange of the terminal base pair protons
compared to those in the interior of the helix.[27,40]
Calculated chemical shifts of the two C·G resonances allow
assignment of the resonance at 12.9 ppm to the C·G in position
one and the 13.55 ppm peak to the C·G in position seven (see
Table VII).[41] The assignments of the A·T base pairs were
made by comparison with the calculated shifts for DNA B
geometry. This enabled us to assign the A·T resonances at
the 6 position to 14.56 ppm with the rest of the A·T base
pairs assigned to region 13.9 - 14.4 ppm.

In the rCU_5G + rCA_5G system we were aided in the assign-
ments by comparison with the system rCA_6 + rCU_5G. Figure
2.10 shows the comparison of the rCA_5G + rCU_5G and rCA_6 +
rCU_5G. This gives unambiguous assignments of the C·G(1)
base pair to 12.6 ppm, A·U(6) to 14.6 ppm and C·G(7) to
13.6 ppm as shown in Figure 2.7. The other resonances in
the rCU_5G + rCA_5G were assigned to the region 13.6 - 13.9
ppm. All chemical shifts at 5°C are given in Table VII.

In the duplex rCA_5G + dCT_5G, assignments were made in
an analogous manner to the procedure used for the dCA_5G +
dCT_5G helix. The C·G resonances again show very different
temperature dependences than the A·T protons. The other
peak assignments were then made using an RNA A geometry

Figure 2.10. Comparison of imino proton region
of rCA_6 + rCU_5G (top) and rCA_5G + rCU_5G
(bottom).

14.8 14.6 14.4 14.2 14.0 13.8 13.6 13.4 13.2 13.0 12.8 12.6 12.4 12.2 PPM
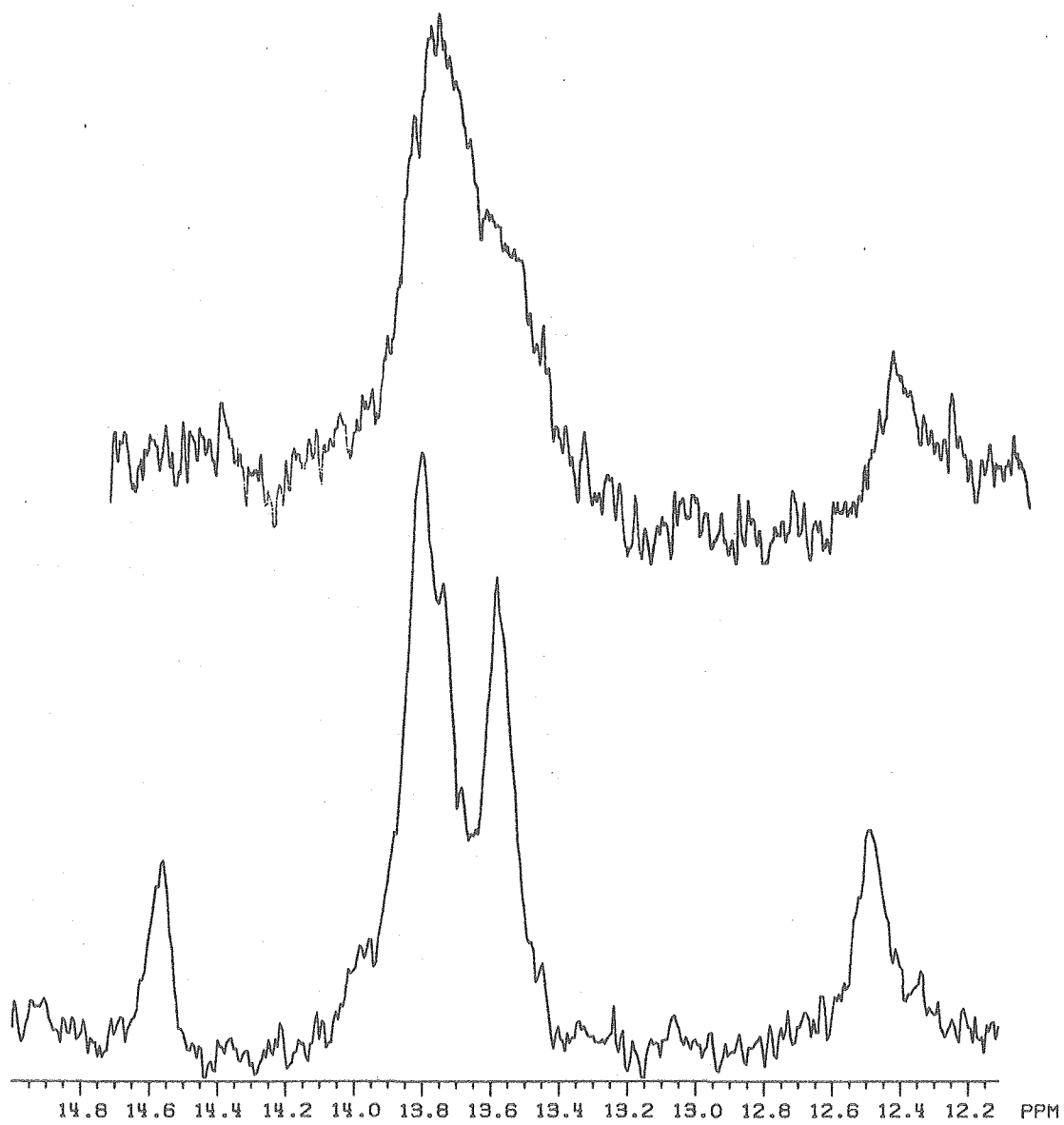
XBL 8011-7496

TABLE VII

EXPERIMENTAL AND CALCULATED CHEMICAL SHIFTS OF THE IMINO

PROTONS IN THE DOUBLE HELIX

#1	#2	#3	#4	#5	#6	#7
C	A	A	A	A	A	G
G	T	T	T	T	T	C

$dCA_5G + dCT_5G$ helix

        12.94 (13.95 14.30 14.08 14.08) 14.56 13.51

$rCA_5G + dCT_5G$ helix

        12.38   13.40 (14.02 13.88 13.80) 14.53 13.52

$rCA_5G + rCU_5G$ helix

        12.52 (13.60 13.76 13.82 13.82) 14.60 13.60

DNA B form calculation

        12.53   13.50 13.80 13.80 13.85   14.15 13.30

RNA A form calculation

        12.80   13.46 13.70 13.70 13.70   14.10 13.50

RNA A' form calculation

        12.72   13.27 13.58 13.58 13.60   14.11 13.47

The calculations were done using numbers derived by Arter
and Schmidt,[41] and we assumed thymine has the same ring
current as uracil. Values in parentheses indicate that we
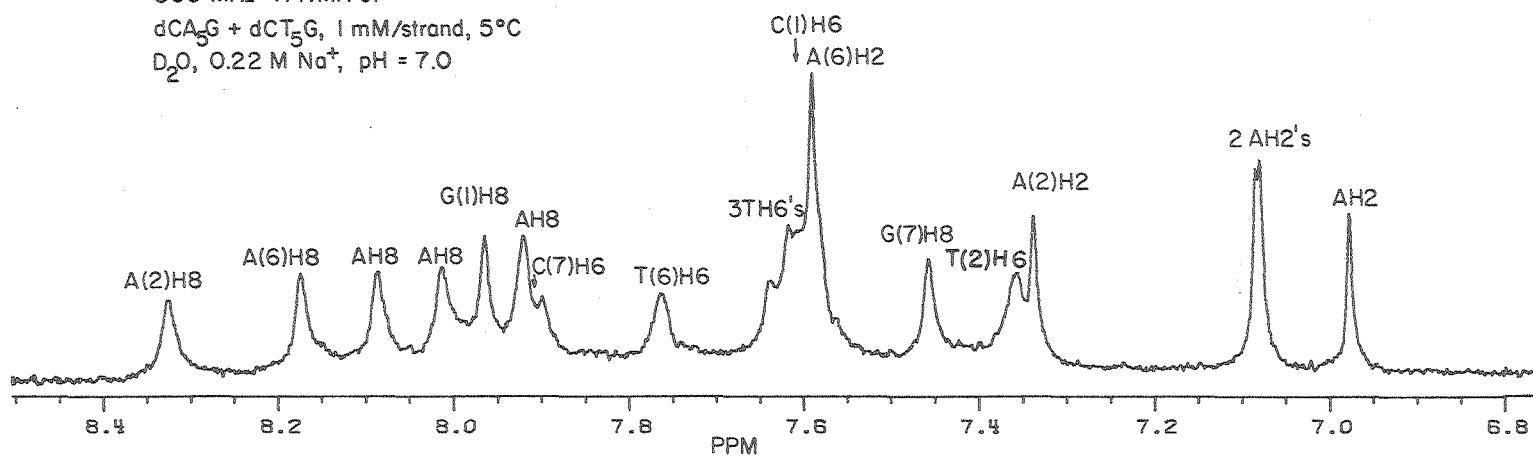were unable to assign these peaks to particular bases.

to calculate ring current shifts for each resonance. For
this hybrid the calculated ring current shifts are shown
for RNA A and A' as well as DNA B form geometry in Table
VII.

C)   Temperature Dependence of the Nonexchangeable Protons
      in the Single Strands

The temperature dependences of the base protons of the
single strands dCA_5G, dCT_5G, and rCA_5G are shown in Figures
2.11, 2.12, and 2.13, respectively. The cytosine H6 and H5,
the adenine H2 and H8, the guanine H8 and the thymine H6 and
methyl proton resonances were observed. The chemical shifts
for all the base protons in dCT_5G show little change with
temperature (< 0.1 ppm from 5 - 65°C, see Figure 2.12).
The largest changes are on the adenine H2 protons in dCA_5G and
the adenine H8 protons on rCA_5G as shown in Figures 2.11 and
2.13. Most of the proton chemical shift changes observed are
not linear with temperature; this is important to note when
analyzing melting curves, as will be discussed in a later
section. There are large differences in chemical shift changes
with temperature between dCA_5G and rCA_5G. The temperature de-
pendences of the chemical shift for a particular proton are
also sometimes in opposite directions for the two strands.
For example, compare the H6 of C(1) and the H8 of A (3, 4,
5 or 6) on the two strands in Figure 2.14. These observations
indicate different conformations for the deoxyribo- and
ribo- strands of CA_5G.

Figure 2.11. Temperature dependence of the base

protons in the single strand of dCA_5G.
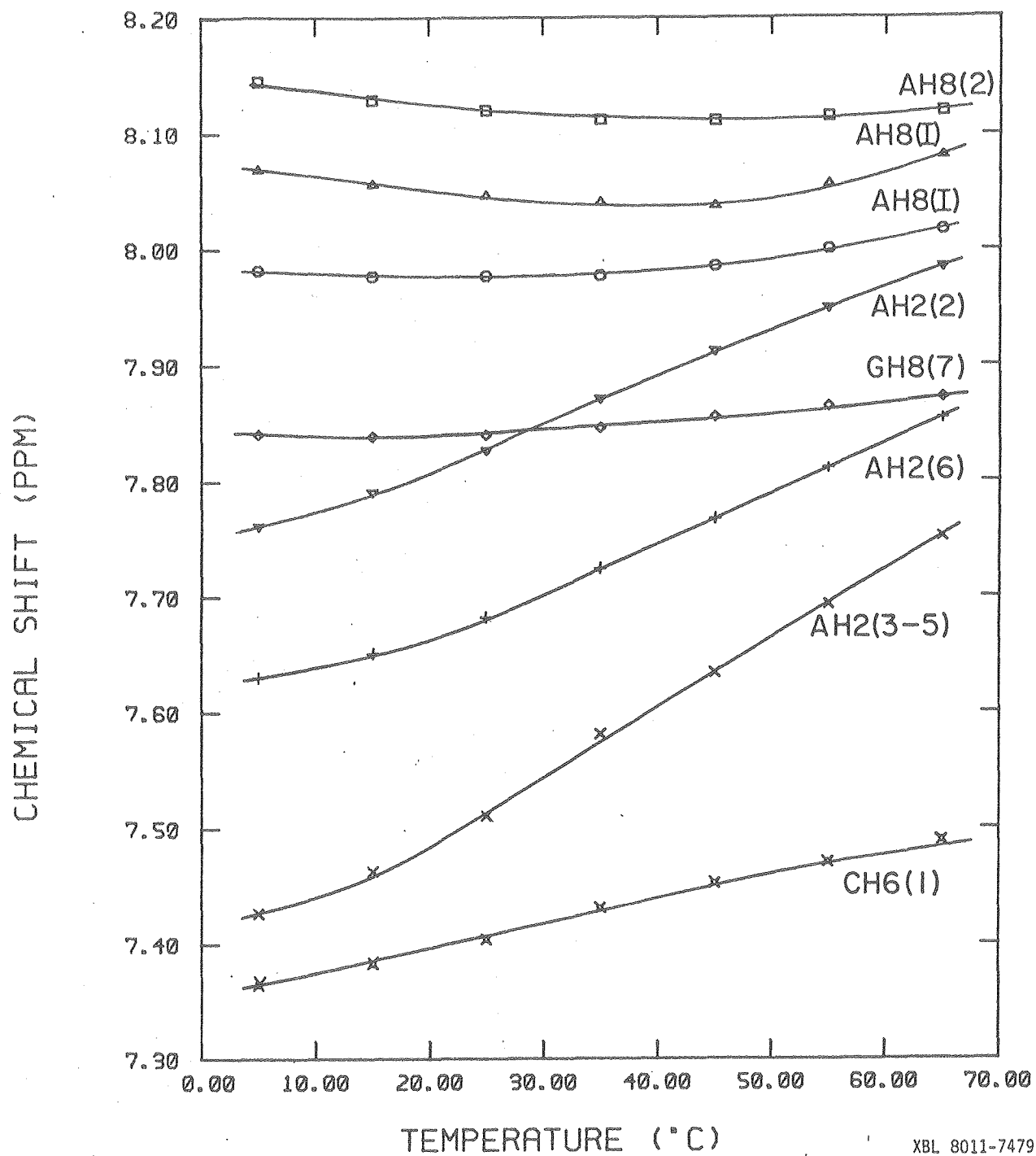
XBL 8011-7479

Figure 2.12. Temperature dependence of base protons in the single strand of dCT_5G.
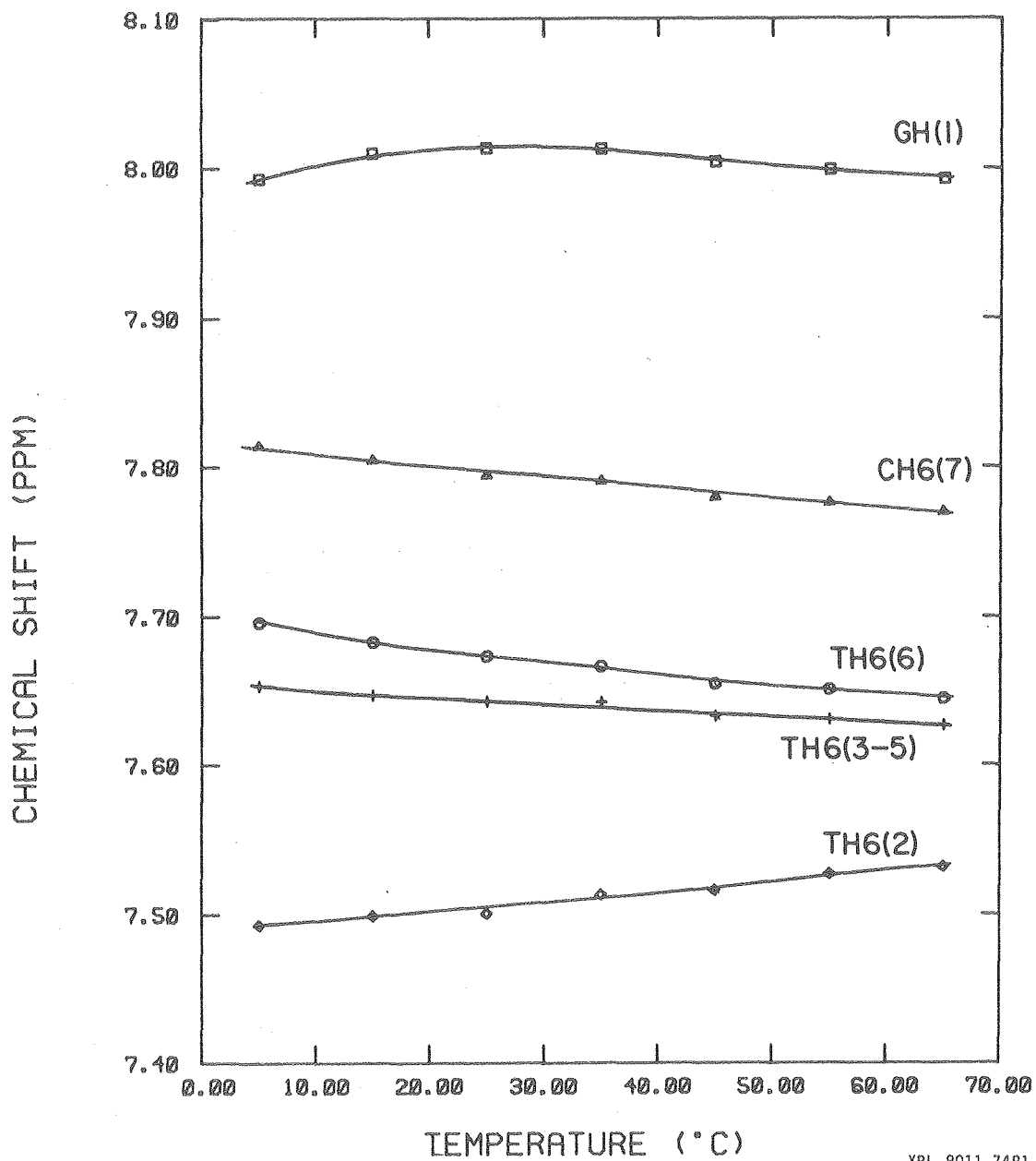
XBL 8011-7481

Figure 2.13. Temperature dependence of base protons in the single strand of rCA_5G.

XBL 8011-7484
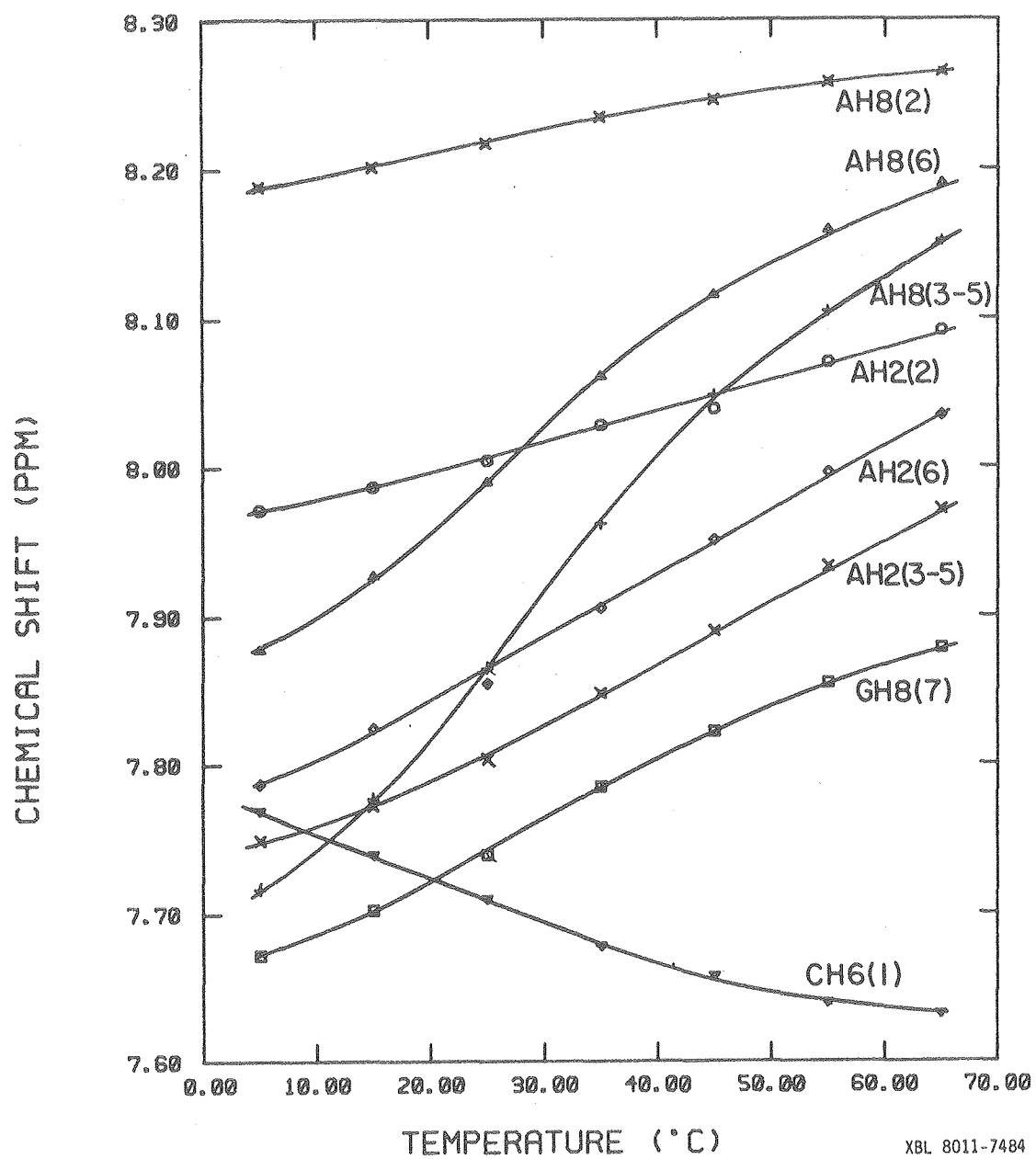
The best measures of base-base stacking from chemical shifts are obtained from the H2 of adenine and the H5 of the pyrimidines.[42] The H8 of adenines and the H6 of pyrimidines have significant effects basides ring currents, which effect their chemical shifts,[42,43] such as the glycosidic torsion angle, and the proximity of the sugar ring oxygens or phosphate groups. Therefore, in order to get an idea of the relative base-base stacking in the dCA_5G and rCA_5G strands, we compared the chemical shifts of the adenine H2 protons. The adenine H2 protons on the ribose strand are always downfield (less shielded) from the same protons on the deoxyribose strand. This is indicative of more base-base stacking in dCA_5G than in rCA_5G.

D)   The Helix to Coil Transition of dCT_5G + dCA_5G and dCT_5G + rCA_5G as Followed by the Chemical Shift of the Base Protons

The temperature dependence of the chemical shifts of the base protons were studied in the oligonucleotides, dCT_5G + dCA_5G, and dCT_5G + rCA_5G. In the helix-to-coil transition of the dCA_5G + dCT_5G, all the base proton chemical shifts were followed from 5 - 65°C. In the intermediate states from 20 - 35°C, it is difficult to obtain exact chemical shifts of some of the protons due to extensive broadening of the resonances undergoing chemical exchange.

Figure 2.14.   Comparison of temperature dependence
of base protons in dCA_5G and rCA_5G.
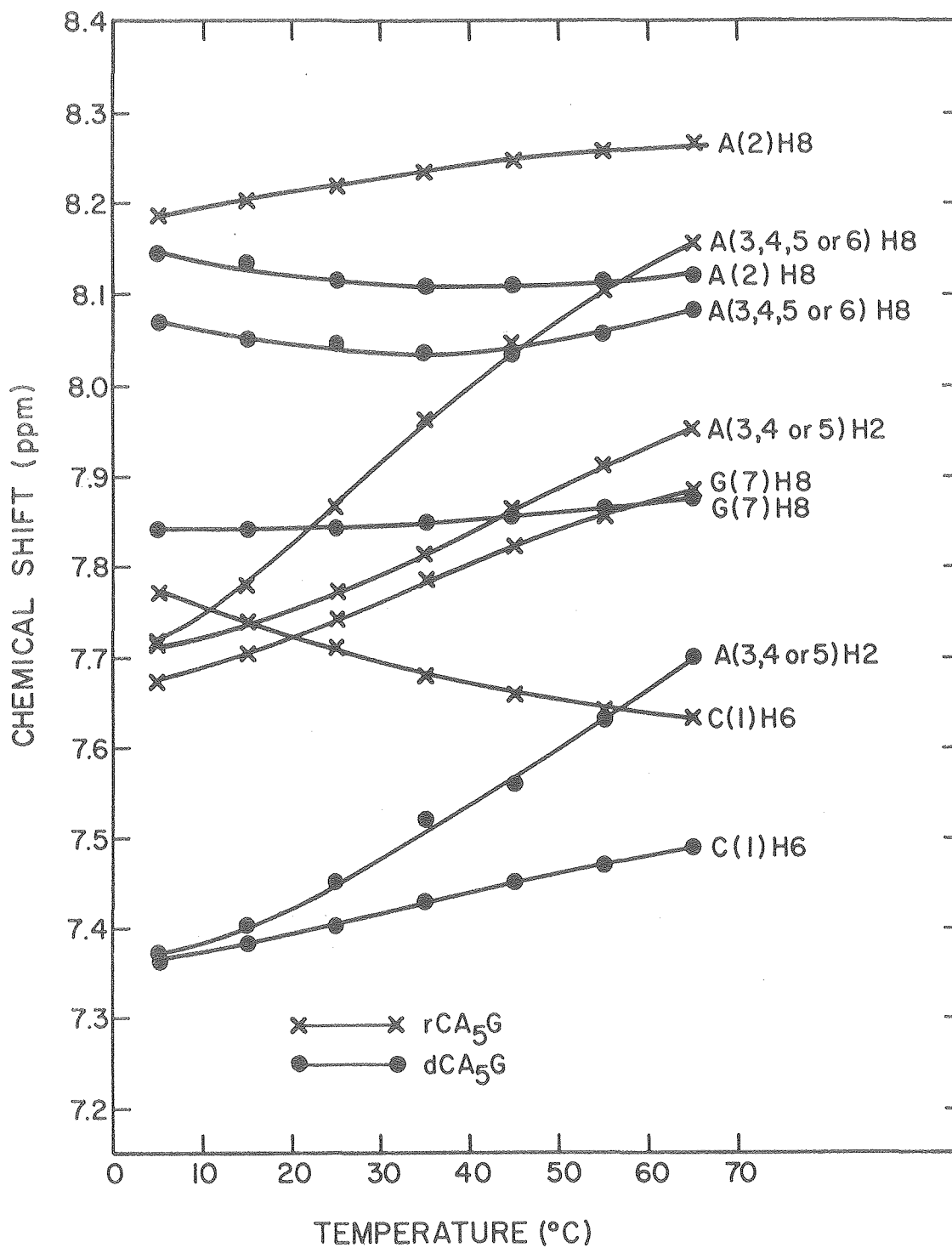
XBL 8011-7467

In the other helix, $dCT_5C + rCA_5G$, the chemical exchange broadening over the 20 - 30°C temperature range prevented the assignment of many of the resonances at lower temperatures. The chemical shift changes with temperature for the base protons in the two helices are shown in Figures 2.15a-e and 2.16a and b.

In order to monitor the helix-to-coil transitions in these oligomers, base protons were chosen which show large changes upon formation of the helical state (> 0.1 ppm). The curves for many of these protons have sigmoidal shapes and characteristics which are very similar to absorbance versus temperature curves for these oligomers.[44] However, the NMR data allows one to follow the properties of individual bases throughout the double-to-single strand transition. Thus NMR is more useful than absorbance studies for finding properties such as differential melting of the helix.[15,27,40]

The T_m's or melting temperatures of different bases were compared to learn if there is any melting on the ends of the $dCT_5G + dCA_5G$ helix. The analysis was the same as that used in optical studies;[25] this requires the melting behavior of the single strand to obtain the T_m. We measure the chemical shifts versus temperature of the single strands directly by using solutions containing only one of the strands. The double strand baseline can only be estimated from the low temperature behaivor of the chemical shifts. We used the

Figure 2.15. Temperature dependence of the following

protons in the helix-to-coil transition of

dCA_5G + dCT_5G.

a) Thymine H6 protons.

b) Terminal guanine H8 and cytosine H6 protons.

c) Adenine H8 protons.

d) Adenine H2 protons.

e) Thymine methyl protons.

a)

b)

XBL 8011-7483

c)
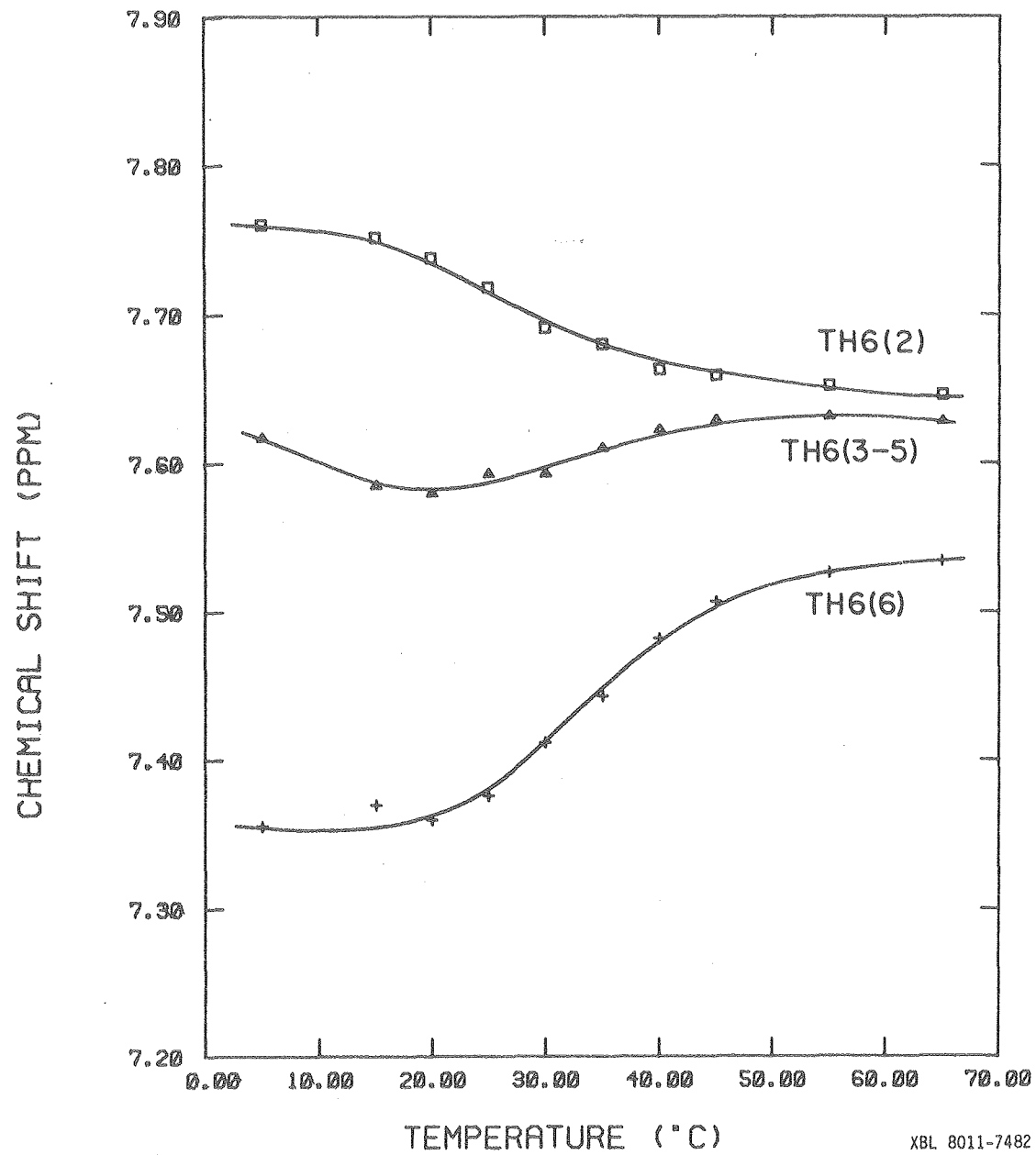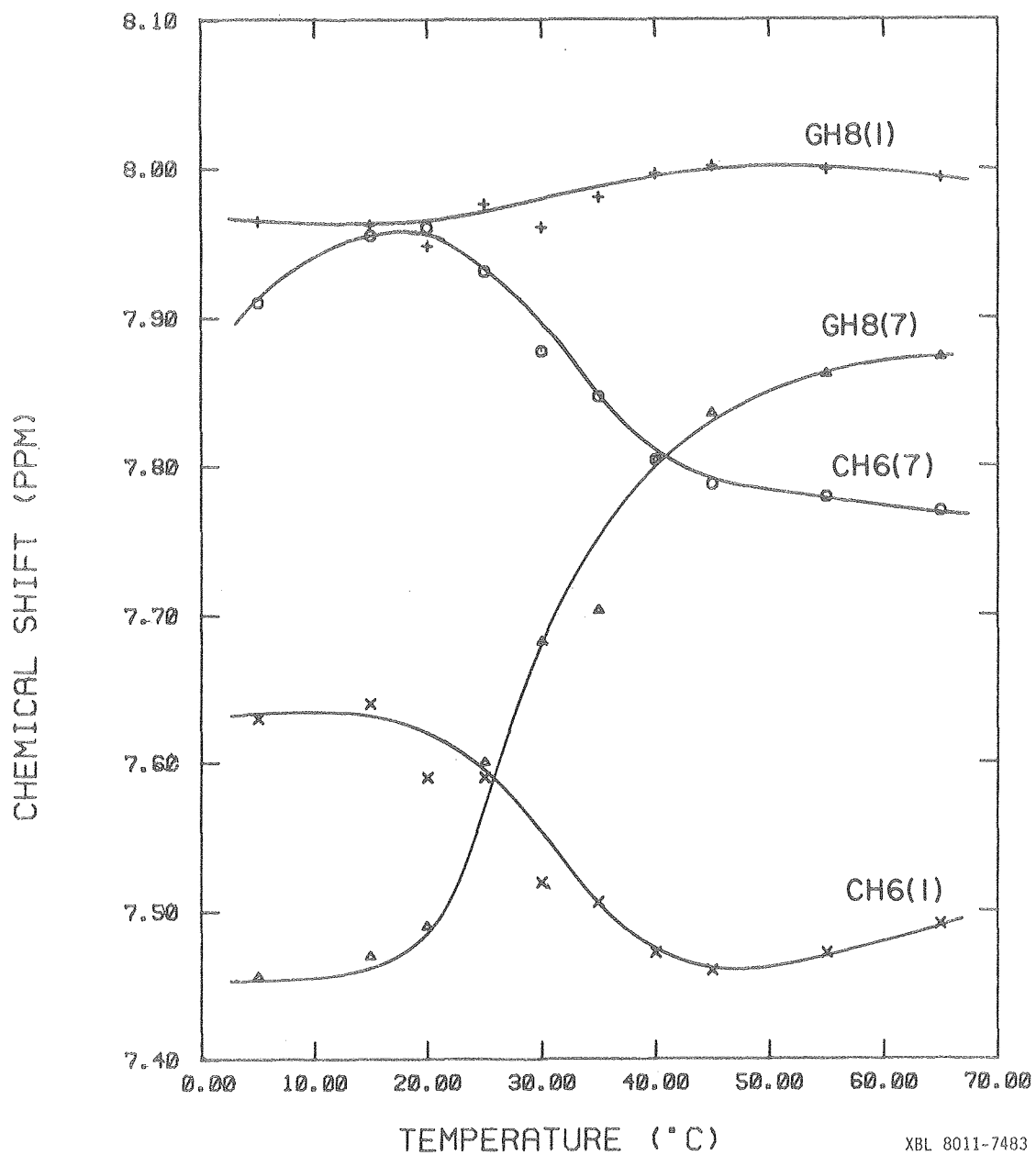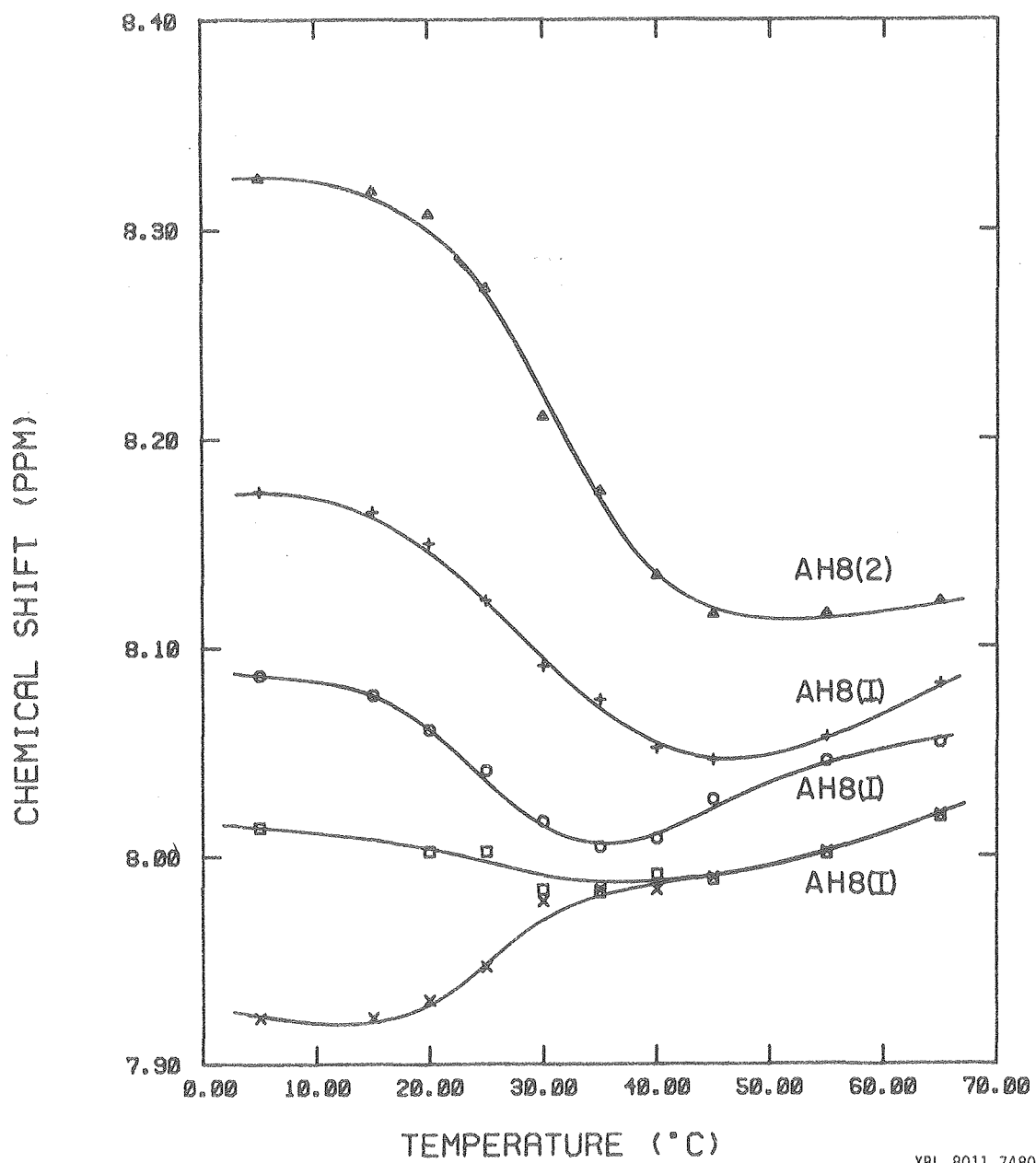
XBL 8011-7480

d)
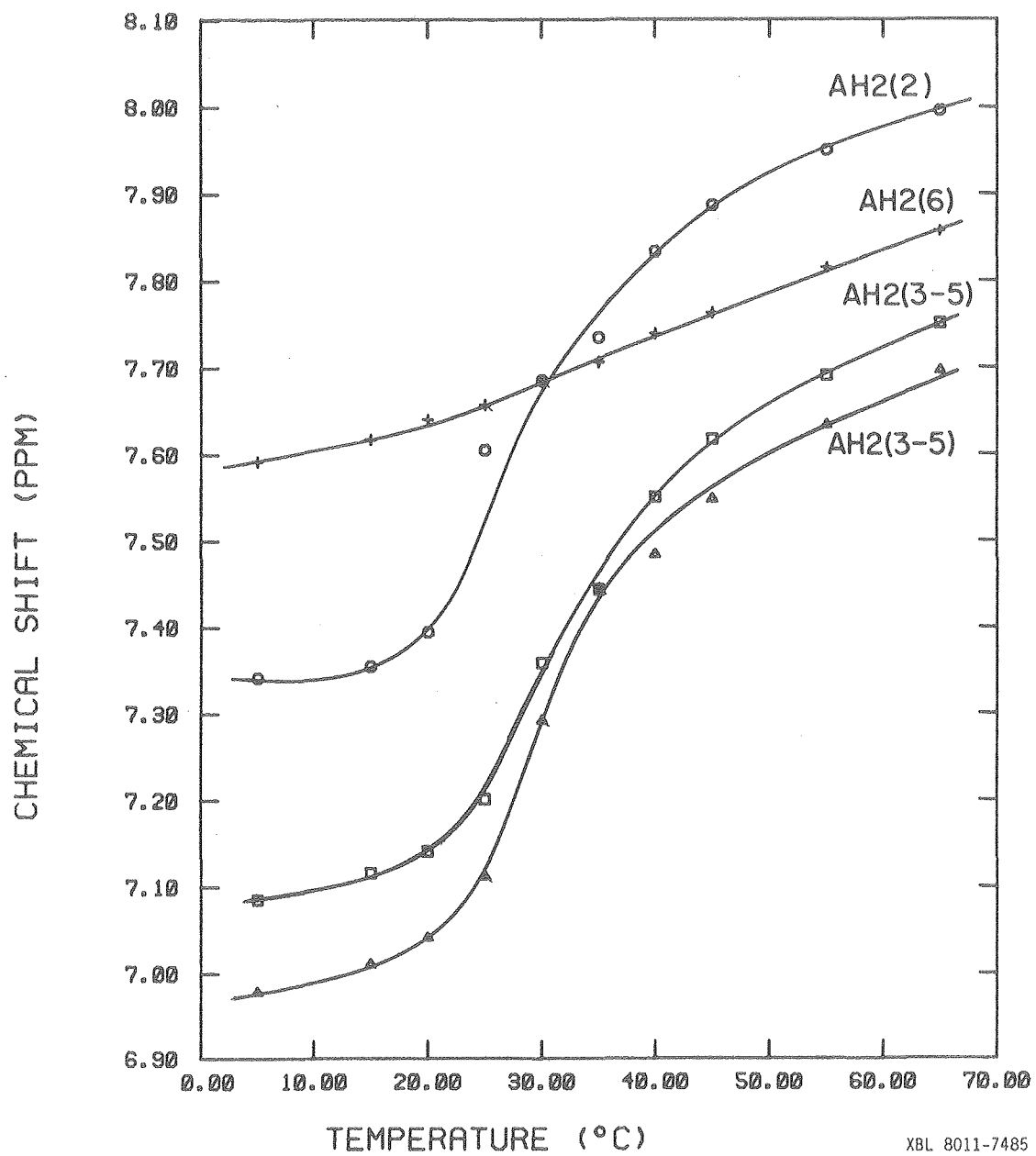
XBL 8011-7485

e)
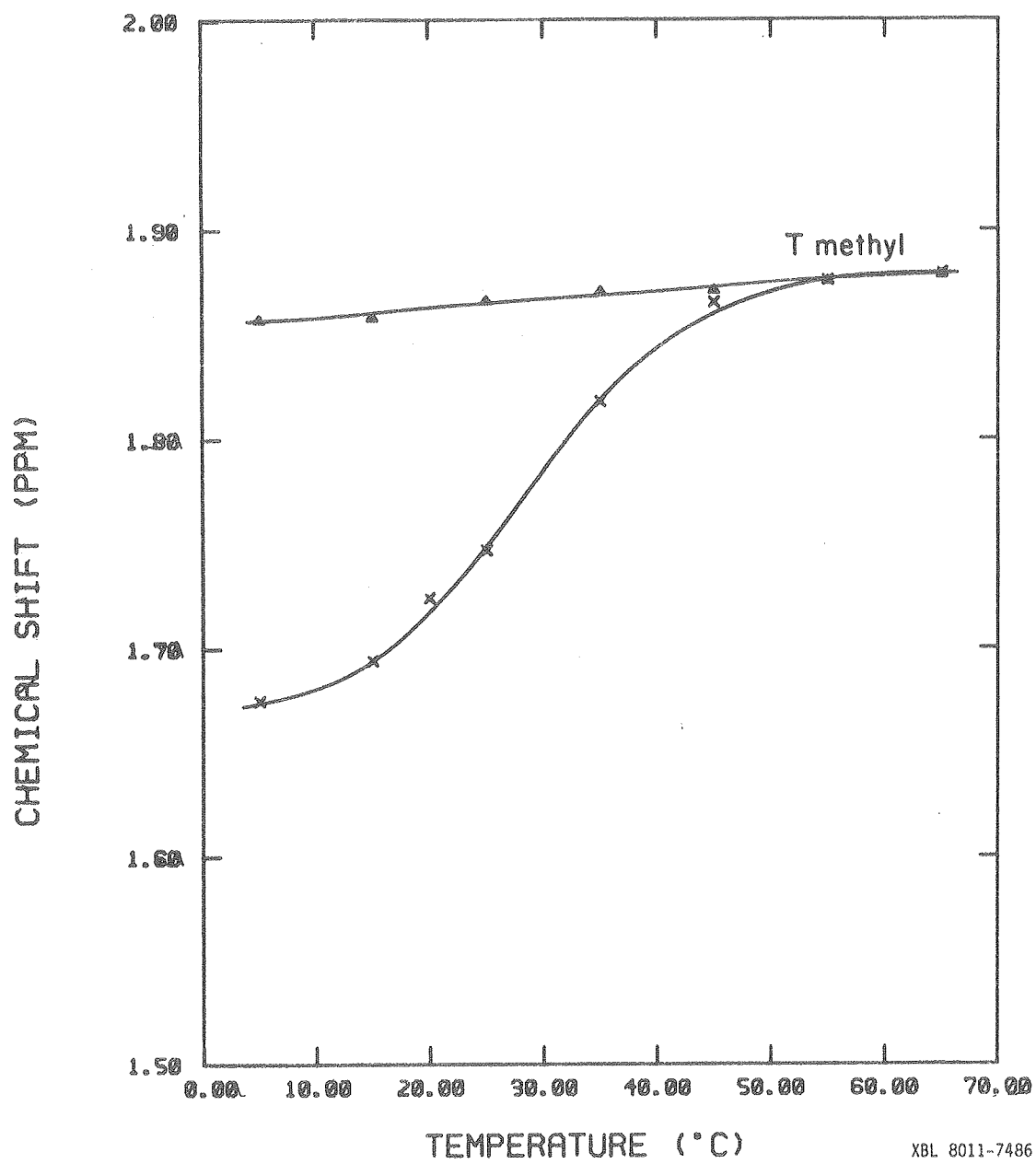
XBL 8011-7486

Figure 2.16. Temperature dependence of the
following protons during the helix-to-coil
transition of dCT_5G + rCA_5G.

a) Adenine H2 protons.

b) Adenine H8 and thymine H6 protons.

a)
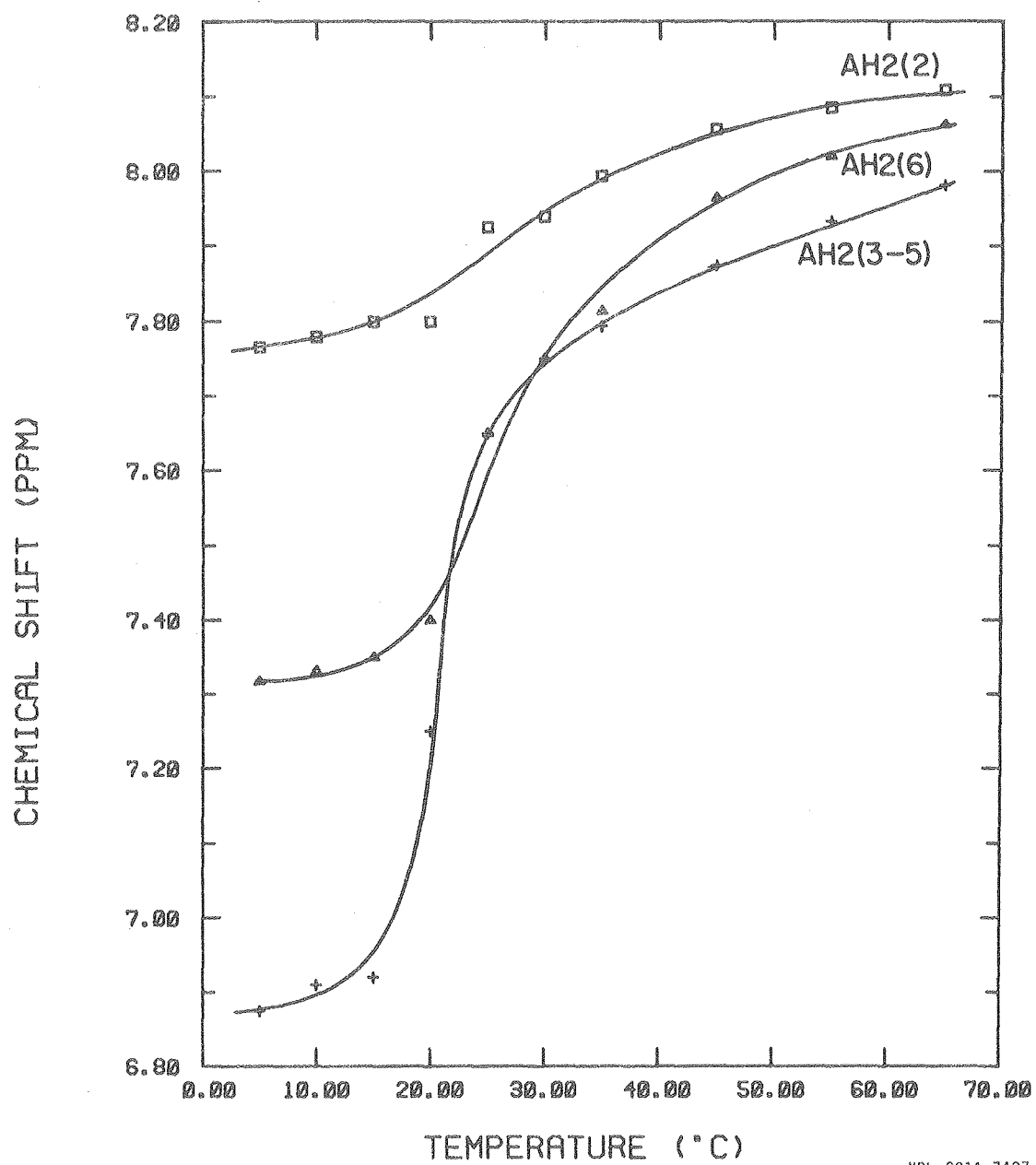
b)
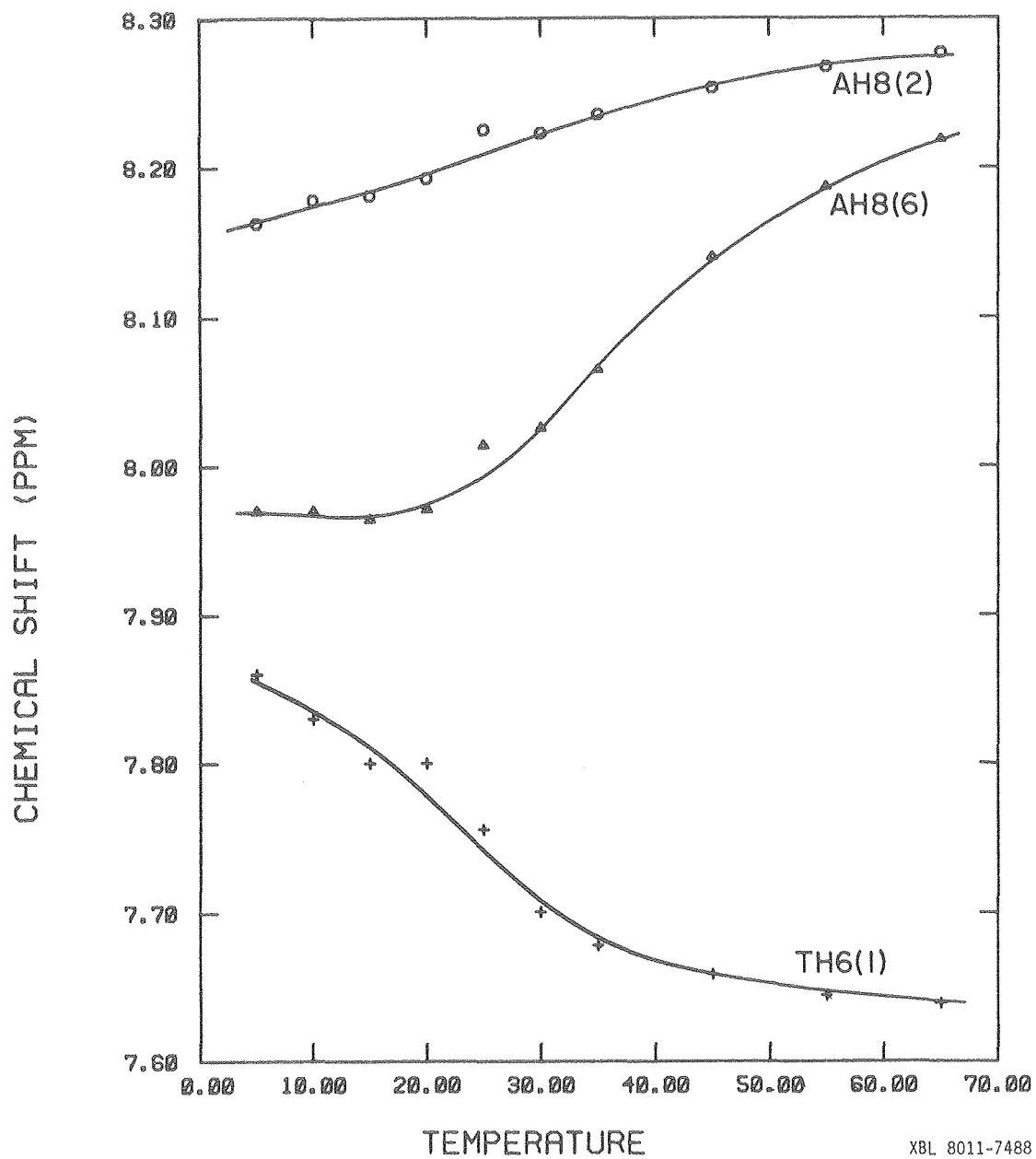
value of the chemical shift measured at 5°C for the lower
baseline. For most of the protons there are very small
chemical shift changes between 5 and 15°C so that the chemical
shift of the completely double strand was taken to be tem-
perature independent. The T_m values are all very similar
for protons in different parts of the helix, with an average
value of 29 ± 2°C at a concentration of 1.0 mM per strand.
Since all the base protons melt at approximately the same
temperature, the concentration of partially formed helices
is small.

Optical melting under identical conditions gives a T_m
of 34 ± 2°C. No change in the melt was seen whether H_2O
or D_2O was used as solvent. The difference in the T_m's
obtained by NMR and optically is probably due to assumptions
about the temperature dependence of the properties of the
double strand, and also errors involved in assuming fast
exchange, on the NMR time scale, throughout the single to
double strand transition. These effects will be discussed
in a later section.

Melting curves for the oligomer dCT_5G + rCA_5G are shown
in Figures 2.16a and b. The temperature dependence of only
a small number of the base protons are shown since exchange
broadening and overlap of too many protons hindered the
identification of many of the protons in the double strand.
In this helix we were unable to follow any of the guanine

or cytosine protons throughout the whole melting transition, so that it was not possible to tell if there was significant melting of the ends of the helix. The average T_m for all the base pairs was 23.5°C at 0.5 mM per strand. The T_m obtained under similar conditions from optical data extrapolated to the same concentration was 25.7°C.[44]

E)   Temperature Dependence of the Exchangeable Imino Protons

The temperature dependences of the imino base protons in $dCT_5G + dCA_5G$ are shown in Figure 2.9. As already discussed in the section on the assignments of the imino protons, it is found that the base pairs on the ends broaden and disappear before the rest of the base pairs in the helix. Similar broadening is observed for the other helices $dCT_5G + rCA_5G$, and $rCU_5G + rCA_5G$ and are shown in Figures 2.17 and 2.18. The broadening phenomenon observed is due to chemical exchange as will be discussed in a later section.[45,46] The C·G imino protons for the three systems broaden and disappear in the range from 17 - 23°C. There is little chemical shift change with temperature for any of these resonances. Differences in the extent of broadening for a particular proton at a given temperature are seen in the three systems; this is due to different lifetimes for exchange of the imino protons with H_2O. This will be discussed in a later section.

Figure 2.17. Melting of imino protons in

rCA$_5$G + dCT$_5$G helix.
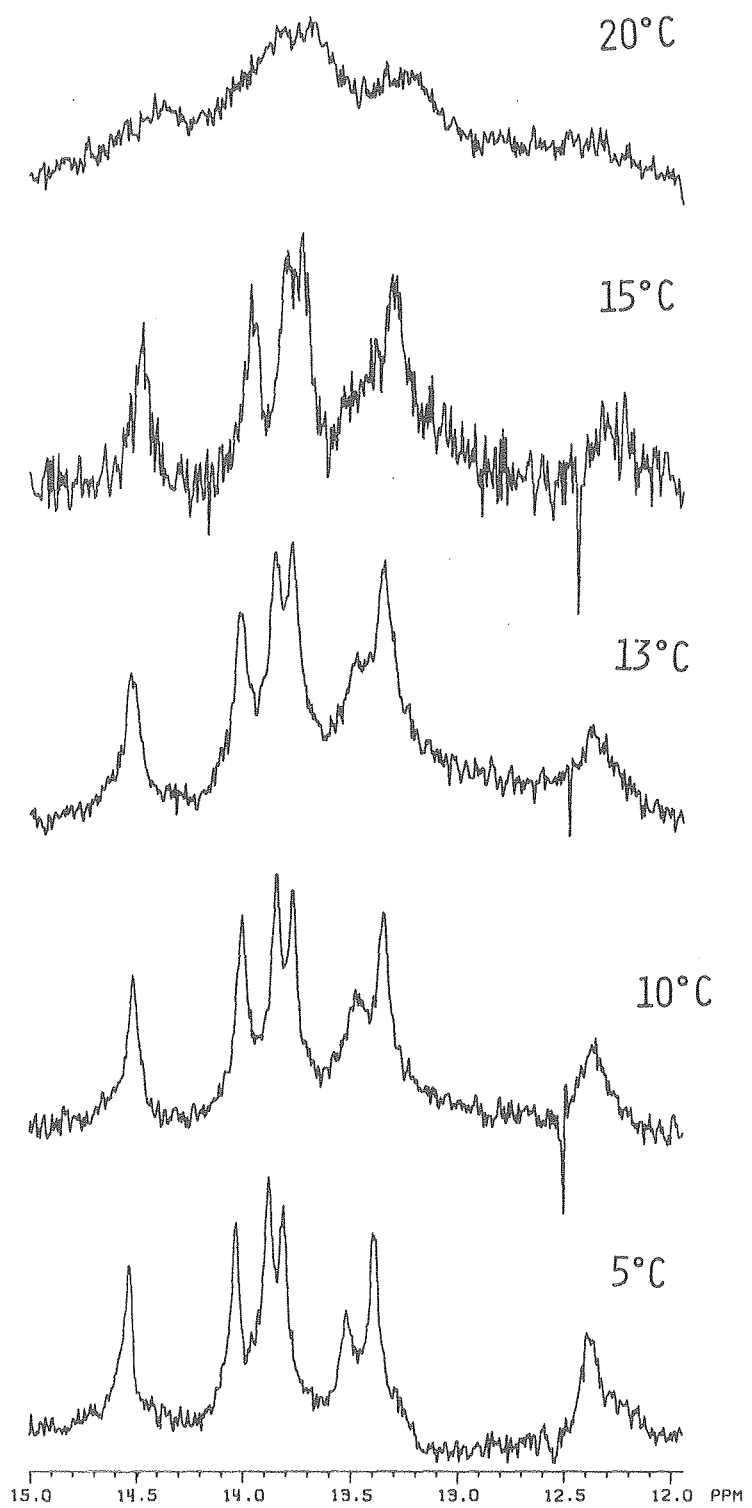
Figure 2.18. Melting of imino protons in

rCA$_5$G + rCU$_5$G helix.
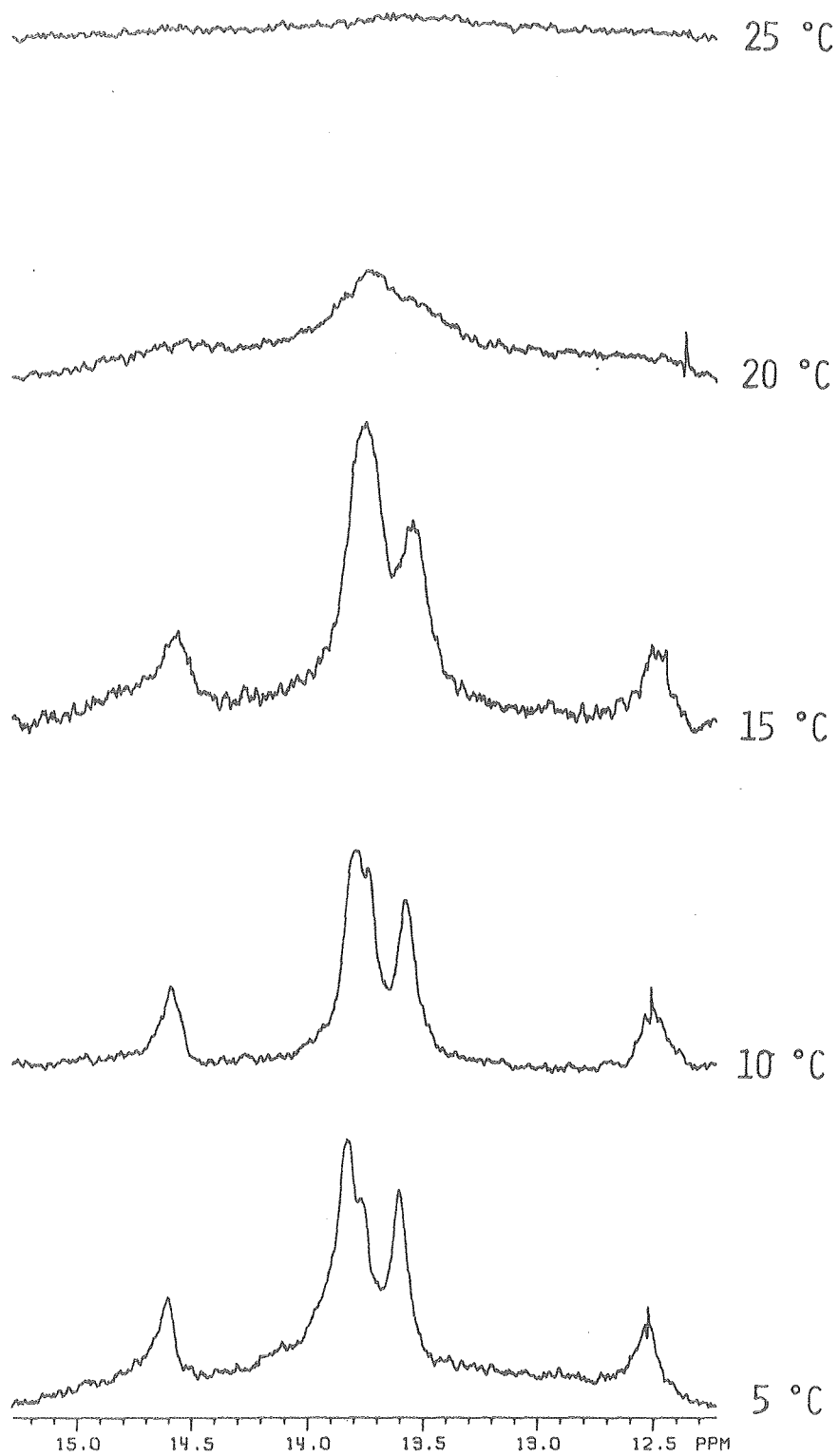
XBL 8011-7489

F)   Sugar Pucker of the Furanose Ring in the Double Strand

In two of the oligomer systems, the sugar pucker for some of the ribose or deoxyribose rings were calculated. The conformation of the ribose or deoxyribose ring has been described by Altona and Sundaralingam (1973) as a two-state equilibrium between type N[C2' exo, C3' endo] and type S[C2' endo, C3' exo]. Figure 2.19 shows an illustration of the different sugar conformations for 2' endo and 3' endo sugar puckers. The ribose ring conformation can then be calculated from the fact that in N type conformation J1'2' = ~ 0 Hz and the S type has J1'2' = ~ 10 Hz. For the deoxyribose ring the N type conformation has the property of J1'2' + J1'2" = ~ 7 Hz while the S type has a value of ~ 16 Hz for this sum.[47]

The assignment of the H1' protons to particular sugars in the oligomers was not possible, and coupling constants were obtained only for those resonances which were well separated from the main group of H1' protons.

Figure 2.20 shows the H1' deoxyribose proton region of dCT$_5$G + dCA$_5$G in the double strand at 5°C. Although the spectrum is fairly noisy, the two H1' peaks at 5.67 and 5.48 ppm had high enough signal to noise, and were well enough resolved, to do simulation. The simulation was done using a Nicolet 1180 computer in the NTCSIM routine. The lower part of the figure shows a blow-up of the simulated and experimental spectra. The best fit is obtained when

81

Figure 2.19. Illustration of the conformation of
the sugar ring in 2' <u>endo</u> and 3' <u>endo</u> sugar
pucker.
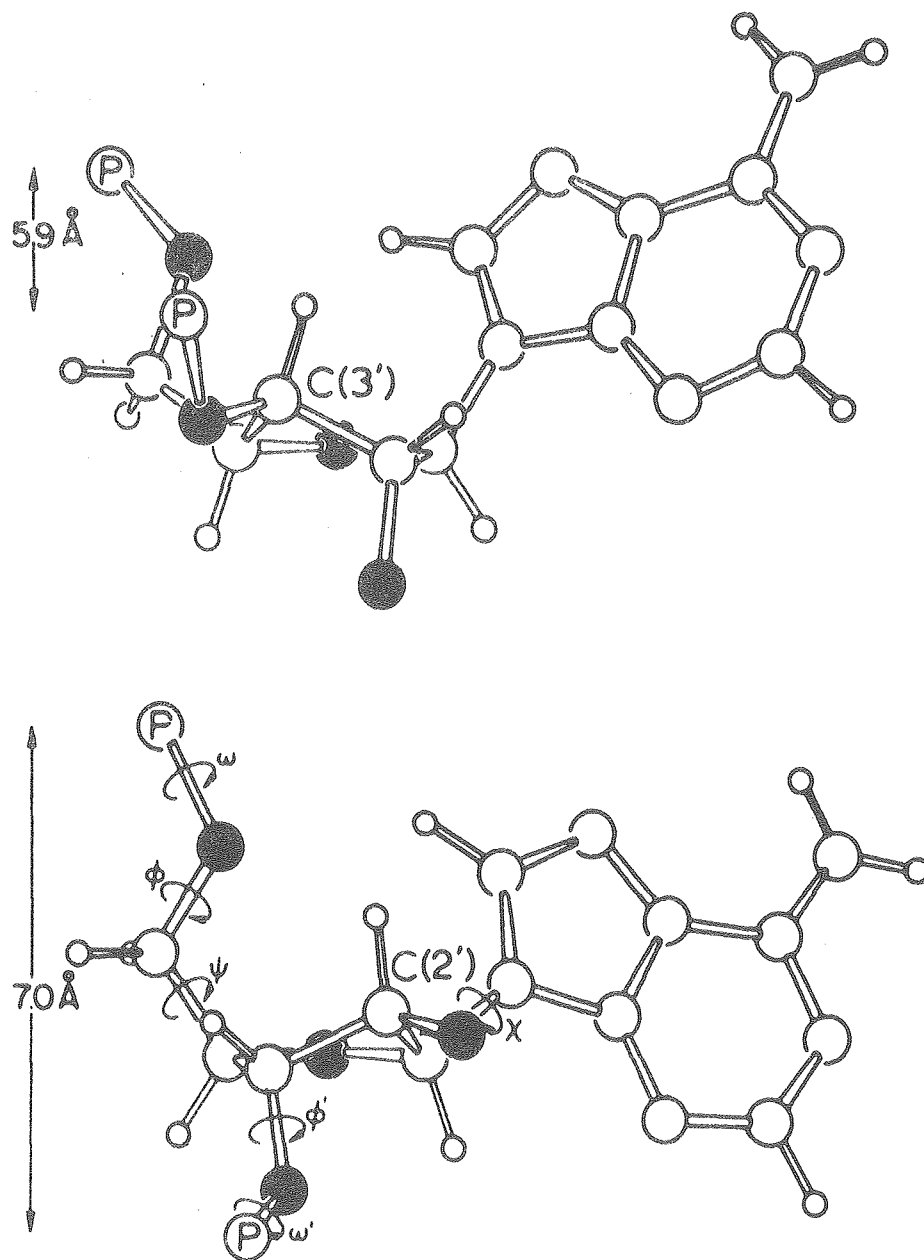
FIGURE 2.   The two preferred or rigid nucleotide units. $C^{3'}$-*endo* (top), $C^{2'}$-*endo* (bottom). The torsion angle Ψ' is *gauche* in C(3')-*endo* and *trans* in C(2')-*endo*. (From Sundaralingam, M., *Structure and Conformation of Nucleic Acid and Protein-Nucleic Acid Interactions*, (Part 5), University Park Press, Baltimore, 1975, 487. With permission.)

XBL 8011-7466

Figure 2.20. Deoxyribose H1' protons in dCA_5G +
dCT_5G double helix at 5°C.

DEOXYRIBOSE H1' PROTONS IN dCT$_5$G + dCA$_5$G AT 5°C
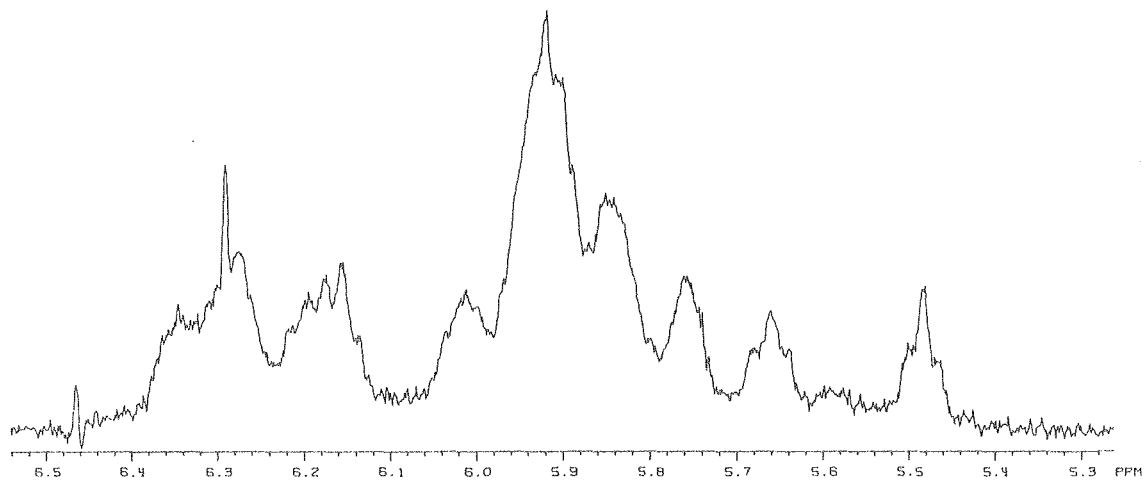
$J_{1'2'} + J_{1'2''} = 15$ Hz $J_{1'2'} + J_{1'2''} = 15$ Hz

SIMULATION
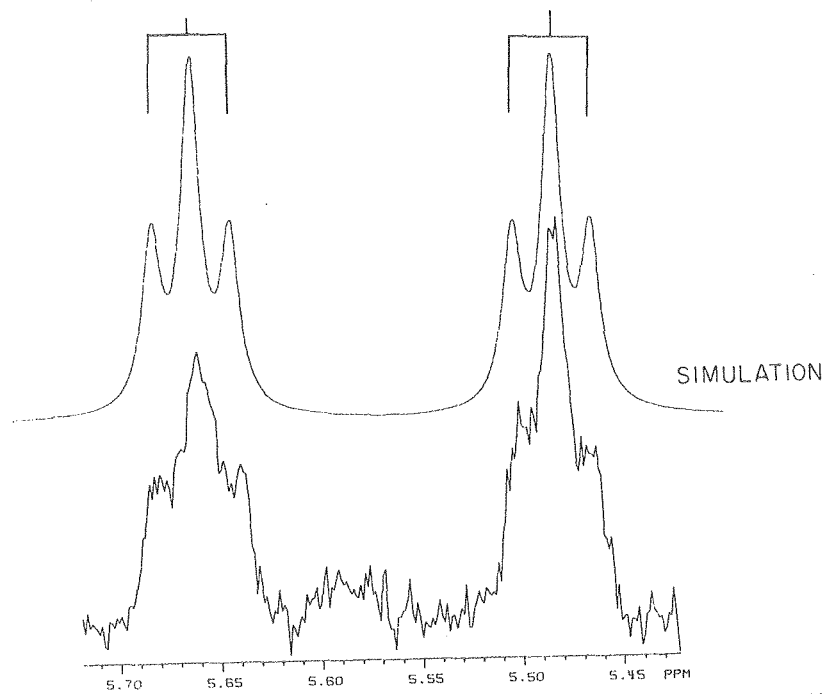
XBL 805-9522

J1'2' + J1'2" = 15 ± 1 Hz. The sugar conformation is then calculated to be 90 ± 10% S type (2' endo). Although we were not able to uniquely assign these two H1' protons, the temperature dependence of these peaks, as well as comparison with the single strands at 65°C shows that both protons are from the dCA₅G strand. The chemical shifts of the H1' protons in the components of dCA₅G indicate that these two protons are from adenine residues. The fact that these deoxyribose sugars are in approximately 90% S type (2' endo) conformation is consistent with a B form type geometry for this helix.

Figure 2.21 shows the H1' ribose region of the double strand dCT₅G + rCA₅G at 5°C. This region contains only the H1' protons from the ribose CA₅G strand, as well as a peak at 5.92 ppm probably from a H1' deoxyribose proton. Simulation of this region shows that the J1'2' coupling constant is less than 1.5 Hz for all the H1' protons. This means that in the helical state there is > 85% N type (3' endo) sugar pucker in all the ribose rings in the rCA₅G strand. This 3' endo sugar pucker is indicative of an A type geometry for this helix.

G)   Linewidths of the Base Protons and Chemical Exchange

For the dCA₅G + dCT₅G system we see extensive broadening of some of the base protons during the melting transition. The fact that some of the resonances broaden while others stay very sharp is clearly seen in Figure 2.4. The reason for

Figure 2.21.   Ribose H1' protons in dCT_5G +
rCA$_5$G double helix at 5°C.

RIBOSE HI' PROTONS IN dCT₅G + rCA₅G AT 5°C

All ribose sugars are in 3'endo conformation on the
rCA₅G strand in the double helix

The HI'2' coupling constant is less than

1.5 Hz for all the ribose rings

SIMULATION

5.95   5.90   5.85   5.80   5.75   5.70   PPM
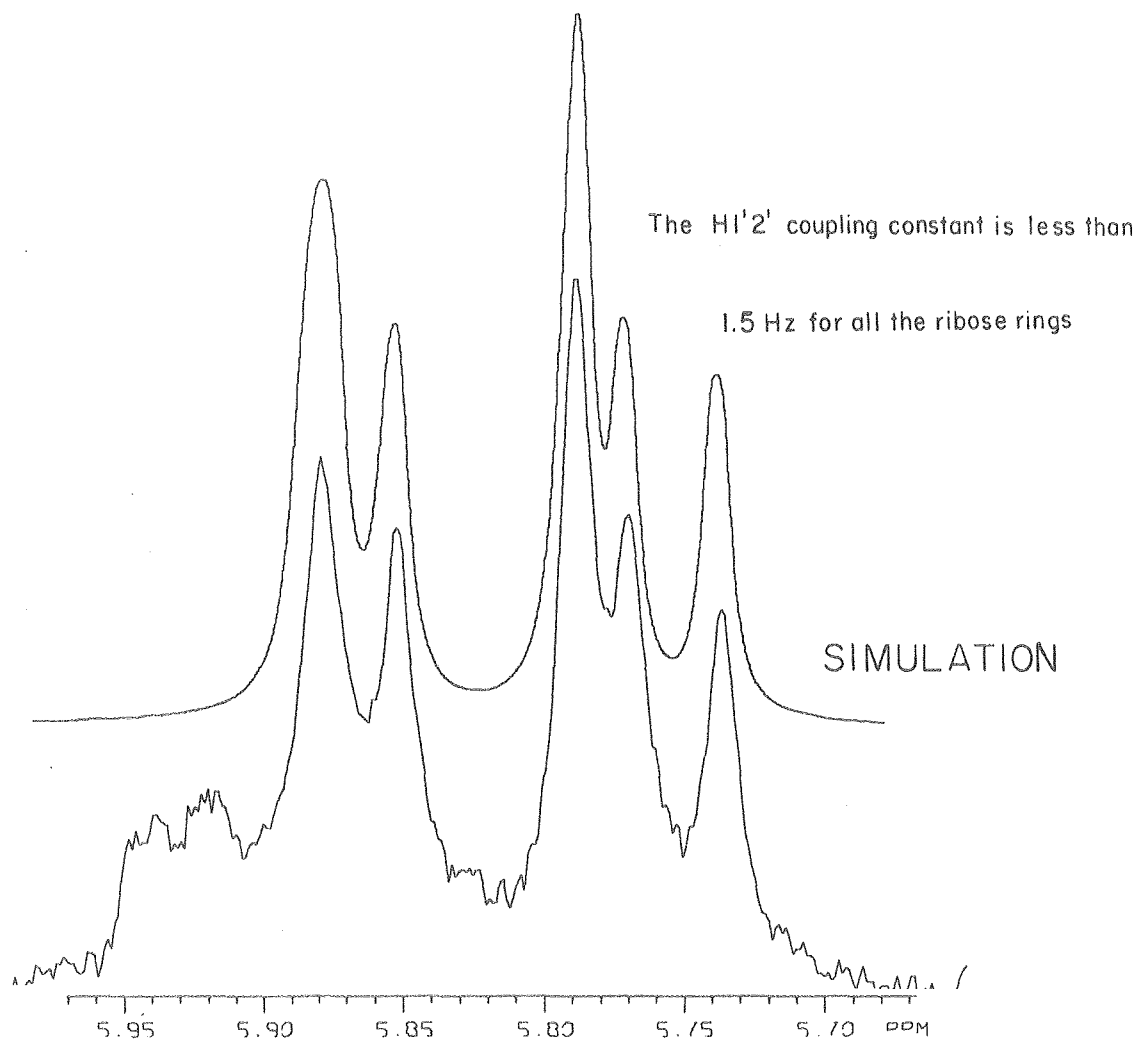
XBL 805-9520

this broadening is the fact that the system is undergoing chemical exchange between the double stranded helix (helix) and the single strands (coil). The rate of exchange, the population difference, as well as the difference in chemical shift between the two states are the factors which lead to broadening of the resonances.[45] Resonances such as the guanine (#1) H8 at 7.95 ppm, the thymines (#3-5) H6 at ~ 7.6 ppm, all shift little, and therefore are sharp throughout the transition. The three interior adenine H2 protons (at 7.09, 7.08 and 7.67 ppm at 5°C) have such large chemical shift differences for the two states that their resonances are almost broadened into the baseline at 25°C.

The (#2) adenine H8 proton (8.32 ppm at 5°C) is well separated from its neighbors and broadens to moderate extent, which makes it[26,27] possible to extract rate constants for the helix-to-coil transition. Equation (1) applies when the system is just short of the fast exchange limit,[46] and has been used to calculate rate constants for the helix-to-coil transitions in other oligonucleotides.[26,27]

$$\frac{1}{\pi T_{2_{obs}}} = \frac{P_C}{\pi T_{2_C}} + \frac{P_H}{\pi T_{2_H}} + 4\pi P_C^2 P_H^2 (\nu_H - \nu_C)^2 (\tau_H + \tau_C) \qquad (1)$$

$1/\pi T_{2_H}$ and $1/\pi T_{2_C}$ are the measured linewidth of the helix and coil states, respectively, while $1/\pi T_{2_{obs}}$ is the observed linewidth in the broadened spectrum. The linewidth of the helix state for a particular proton is assumed to be

independent of temperature and is thus the measured line-width of the helix at 5°C. The linewidth of the coil was taken from the measured linewidths during the melting of the single strand. ν_H and ν_C are chemical shifts of the protons in the helix and coil given in Hz, again ν_H is assumed to be the chemical shift of the helix at 5°C, while ν_C is measured from the melting of the single strand. P_H and P_C are the populations at a given temperature for the double and single strands, respectively. The populations were obtained from analysis of the absorbance versus temperature melting curve. τ_H and τ_C are the lifetimes of the helix and coil states; by the definitions, $P_H\tau_C = P_C\tau_H$.

We chose to calculate lifetimes of the helix and coil from the broadening of the #2 adenine H8 proton at 25°C, because at this temperature we can be fairly sure that equation (1) is applicable. Figure 2.22 shows that at 35°C the line-width of this resonance is only 3.5 Hz, whereas for 25°C the linewidth is 16 Hz. At 35°C there are approximately equal populations of the helix and coil, so the system must be in fast exchange in order to get this linewidth. By 25°C the exchange lifetimes have changed to such an extent that one sees broadening of the peak and equation (1) can be used to model this broadening. At 25°C, from the data given in Table VIII, we calculate the lifetimes of the helix and coil to be 14 msec and 2 msec respectively. Similar studies

Figure 2.22. Linewidth _versus_ temperature for
#2 H8 adenine proton in dCA_5G for double and
single strands.

XBL 8011-7475
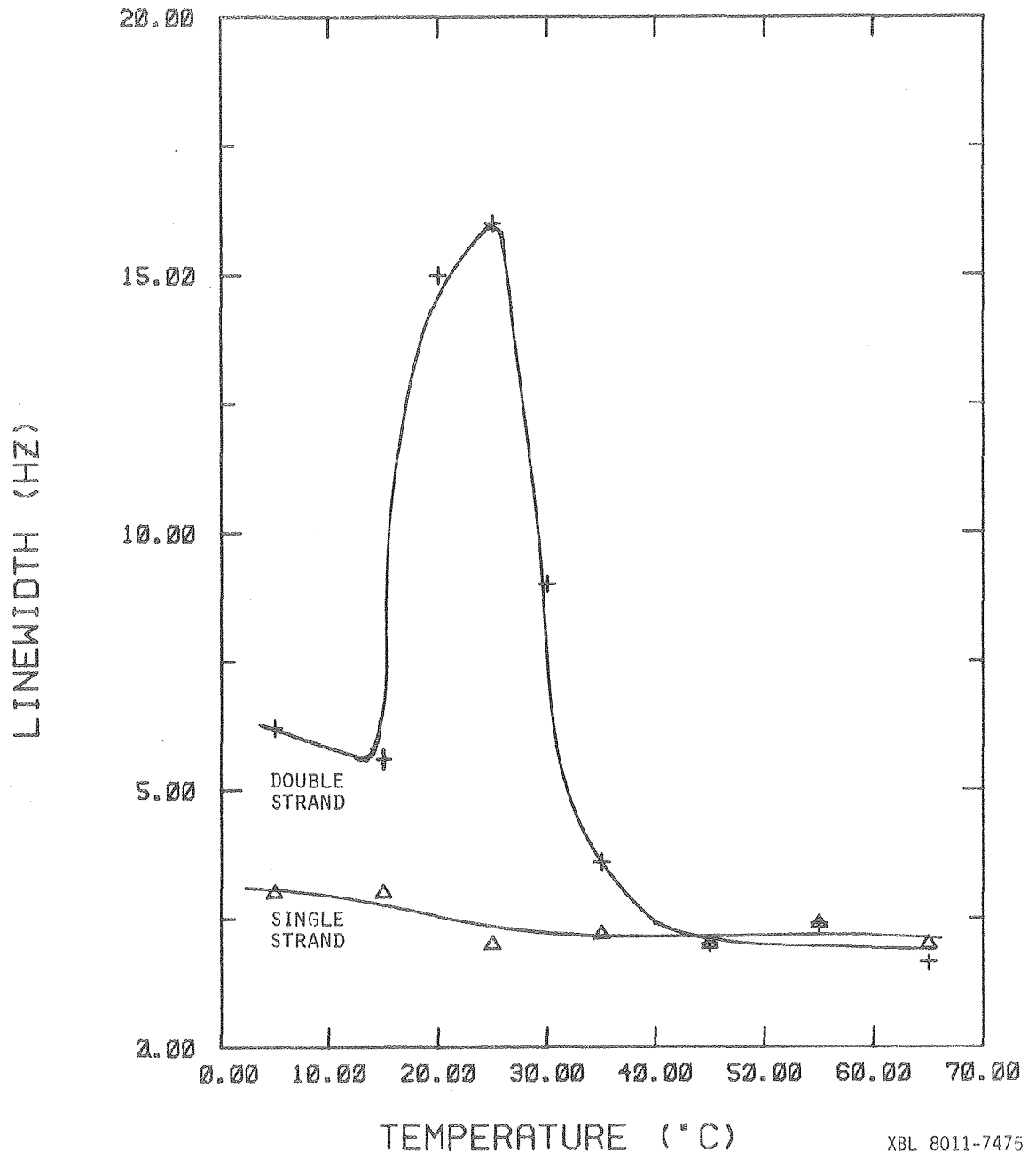
TABLE VIII

LINEWIDTH DATA FOR #2 ADENINE H8 PROTON

IN $dCA_5G + dCT_5G$ DOUBLE HELIX

360 MHz at 25°C

$1/\pi T_{2obs} = 15$ Hz $\qquad 1/\pi T_{2c} = 2$ Hz $\qquad 1/\pi T_{2H} = 6$ Hz

$p_H = 0.88 \qquad p_c = 0.12 \qquad \nu_H - \nu_c = 72$ Hz

Using equation (1) and $p_H \tau_c = p_c \tau_H$ we calculate

$\tau_H = 14$ msec $\qquad$ and $\qquad \tau_c = 2$ msec

270 MHz at 24°C

$1/\pi T_{2obs} = 15$ Hz $\qquad 1/\pi T_{2c} = 2$ Hz $\qquad 1/\pi T_{2h} \approx 6$ Hz

$p_H \cong 0.88 \qquad p_c \cong 0.12 \qquad \nu_H - \nu_c = 55$ Hz

we then calculate

$\tau_H = 19$ msec $\qquad$ and $\qquad \tau_c = 2.5$ msec

were done on the 270 MHz instrument at 24°C with the data

given in Table VIII. The lifetimes are probably not very

meaningful at temperatures other than 25°C because at

higher temperatures the broadening caused by exchange is not

much larger than the natural linewidth of the peak, so the

errors involved in calculating the lifetimes are very large.

At temperatures lower than 25°C the assumption of close to

fast exchange and the use of equation (1) may not be valid.

The fact that the lifetimes calculated at 25°C from data ob-

tained at two different frequencies are in good agreement, is

indicative that at this temperature equation (1) is applicable

to our system. These lifetimes and their rate constants are

consistent with kinetic results obtained on other oligo-

nucleotides by temperature jump methods.[48,49]

H) Base Pair Overlap in the Double Strand

The chemical shifts of the nonexchangeable protons for

the helix dCA_5G + dCT_5G have been compared with the calcu-

lated chemical shifts assuming a B form DNA geometry. The

calculations for the double helix were done using the model

by Arter and Schmidt,[41] which incorporates next nearest

neighbor effects as well as the effects of the closest

base pairs. The data shown in Table VI gives the chemical

shifts for a B DNA geometry and the observed shifts for this

helix. The prediction of the chemical shifts of the base

protons in A RNA and A'RNA geometry using Arter and Schmidt's

numbers are also given in Table VI.[41] One can see that these predictions do not give a better fit to the experimental numbers than the B DNA form.

The observed chemical shifts of the base protons which we were able to assign for the helix $dCT_5G + rCA_5G$ at 5°C are shown in Table VI. These can then be compared with predicted chemical shifts from the three geometries also given in Table VI. None of the fits between the calculated and the experimental data are very good for the base protons, so the imino protons seem to be more useful in these comparisons.

4.   DISCUSSION

A)   Comparison of the Structure of Oligonucleotide Complexes
      In Solution

      I.   The double Stranded Structures

      Figures 2.7a-c show the low field spectra of the three double stranded systems at 5°C. There are seven imino protons in each spectrum, one for each base pair in the double helix. From examining the chemical shifts of the imino protons in the three double strand, one sees distinct differences in the peak positions of many protons. This is indicative of different conformations for each system. The best fits for calculated and experimental results are for the $dCT_5G + dCA_5G$ in a DNA B type geometry, while the $dCT_5G + rCA_5G$ and $rCU_5G + rCA_5G$ are in an RNA A or A' type geometry.

The fits of the DNA B form to the deoxyribose double
helix is excellent in the relative positions of the imino
protons, but are not as good in their predictions of the
exact positions, as seen in Table VII and Figure 2.23.
The predicted resonances are all about 0.3 ppm higher field
than the experimental results. Since the conformations of RNA
and DNA helices are different, it is likely that the intrinsic
positions of these isolated base pairs are also different.
As more proton NMR work is done on deoxyribo-oligonucleotides,
it may be possible to obtain empirical results for the chemical
shifts of the isolated A·T and C·G imino protons in deoxy-
ribose systems.

RNA structures are found to be more rigid and less
susceptible to conformational changes than their DNA
counterparts.[3] We would then expect that the RNA helix in
our study would be close to an RNA A form geometry. As
seen in Table VII and Figure 2.23, there are large
differences between the experimental results and the calcu-
lations of the chemical shifts for an RNA A or A' geometry.
These differences can be due to several factors such as
inaccurate values for the ring currents used in the calcu-
lations, incorrect geometries assumed in the calculations,
sequence dependent geometries, or other parameters besides
ring currents having significant effects on the chemical
shifts of the imino protons (see Borer et al., 1975, for
discussion of these effects).[15] Aggregation will also
directly effect the chemical shifts of the terminal base

Figure 2.23.   Comparison of experimental and

calculated chemical shifts of the imino

protons.

COMPARISON OF CALCULATED AND EXPERIMENTAL
CHEMICAL SHIFTS OF THE IMINO PROTONS

XBL 8011-7491
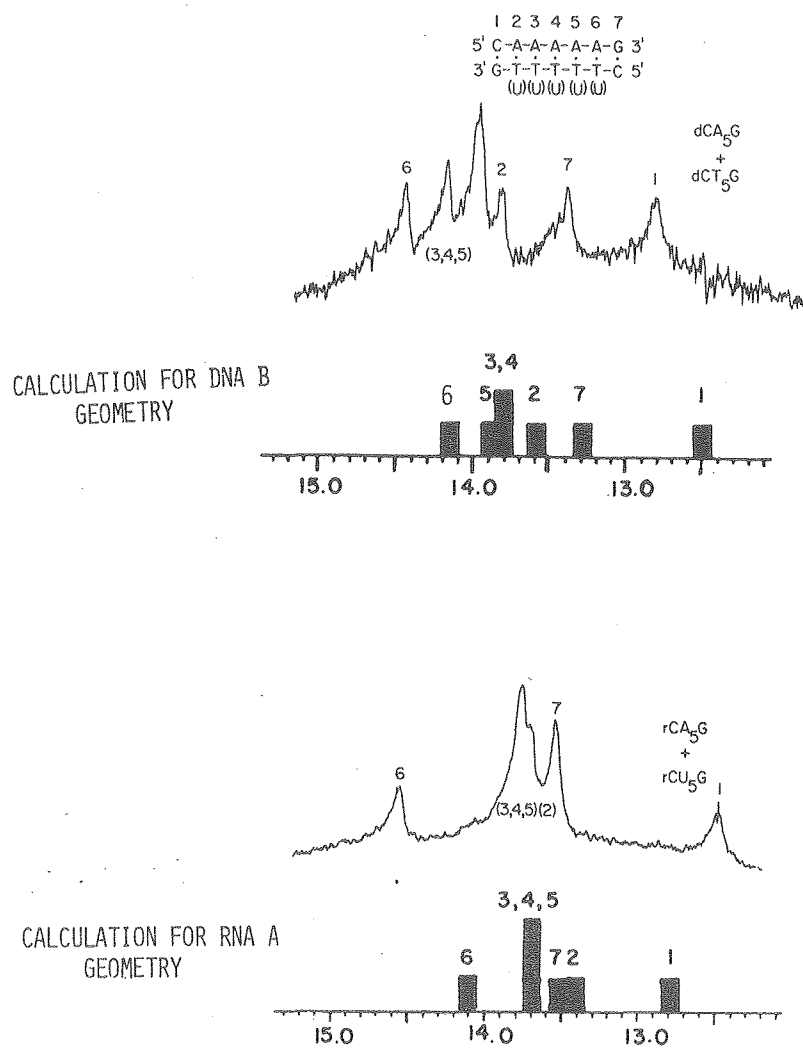
pair protons. Equilibrium sedimentation on similar oligo-
nucleotides have shown that there is significant aggregation
at these concentrations, so the chemical shift of the terminal
base pairs may be affected.[44]

The chemical shifts of the base protons are compared with
the calculated results for several of the oligonucleotide
double helices in Table VI. One sees large discrepancies
between the experimental and calculated chemical shifts
for the dCA_5G + dCT_5G system. We are investigating the
discrepancies to see if the differences are due to the
oligonucleotide being in a slightly different geometry
than the classical DNA B form. Calculations of the chemical
shifts for other energy minimized geometries are presently
being performed (D. Keller, unpublished) to see how slight
changes in helical parameters, such as winding angle,
twist, and tilt, effect the chemical shifts of the base
protons.

The coupling constants and chemical shifts of the ribose
and deoxyribose protons have been extensively used in the past
to obtain conformational information on oligonucleotides in
solution.[8,9] One of the most meaningful parameters in the
geometry of the nucleic acid is the conformation of the
sugar ring.[50] In the dCT_5G + dCA_5G double helix, two of the
deoxyribose sugar rings in the dCA_5G strand were found to be
90% in a 2' endo conformation. The 2' endo sugar puckers
are found in B form geometries which is consistent with this
helix being in a B type conformation.

The hybrid $dCT_5G + dCA_5G$ was also well enough resolved in the H1' proton region to obtain coupling constant data. The evidence of a 3' <u>endo</u> conformation of the ribose strand is indicative of an A type geometry. Knowing the sugar pucker of the helix greatly restricts the range of conformations for the sugar phosphate backbone, thereby ruling out many possible geometries for the helix. This fact is especially useful in conjunction with the ring current calculations, and may make it possible to define conformations more exactly than the qualitative "A" type or "B" type geometries.

II. Triple Strand

The system $rCU_5G + dCA_5G$ forms a triple strand under our conditions. The low field imino proton spectrum of this mixture is quite different than the other spectra shown in Figure 2.7. For example, there is a broad resonance at very low field around 15.0 ppm in Figure 2.7d, the normal Watson-Crick imino protons are not found to resonate higher than ~ 14.6 ppm. This resonance as well as those centered at 14.6 ppm are most likely due to reverse Hoogsteen base pairs involved in the triple strand.

Geerdes and Hilbers have studied [oligo A - (oligo U)$_2$] triplexes in solution by ^{1}H NMR.[23] From the imino protons in this system they concluded one assignment for the intrinsic position of the Watson Crick A·U pair in the triple strand would be ~ 14.3 ppm, whereas the Hoogsteen pair was found

at 14.8 ppm. Robillard and Reid have recently attempted
calculations which empirically optimize the magnitudes of
the chemical shifts of the isolated base pairs by a method
which assumes a strong similarity between the crystal and
solution structure of tRNA.[6] They found the optimized
intrinsic position of the reversed Hoogsteen A·U to be at
14.9 ppm. Kallenbach et al. have studied triple stranded
structures in which oligo U_{15} and rAMP formed two sets of
imino resonances, presumably one for the Watson-Crick and one
for the reverse Hoogsteen base pairs.[19] They concluded that
the A·U reverse Hoogsteen base pair's most probable
intrinsic chemical shift was 14.1, but were unable to rule
out an alternate assignment which would have switched the
position of the two types of base pairs, and given the
intrinsic shift of the reverse Hoogsteen as ∿ 14.8 ppm.

In our system we are unable to make unambiguous
assignments of the imino protons, but we think that the
broad resonance at ∿ 15.0 ppm is due to an A·U reverse
Hoogsteen base pair. It seems to resonate at too low field
to be from a normal Watson-Crick type A·U resonance, and the
above studies on triplexes indicate that the reverse Hoogsteen
base pair's intrinsic shifts may be in the region of 15.0
ppm. This would indicate that the other resonances at 14.2 –
14.5 ppm would also be mostly from reverse Hoogsteen base
pairs. The intrinsic shift of an rU·dA·rU reverse Hoogsteen
pair would then be ≥ 15.0 ppm.

The fact that there are so many types of resonances in the low field region of the dCA_5G + rCU_5G system, many more than the seven protons one sees in the double helical systems, indicates that the oligomers are fully or partially in the triple strand conformation.

B)   Analysis of Thermodynamic Parameters by Chemical Shift
       Versus Temperature Plots of the Base Protons

The validity of the T_m or enthalpy values from melting curves is often dependent upon the method of analysis. In order to get useful results from a melting curve, one must estimate the temperature dependence of the double and single stranded molecules.[15,17] One major advantage in using non-selfcomplementary oligonucleotides is that the properties of the single strand can be studied separately from the double to single strand transition. The temperature dependence of the chemical shifts of the base protons in single stranded molecules have been studied in many systems. In some cases the changes in chemical shifts of the base protons are linear with temperature,[16] but for many other protons there are large deviations from linearity (see Figures 2.12 - 2.14 and Shum).[51] For non-selfcomplementary molecules, one can experimentally obtain the temperature dependence of the chemical shifts of the single strands, while for selfcomplementary molecules, one is forced to assume linearity for the chemical shifts. This assumption can lead

to large errors in the T_m.   For example in the system

$dCA_5G + dCT_5G$ the analysis of the curves with and without

the experimental temperature dependence of the single

strand gives T_m values which differ by up to 5°C for some

of the protons.   This problem seems to be much more im-

portant in NMR melts than optical studies, and should be

taken into account when interpreting thermodynamic parameters

derived from NMR melting curves.

 There is a similar problem involved in the estimation

of the lower baseline of the melting curve.   The temperature

dependence of the chemical shifts of the double strand may

not be linear with temperature, and this can also lead to

errors in the T_m.

 Difficulties involved in obtaining equilibrium constants

from chemical shift data have recently been discussed.[52]

One usually assumes that the system is always in fast exchange,

on the NMR timescale, and that the measured chemical shift

is a weight average of all the states.   The validity of this

analysis breaks down when the system is not in the fast

exchange domain, which happens during the melting of most

oligonucleotides.   The errors made in assuming fast exchange

can be large in many cases.

 We have constructed a model system which calculates the

lineshape of the resonances for any exchange rates linking

two states.   The expression used is essentially that derived

by Gutowsky and Holm,[45] except that their assumption of the linewidth of the two states being equal was not made. The expression for the intensity of absorption for a two state system with exchange is given by

$$v(f) = \frac{- K[J(1 + \tau(p_A\omega_B + p_B\omega_A)) + QR]}{J^2 + R^2} \qquad (2)$$

where

$$\tau = \tau_a\tau_b/(\tau_a + \tau_b) \qquad \omega_n = \pi(\text{linewidth of state n})$$

and

$$J = \tau[\omega_A\omega_B - (\pi(f_A + f_B) - f)^2 + \pi^2(f_A - f_B)^2] + p_A\omega_A + p_B\omega_B$$

$$Q = \tau[\pi(f_A + f_B) - f - \pi(p_Ap_B)(f_A - f_B)]$$

$$R = \pi(f_A - f_B)(p_A - p_B) + \tau\pi(f_A - f_B)(\omega_B - \omega_A)$$
$$+ [\pi(f_A + f_B) - f][1 + \tau(\omega_A + \omega_B)]$$

where τ_n, f_n, and p_n are the lifetime, the frequency (in Hz), and population, respectively, of state n.

The program which calculates the lineshape of a two state system with exchange is called WIDTH2 and given in Appendix II. The program uses equation (2) plotted with a program called PLOT written, and kindly provided by Mr. David Keller. WIDTH2 also finds the chemical shift and linewidth of the largest peak in the system. These can then be compared with the experimental results, and the parameters such as exchange rates varied until a good fit is found between the experimental and calculated results.

The program WIDTH2 was modified to a program called ITWIDT which changes the mean exchange lifetime τ (where $\tau = \tau_a\tau_b/(\tau_a+\tau_b)$) until the best fit is found between the calculated and experimental chemical shift of the largest peak. For a given population of the two states it iterates until the closest fit is found between the experimental and calculated results.

These programs were used to model an NMR melting curve to see how large the errors can be in extracting thermodynamic data by always assuming fast exchange. If the system were in fast exchange throughout the whole helix-to-coil transition, then the chemical shift observed is a weight average of the two states. The observed chemical shift would then be a direct measure of the populations of the two states (assuming one knows the chemical shift of the helix and the coil). For this analysis we will refer to the measured chemical shifts as those which are found if the system were from equation 2. If the fast exchange chemical shift and measured chemical shift are different, then for that population and exchange rates the normal analysis of the melting curve is not valid.

Figure 2.24 shows the melting curves for a model system which mimics the behavior of an interior adenine H2 proton in $dCA_5G + dCT_5G$. What was found was that the fast exchange chemical shifts agree well with the measured chemical shifts

Figure 2.24. Comparison of melting curves when system is in fast exchange and when it is no longer in the fast exchange region (measured curve).
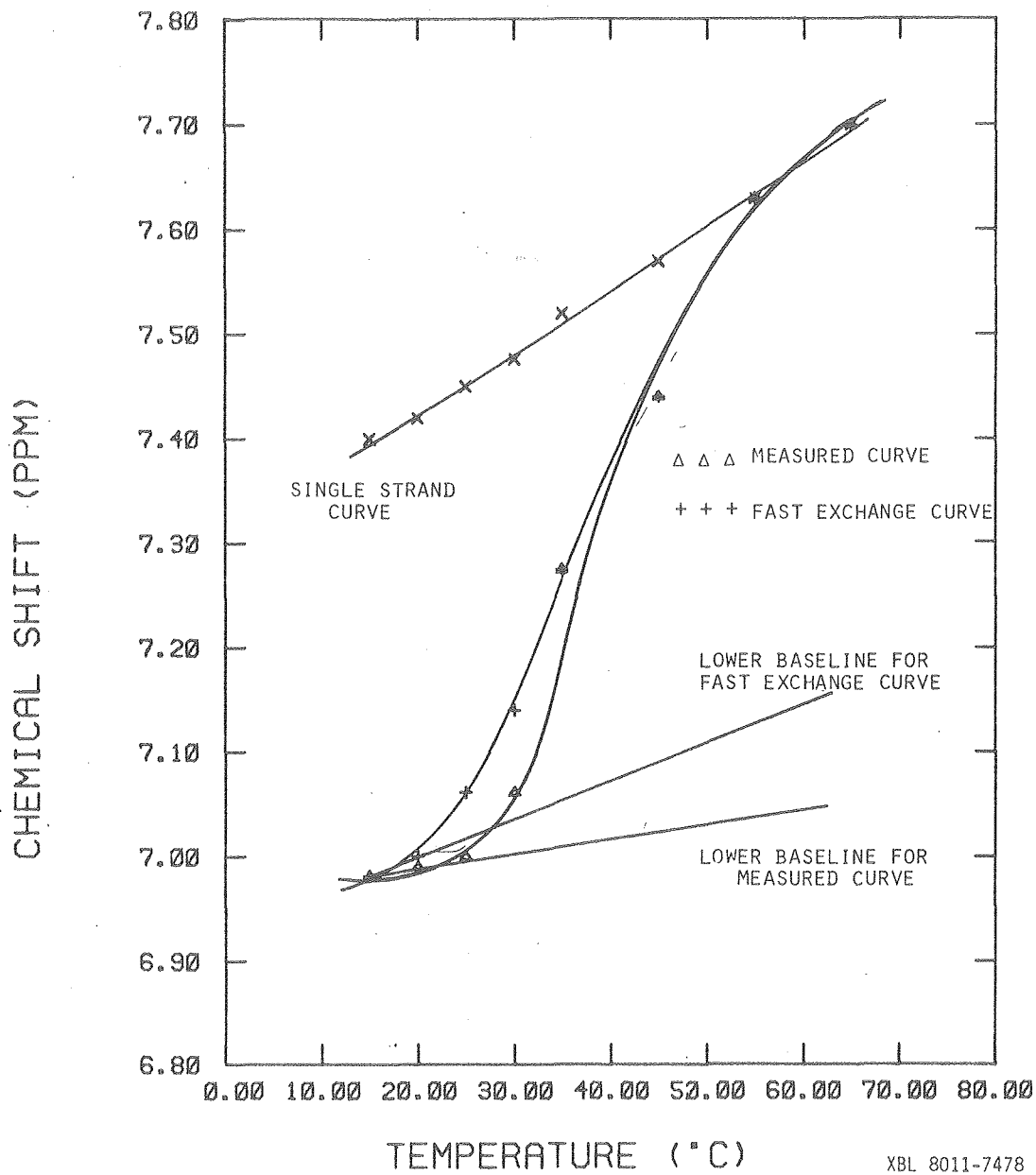
above the T_m of the system. This is because the system
actually is in fast exchange over this temperature range
for all the protons. Below the T_m, many of the protons are
no longer in fast exchange, so we see lines which are
broadened due to exchange. The chemical shift is no longer
the weight average, but skewed toward the chemical shift of
the state with the largest population. This will have the
effect of raising the T_m above its real value. In most of
the model systems studied this effect was fairly small,
with the largest change being 2 - 4°C in the T_m. The
error is in the wrong direction to explain the 5°C discrepency
between the optical and the NMR T_m of the $dCA_5G + dCT_5G$
system, and this effect does not seem to be important in
our case.

Another error produced in assuming fast exchange which
is probably much larger in our system involves the estimation
of the lower baseline in the melting curve. When the system
is 80-100% in the double strand, many of the protons are near
the slow exchange limit so there should be two peaks observed,
weighted according to the populations of the two states. It
will often be difficult, if not impossible, to see the peak
which corresponds to a state with less than 20% population,
due to the large number of resonances and the fact that many
of them may still be exchange broadened. Thus the chemical
shift that we measure will only be the chemical shift of the
state with population of > 80%, and not a weight average

chemical shift. This error will affect the shape of the
lower baseline drawn in the analysis of the melting curve.
The measured curve will overestimate the population of the
double helix and thus make the lower baseline slope less
than it actually is. As seen in Figure 24, this has the
effect of lowering the T_m of the measured curve below
the real T_m.

In the system $dCA_5G + dCT_5G$, the T_m found optically had
a value 5°C higher than the T_m obtained by NMR, which showed
all the resonances melting at 28-30°C. The reason for this
difference is the invalid assumption of fast exchange
throughout the transition, which causes an incorrect exti-
mation of the lower baseline of the NMR melting curve. In
these molecules we took all the lower baselines to be flat,
so that the error is probably systematic and will be similar
for all the protons. Modeling this system gives the same
conclusion, that the errors due to assuming fast exchange are
approximately the same for all the protons. Therefore we
think that for $dCT_5G + dCA_5G$ the terminal and interior base
pairs melt at the same temperature, within 2 - 3°C, and
that an all-or-none transition is a good approximation for
this system.

C)   Fraying Versus Melting of Oligonucleotides

It is important to understand the distinction between fraying of the ends and the differential melting of the ends of an oligonucleotide. Here we refer to the melting of a base pair in the oligomer with respect to the fraction of the base pair which is formed, or involved in hydrogen bonding. An 80% melted base pair would have an equilibrium concentration of oligonucleotides with 80% of the base pair broken and 20% of the base pair formed. Melting thus reflects an equilibrium effect and is dependent only upon the concentration of the two states.

Fraying is defined as the rapid opening and closing of a base pair.[53-55] It is thus a kinetic effect and the important parameters involved are the rate constants linking the open and closed states. Fraying can manifest itself in the H-bonding imino protons where the exchange rate of the proton is reflected by the linewidth of the resonance (see Crothers et al.,[56] and Hilberts,[53] for discussion of exchange of imino protons with H_2O). In our oligomer systems the C-G base-paired imino protons broaden and disappear before the interior base pairs, which is indicative of fraying of the ends of the helix. This does not mean the end base pairs are melted at the temperature where the resonance has disappeared. For example, in the helix $dCT_5G + dCA_5G$ at 25°C, the imino proton region is extremely broad, and by 30°C the resonances have disappeared into the

baseline (see Figure 2.9). This is not representative of the equilibrium concentrations of these states, the oligomer is fraying at this point but it is not melted. In fact, the chemical shift versus temperature data of protons on all bases and optical studies of this oligomer show that it is > 50% in the double strand at 30°C, where all the imino protons have disappeared. The temperature dependence of the broadening of the imino protons ismainly a kinetic, not an equilibrium, effect. Thus an end base pair can be fraying and not "melted" at the same time. In our system, although we see fraying of the ends of the helix, i.e., the end bases are opening and closing faster than the interior base pairs, the ends do not melt appreciably lower than the rest of the helix. It is worth noting that fraying and melting reflect not only different processes, but there may also be different states involved in the two processes. For example, in order for an imino proton to exchange with water, the base pair must open to some extent. This opened state most likely differs from the "melted" state in a molecule with differential melting on the ends of the helix. Care should be taken in dis-tinguishing between fraying and melting, as well as the effects ascribed to them.

5.   CONCLUSION

We have studied the following oligonucleotides separately, and in their complementary mixtures by proton NMR: dCA_5G, dCT_5G, rCA_5G and rCU_5G. Results on the single strands show that the ribose and deoxyribose strands of CA_5G have different conformations in solution, and specifically that there is more base-base stacking in the deoxyribose strand.

Results on the mixtures indicate that rCU_5G + dCA_5G at least partially forms a triple strand with a 2:1 rCU_5G:dCA_5G helix, while rCU_5G + rCA_5G, rCA_5G + dCT_5G, and dCT_5G + dCA_5G form double helical structures. Comparison of the three double strands shows that they all have different structures in solution. The chemical shifts of the imino protons and the calculations of sugar ring pucker in these systems indicate that the deoxyribose helix (dCA_5G + dCT_5G) is in a B type geometry, whereas the ribose (rCA_5G + rCU_5G) and hybrid (rCA_5G + dCT_5G) helices are in an A or A' type geometry.

The melting of the helix dCA_5G + dCT_5G as followed by the chemical shift changes of the nonexchangeable base protons shows that base pairs on the ends of the helix melt at approximately the same temperature as the interior base pairs. The temperature dependence of the imino protons indicates there is fraying of the ends of the helix. Thus this helix exhibits fraying of the ends, but very low concentrations of partially formed helices at the same time. These results

indicate that a two-state model is a good approximation of the helix-to-coil transition in this oligonucleotide, as often assumed in optical studies. Some of the biological implications due to the differences in stability of these oligonucleotides have been discussed elsewhere.[24] The differing conformations for these DNA, RNA, and hybrid helices are probably also important in enzymatic recognition of different types of helices.

Studies on the kinetics of these oligonucleotide helices, as well as the changes in the conformation and stability of double helical oligonucleotides when there is a mismatched base on one strand, or when frameshift mutagens are bound, are presently being pursued.

CHAPTER III

1. INTRODUCTION

It is important to study the exchange of the H-bonding protons in nucleic acids if one is to understand their stability, structure, and flexibility in solution. In order for a proton to exchange, the H-bond must be broken which will require at least some change in the conformation of the helix. The breathing of a helix and the structural stability of a particular region may be important in enzyme-nucleic acid interactions, and also mutational events.[39] Disruption of the base pairs will be important in transcription and replication of DNA.

Exchange in polynucleotides has been studied by tritium exchange experiments,[57-59] and also by H-D exchange as monitored by a kinetic difference spectrum in the UV. These results have been recently reviewed by Kallenbach et al.,[60] and demonstrate the importance of the dynamics and fluctuations of DNA and RNA.

Proton NMR has also been used to study exchange of H-bonded protons in tRNA and oligonucleotides. (See Hilbers[53] for a review of exchange in nucleic acids as studied by NMR.) Crothers et al.[56] studied the thermal unfolding of tRNA^{fMet} by the broadening of the low field imino protons in the molecule. The broadening of these resonances is due to exchange with water, and the equations used to relate the width and chemical shift of the resonance to exchange rates are given there.

Studies of exchange in oligonucleotides have been done by Patel and Hilbers on dATGCAT,[54,55] and by Kallenbach et al.[19] on dAAAGCTTT, by monitoring the behavior of the imino protons. They concluded that the internal G imino proton exchanged in an open limited case, which means the rate of exchange is limited by the opening of the base pair and not by exchange with H_2O. For the other A·T base paired imino protons, exchange took place from partially formed double helical states. This indicates fraying of the ends of the helix, which means the ends of the helix were rapidly opening and closing.

These earlier studies of exchange by NMR involved interpreting the linewidth and chemical shift of the imino protons. Redfield developed the method of transfer of saturation to study exchange rates of H-bonded protons with H_2O.[61-63] This method involves perturbing part of the system, and then monitoring the system as it exchanges with an unperturbed part of the system. Johnston and Redfield studied exchange rates in tRNA by this method.[62,63]

In this chapter we will investigate the exchange of the imino protons on a deoxyribo-oligonucleotide $dCA_5G + dCT_5G$, and also a hybrid helix $dCT_5G + rCA_5G$. The fraying on the ends of the helix as well as the exchange of protons on the interior of the helix will be discussed.

2. Experimental Methods

The samples used in these studies were the same ones used to study the imino protons in the oligonucleotides. The experiments were done on the 360 MHz instrument at Stanford Magnetic Resonance Laboratory, and the 270 MHz instrument at the Laboratory of Chemical Biodynamics. The Redfield 214 pulse sequence setup and the saturation recovery experiment are routinely done on the Stanford facility, and are well documented there. For the 270 MHz instrument slight modifications of the existing setup had to be made in order to do the Redfield pulse sequence and the saturation recovery experiments. Since this procedure is not documented elsewhere,[64] the modifications made on the system will be discussed later.

A description of the theory of the Redfield 214 pulse sequence is given elsewhere.[65] The idea of the pulse sequence stems from the fact that the frequency width of a radio frequency (Rf) pulse is inversely proportional to the length of the pulse. A typical 90° pulse is usually on the order of 2 - 30 μsec, and covers a much wider frequency range than the normal absorption frequencies of protons in solution. If one wants to reduce the frequency width of the Rf pulse, then the time of the pulse is simply increased. One method of water suppression similar to the Redfield sequence is a long low power pulse. The Rf pulse

Figure 3.1.   Comparison of the shapes of an Rf

pulse for:

a) a 90° pulse.

b) a long low power pulse.

c) a Redfield 214 pulse.

PULSE SEQUENCE COMPARISON

a)

90° Pulse

τ

H_2O
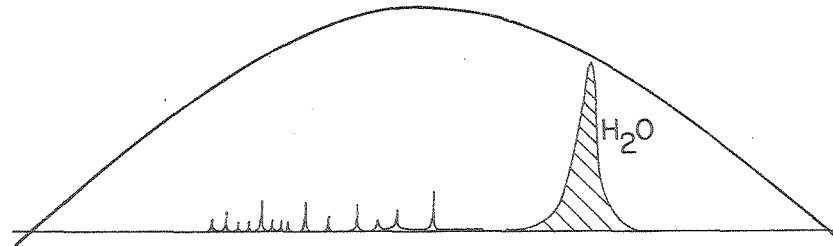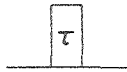
b)

Long Pulse (low power)

10τ

H_2O
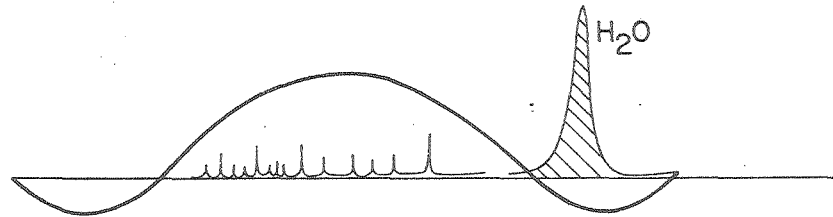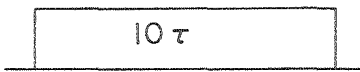
c)

Redfield 214 Pulse (low power)

2τ 4τ 2τ

τ τ

H_2O

XBL 801-7672
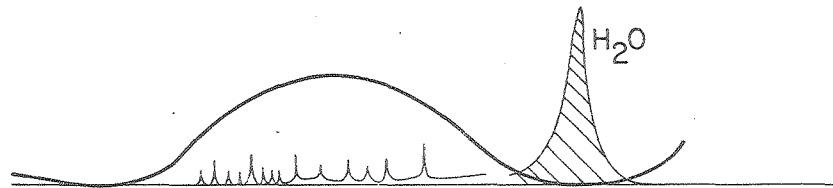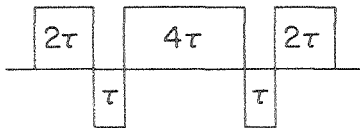
is centered at the frequency of the signals of interest, (they must be > 1 ppm away from the water signal), and the length of the pulse is adjusted so that the null in the Rf pulse is on top of the water signal. This reduces the intensity of the H_2O signal relative to the rest of the spectrum. The shape and the frequency width of a short 90° pulse and a long pulse are schematically shown in Figures 3.1a and 3.1b. Redfield improved the suppression of the water signal by broadening the null in the Rf pulse with use of two 180° phase shifts during the pulse. The shape of the Redfield 214 pulse is compared schematically with the long pulse in Figure 3.1.

The Redfield sequence allows the H_2O signal to be reduced approximately 100 fold in most cases, thus cutting down the huge dynamic range problem encountered when doing ^{1}H NMR in H_2O. Audio filtering can also be used to further reduce the H_2O signal, and in most of our saturation recovery experiments the cutoff filter was set so as to filter the water signal, reducing its magnitude. The problem with this procedure is that it causes baseline distortions and phasing problems, over the area being filtered. Since the imino protons that we are interested in are 8-9 ppm downfield from water, there was little pertubation in the imino proton region, but it is impossible to correctly phase the whole spectrum. Another method of audio filtering which is far

superior to the cutoff filter in these experiments, is the use of a tunable notch filter to suppress the H_2O signal.[67] The notch filter reduced the water signal to a much larger extent, and also induced far less baseline distortion than the cutoff filter. Most of the saturation recovery experiments described here were done using the cutoff filter since the notch filter was not yet available. Comparison of the size of the water signal in the Redfield sequence with and without the notch filter is shown in Figure 3.2.

For the 270 MHz NMR spectrometer, instrumental details for normal Fourier transform operation are given elsewhere,[64] and only modifications needed for these experiments will be discussed. The Redfield 214 pulse sequence requires a long low power pulse, as well as the ability to make two 180° phase shifts during the pulse. In our experiments a low power linear amplifier was used for the Redfield 214 pulse in place of the normal high power proton amplifier. The same amplifier was also used in the saturation recovery experiments on the decoupling channel to saturate the imino resonance. Figure 3.3 shows the experimental setup for the observe channel when using the Redfield pulse sequence. Figure 3.4 shows the setup for the decoupling channel when running the saturation recovery experiments.

When using the Redfield sequence, all the protons over a frequency range are not equally excited. This can present problems in comparison of the relative intensities of peaks

Figure 3.2. Comparison of Redfield sequence
    spectra without notch filter (top) and with
    notch filter (bottom).

X 20

XBL 8011-7497
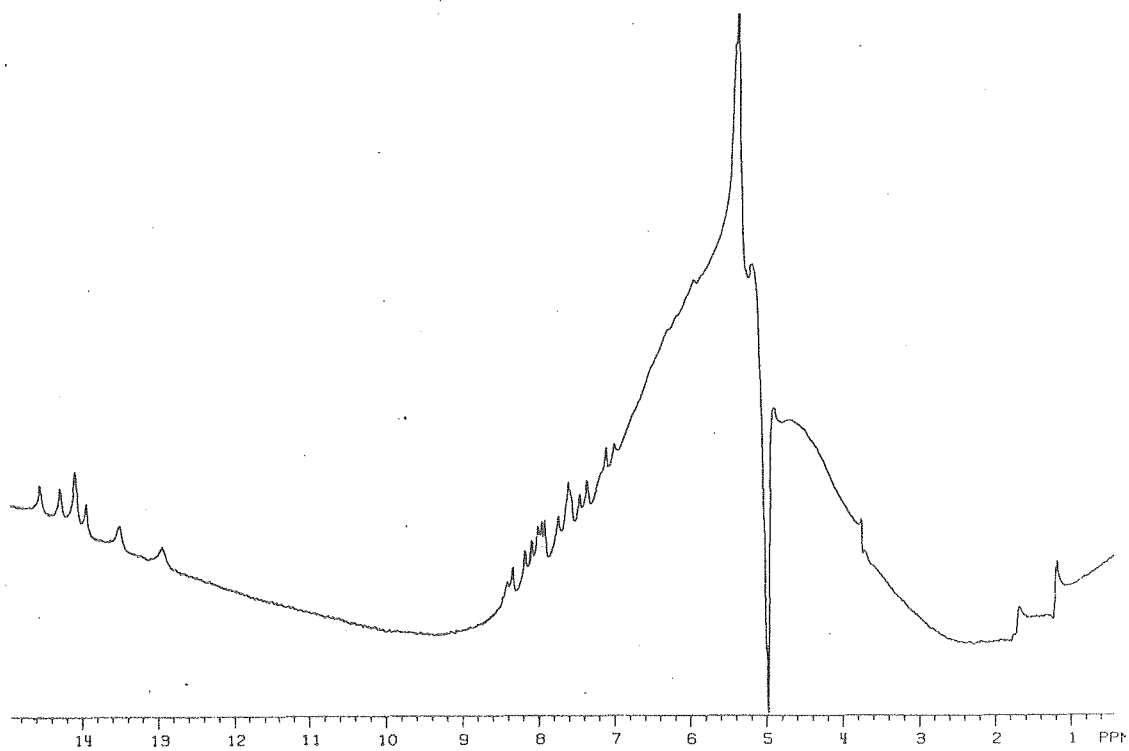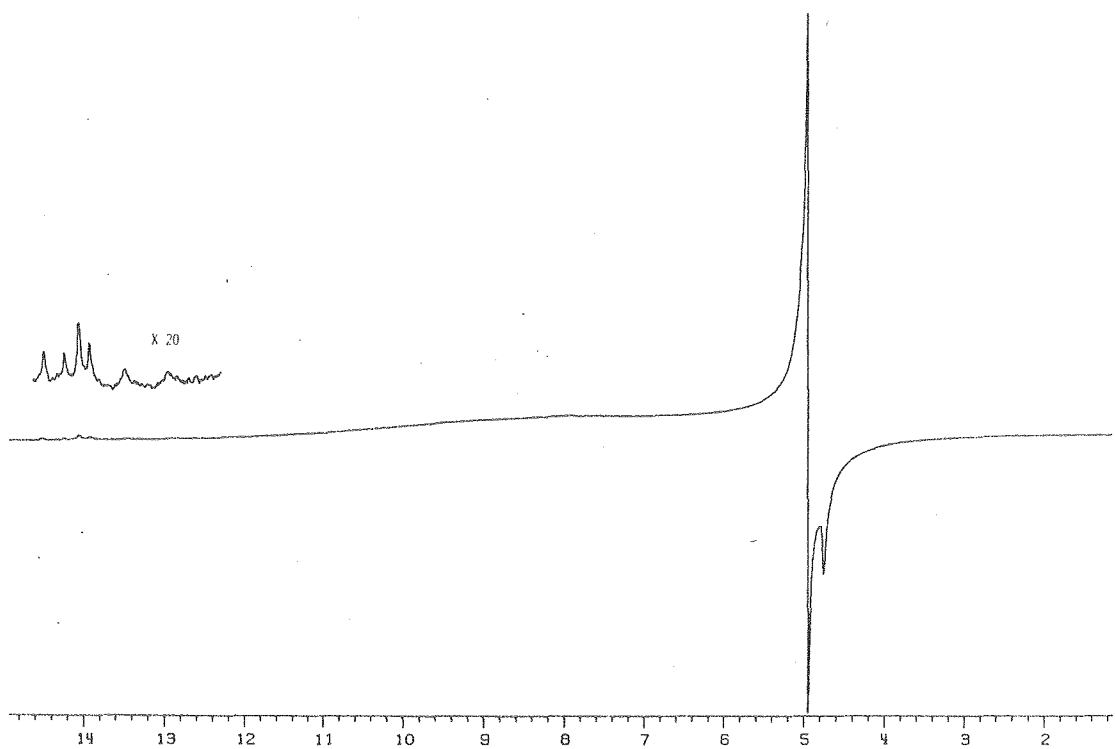
Figure 3.3. Block diagram of the observe channel

for the Redfield pulse sequence setup on

the 270 MHz NMR spectrometer.

Observe Channel SSB Generator

HP 5105A
Frequency
Synthesizer

10X206

38-300MHz
input

8-270MHz
output

Gate

30MHz input

SP3
control
line from
1180

3V

flag
box
input
+15v

-15v
output

300Ω
2W 5%

R
HP
X 10514A

L

Observe channel for the

Redfield pulse setup

on the 270.

30MHz output
10X207
Four Phase
Generator

0°
90°
180°
270°

control
line
(to 16X892)

Rf
input

Linear
Power Amp.
Boonton
or
E.N.I.

Rf output

10X1N4447

5

Brrd 4314
Thruline
Wattmeter

-40dB
monitor

to probe
(T/R switch)

Figure 3.4. Block diagram for the decoupling
channel in the saturation recovery ex-
periment on the 270 MHz spectrometer.

Decouple Channel SSB Generator

Alternate Frequency Source HP5105A

10X206
38-300MHz input
8-270MHz output
Gate
30MHz input

Null T

Rf Pulse from SSB Generator

Rf input
Linear Power Amp Boonton or E.N.I.
Rf output

H.P. Noise Generator HOI-3722A
Variable output (binary)

300Ω
2W5%

R
HP
10514A
X
L

10X1N4447

5

Tectonic TEB 50-X2
0-10.9dB Step Attenuator
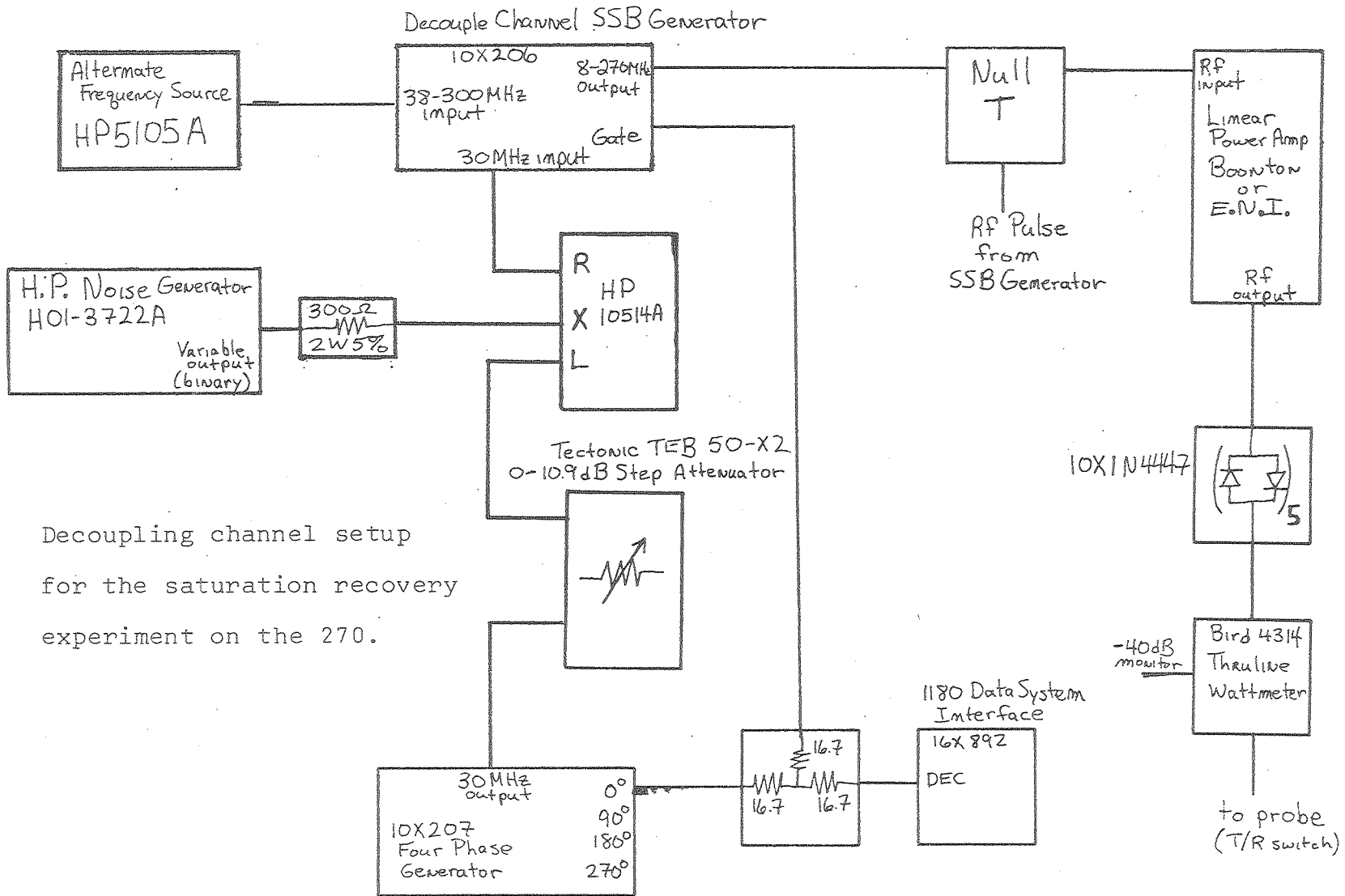
Decoupling channel setup
for the saturation recovery
experiment on the 270.

Bird 4314 Thruline Wattmeter

-40dB monitor

to probe (T/R switch)

1180 Data System Interface

16X892
DEC

16.7
16.7   16.7

30MHz output   0°
                      90°
10X207   180°
Four Phase   270°
Generator

in different parts of the spectrum. For this reason the center of the Rf pulse was placed as close to the center of the imino proton region as possible. Over the three ppm range of the imino protons in nucleic acids, there is only a small intensity difference in the Rf pulse, typically less than 5%, so there was little effect on the intensities of the peaks due to the pulse width. Figure 2.8 shows the integration of the imino proton region of the DNA helix.

In order to find optimum conditions for the Redfield pulse sequence, th power of the Rf pulse must be changed. A 90° pulse is normally obtained by changing the length of the pulse and holding the power of the pulse constant. Equivalently, one can keep the pulse length constant and change the power. The Redfield sequence requires a pulse length which is set by the frequency difference between the center of the pulse and the H_2O signal, so one must change the power of the pulse in order to change the flip angle. The optimum power for the Redfield pulse of a given length was found by maximizing the signal to noise of the 3 imino proton in a sample of 50 mM 3' UMP at pH = 4.5 in H_2O. This signal is found around 10.8 ppm at this pH and 25°C. The power level was increased until the largest signal to noise was found; whether this power level represents a 90° pulse under these conditions is not known, but higher power levels gave lower signal to noise.

Saturation recovery experiments were performed on the imino protons of the oligonucleotide helices $dCA_5G + dCT_5G$ and $rCA_5G + dCT_5G$. The experiment involves the saturation of one or several of the imino protons followed by a variable delay time before taking the observation Redfield pulse. An example of the data for $dCA_5G + dCT_5G$ is shown in Figure 3.5. Here the saturation pulse is centered at 14.1 ppm and as the delay time increases, the intensity of the saturated peak also increases. The peak recovers due to exchange with unperturbed water and by other relaxation processes such as the spin-lattice relaxation of the imino protons. (This will be discussed in a later section.)

The rate of exchange is at least partially dependent upon the rate of opening of the helix under these conditions and since the rate of opening of the helix is highly tempera-ture dependent, i.e. has a large activation energy, the exchange rates measured may also be temperature dependent. For this reason special precautions were taken to test the temperature of the sample while in the NMR probe. Temperature regulation on the NMR spectrometers is done by flowing a stream of N_2 gas past the sample and monitoring the temperature of the gas.[64] The thermocouple which monitors the gas is usually close to, but not at the same point as the sample tube. The temperature at the sample was obtained by measuring the chemical shift differences of neat methanol, which is

Figure 3.5. Saturation recovery experiment on

dCA$_5$G + dCT$_5$G double helix.

SATURATION RECOVERY EXPERIMENT USING
REDFIELD 214 PULSE SEQUENCE

270MHz SPECTRA OF dCA_5G + dCT_5G AT 5°C IN H_2O

500msec delay

150msec

50msec

SATURATION PULSE

1msec

14.6 14.4 14.2 14.0 13.8 13.6 13.4 13.2 13.0 12.8 12.6

PPM
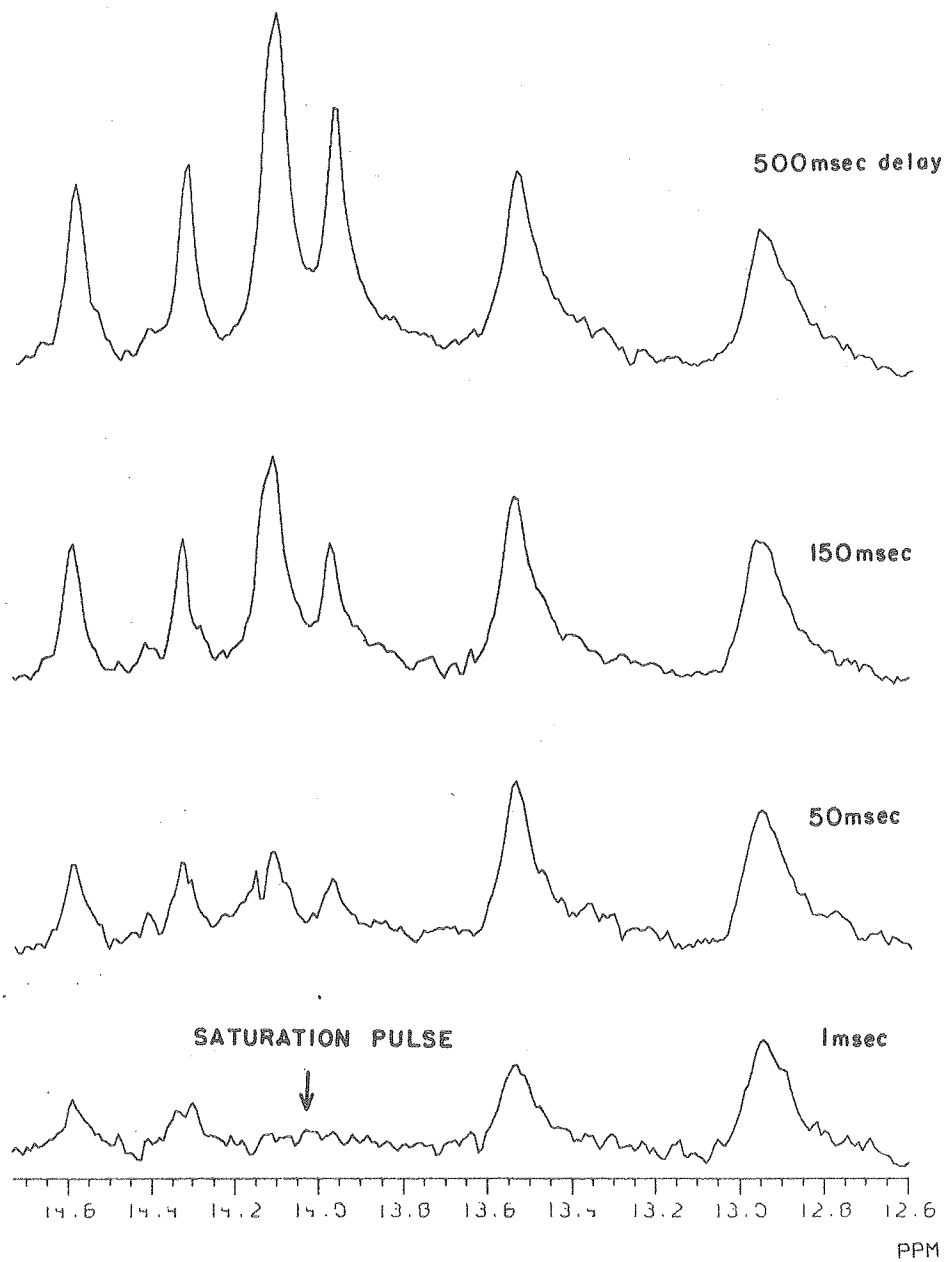
XBL 805-9523

calibrated with temperature. This procedure is not
as accurate but is more convenient than the other method
used which involves inserting a small thermocouple directly
inside an NMR tube and then putting the tube in the probe.
This gives a direct measure of the sample's temperature on
a digital thermometer connected to the thermocouple. Both
the long term (month to month) and the short term (time of
experiment) stability and accuracy of both the 270 MHz and
360 MHz instruments were found to be very good, with an
error of no more than ± 1°C, at fairly high N_2 flow rates.

3.   RESULTS

A)   Saturation Recovery Experiments

Relaxation rates for the imino protons were analyzed
in the following way. The imino protons exchange between
three different environments: the helix, the coil, and
water as shown below.

$$H_h \underset{k_{cl}}{\overset{k_{op}}{\rightleftharpoons}} H_c \qquad\qquad (1)$$

$$H_c + HOH^* \underset{k_{cw}[\text{catalyst}]}{\overset{k_{cw}[\text{catalyst}]}{\rightleftharpoons}} H_c^* + HOH$$
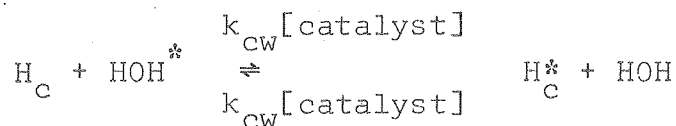
where H_h and H_c are the imino protons in the helix and coil
respectively. Crothers et al.[56] derived the Bloch equations
for exchange between three different environments, an extension

of McConnell's two state derivation.[65] The decay of M_z, the magnetization along the z axis, for each state is given below; with all the M_x's and M_y's equal to zero.

$$\frac{dM_{zh}}{dt} = - \frac{M_{zh}}{\tau_{op}} + \frac{M_{zc}}{\tau_{cl}} + \frac{M_{zh^o} - M_{zh}}{T_{1h}} \qquad (3)$$

$$\frac{dM_{zc}}{dt} = - \frac{M_{zc}}{\tau_{cl}} - \frac{M_{zc}}{\tau_{cw}} + \frac{M_{zh}}{\tau_{op}} + \frac{M_{zw}}{\tau_{wc}} + \frac{M_{zc^o} - M_{zc}}{T_{1c}} \qquad (4)$$

$$\frac{dM_{zw}}{dt} = - \frac{M_{zw}}{\tau_{wc}} + \frac{M_{zw}}{\tau_{cw}} + \frac{M_{zw^o} - M_{zw}}{T_{1w}} \qquad (5)$$

where M_{zh}, M_{zc}, and M_{zw} are the magnetizations along the z axis of the helix, coil, and water respectively; M_{zh^o}, M_{zc^o}, and M_{zw^o} are the equilibrium magnetizations of the helix, coil, and water respectively; and T_{1h}, T_{1c}, and T_{1w} are the longitudinal relaxation times in the helix, coil, and water, respectively. The lifetimes are: $\tau_{op} = 1/k_{op}$, $\tau_{cl} = 1/k_{cl}$[single strands] and $\tau_{wc} = \tau_{cw} = 1/k_{cw}$[catalyst]. This system is greatly simplified under our conditions by the fact that $1/\tau_{cw} = k_{cw}$[catalyst] $\gg 1/T_{1c}$. This means there is essentially no relaxation due to the T_1 of the coil, because the coil is in such fast exchange with water: a proton spends so little time in the coil state that there is negligible relaxation from that state. A second, similar assumption is that $1/\tau_{cw} \gg 1/\tau_{cl}$, which implies that everytime the helix opens to the coil state the protons exchange with water. These two assumptions allow a two-

state analysis of this system with just the helix and
water states. One can now write the equilibrium as

$$H_h \underset{k_{wh}}{\overset{k_{hw}}{\rightleftharpoons}} \text{water} \tag{6}$$

and the modified Bloch equations as

$$\frac{dM_{zh}}{dt} = -\frac{M_{zh}}{\tau_{hw}} + \frac{M_{zw}}{\tau_{wh}} + \frac{M_{zh}\textdegree - M_{zh}}{T_{1h}} \tag{7}$$

$$\frac{dM_{zw}}{dt} = -\frac{M_{zw}}{\tau_{wc}} + \frac{M_{zh}}{\tau_{cw}} + \frac{M_{zw}\textdegree - M_{zw}}{T_{1w}} \tag{8}$$

In the saturation recovery experiment performed here water
is not perturbed, so both equation (8) drops and $M_{zw} = M_{zw}\textdegree$
in equation (7). The steady state condition of $M_{zh}\textdegree/\tau_{hw} = M_{zw}\textdegree/\tau_{wh}$ gives the following equation

$$\frac{dM_{zh}}{dt} = \frac{-M_{zh} + M_{zh}\textdegree}{\tau_{hw}} + \frac{M_{zh}\textdegree - M_{zh}}{T_{1h}} \tag{9}$$

which can be integrated with the initial condition of $M_{zh} = 0$
at $t = 0$ to

$$M_{zh}(t) = M_{zh}\textdegree(1 - e^{-t[(1/\tau_{hw}) + (1/T_{1h})]}) \tag{10}$$

Data reductions were done on a Nicolet 1180 computer
which performs a least squares fit on the above equation by
changing $M_{zh}\textdegree$ and $[(1/\tau_{hw}) + (1/T_{1h})]$. The program then
gives the best fit to the lifetime $[(1/\tau_{hw}) + (1/T_{1h})]$, and
the equilibrium intensity of the peak $M_{zh}\textdegree$. The experimental

intensities of the peaks were obtained by measuring their
heights or areas, with areas used for broad resonances
since this procedure seemed to produce more accurate results
than the heights. The areas were measured by weighing
traces of the peaks on an analytical balance.

An example of the fits are given in Figure 3.6.
Experiments were usually done with 10-20 data points and
never less than 8 points. At least one point was taken
at a very short delay time, 0.25 or 0.5 msec, in order to
estimate the extent of saturation at zero time. The power
of the saturation pulse was usually set so as to get complete
saturation at the shortest time, but peaks nearby may be only
partially saturated. It is possible to get relaxation informa-
tion from partially saturated peaks by subtracting the intensity
of the peak at time zero from all the other delay times. A
point was also usually taken where the peak was fully re-
covered in order to get an idea of the equilibrium intensity.
This was done by using a delay time which is much larger
than (4 - 5 times) the relaxation time, or taking a spectrum
where no power was put in the saturation pulse. For a
given experiment all the spectra had the same number of scans
and were processed in the same way, so that their intensities
could be directly compared. The error on the relaxation time
of an individual calculation was on the order of 5 - 30% and
dependent on the number of delay times measured and also the
signal to noise of the individual spectra.

Figure 3.6. Fit of lifetime for saturation
   recovery experiment of dCA$_5$G + dCT$_5$G
   helix at 5°C. The line shows the calculated
   curve and the circles show the experimental
   points.

FIT OF LIFETIME FOR SATURATION RECOVERY EXPERIMENT

INTERIOR A·T RESONANCE AT 14.0 ppm IN dCA$_5$G + dCT$_5$G AT 5°C

0.0   0.2   0.4   0.6   0.8   1.0   SEC
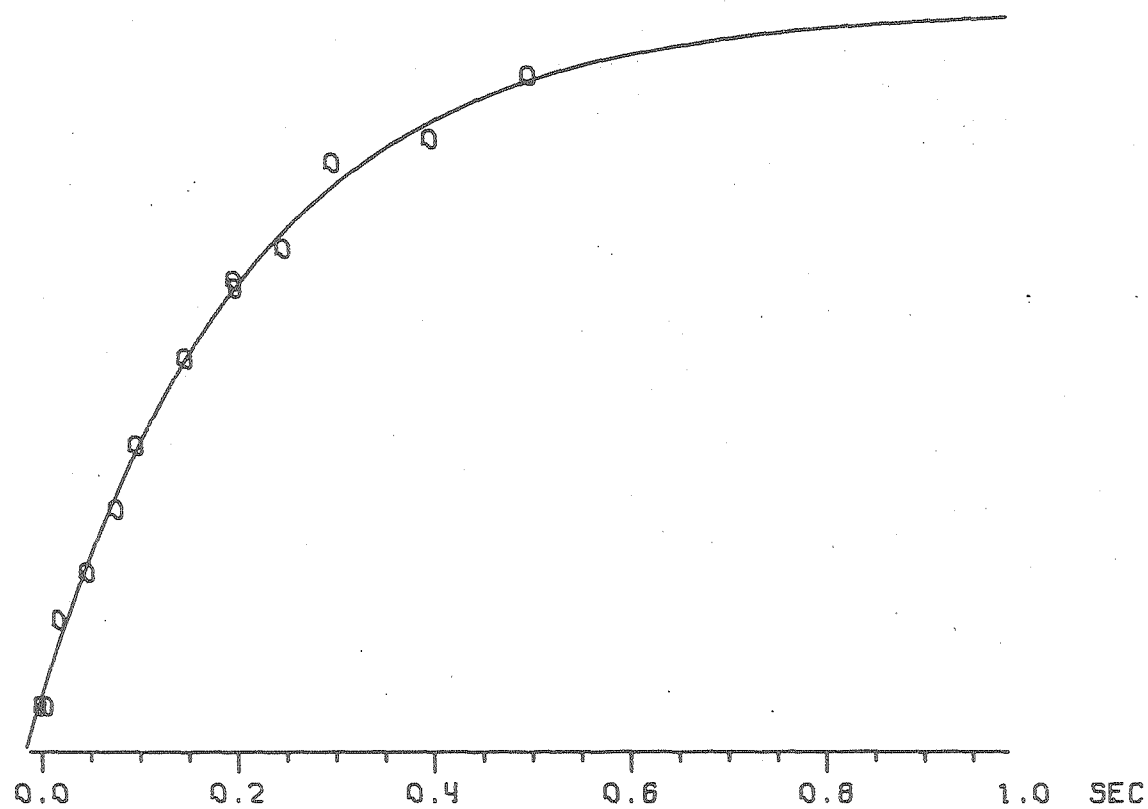
XBL 8011-7494

B)   Lifetimes of the Imino Protons for dCA_5G + dCT_5G at 5°C

Saturation recovery experiments on the imino protons of dCA_5G + dCT_5G at 5°C show varied lifetimes for protons in different parts of the helix. Table IX and Figure 3.7 show the lifetimes measured using equation (10) for this helix. The numbers given are the average of at least four measurements, with the errors representing the standard deviation of these measurements. No field dependence between the 270 MHz and 360 MHz instruments was seen for these lifetimes. Neither the length of the saturation pulse, nor the power of that pulse affected the lifetimes of the imino protons. The two peaks at 13.8 ppm (see Figure 3.7) are due to two interior A·T imino protons and were analyzed as one peak which recovered with one rate.

C)   Temperature Dependence of the Relaxation Rates for
      dCA_5G + dCT_5G

The temperature dependence of the lifetimes for two of the protons in the deoxy helix were observed. One proton at 14.3 ppm was on an A·T base pair on the interior of the helix, while the other at 12.93 ppm was the terminal #1 C·G base pair. The temperature dependences are given in Table X. There are only three temperature points for the #1 C·G proton, while the interior A·T proton had four temperature points. The discussion of these data will be left to a later section.

TABLE IX

LIFETIMES OF IMINO PROTONS IN dCT$_5$G + dCA$_5$G

DOUBLE HELIX AT 5°C (msec)

chemical shift of peak	12.93 C·G(#1)	13.5 C·G(#7)	13.9 A·T(Int)	14.1 A·T(Int)	14.3 A·T(Int)	14.6 A·T(#6)
360 MHz (# of points)	16±2.4 (5)	47±10 (4)	208±20 (3)	237±20 (3)	220±18 (6)	173±20 (3)
270 MHz (# of points)	17 (1)	–	228 (2)	180 (1)	–	143±20 (2)
Average lifetimes using points at 360 and 270 MHz	16±2.2	47±10	217±20	220±31	220±18	161±26

Figure 3.7. Lifetimes of the imino protons in

dCA_5G + dCT_5G helix at 5°C.

LIFETIMES OF IMINO H-BONDING PROTONS IN
THE HELIX dCA$_5$G + dCT$_5$G AT 5°C

XBL 8011-7492
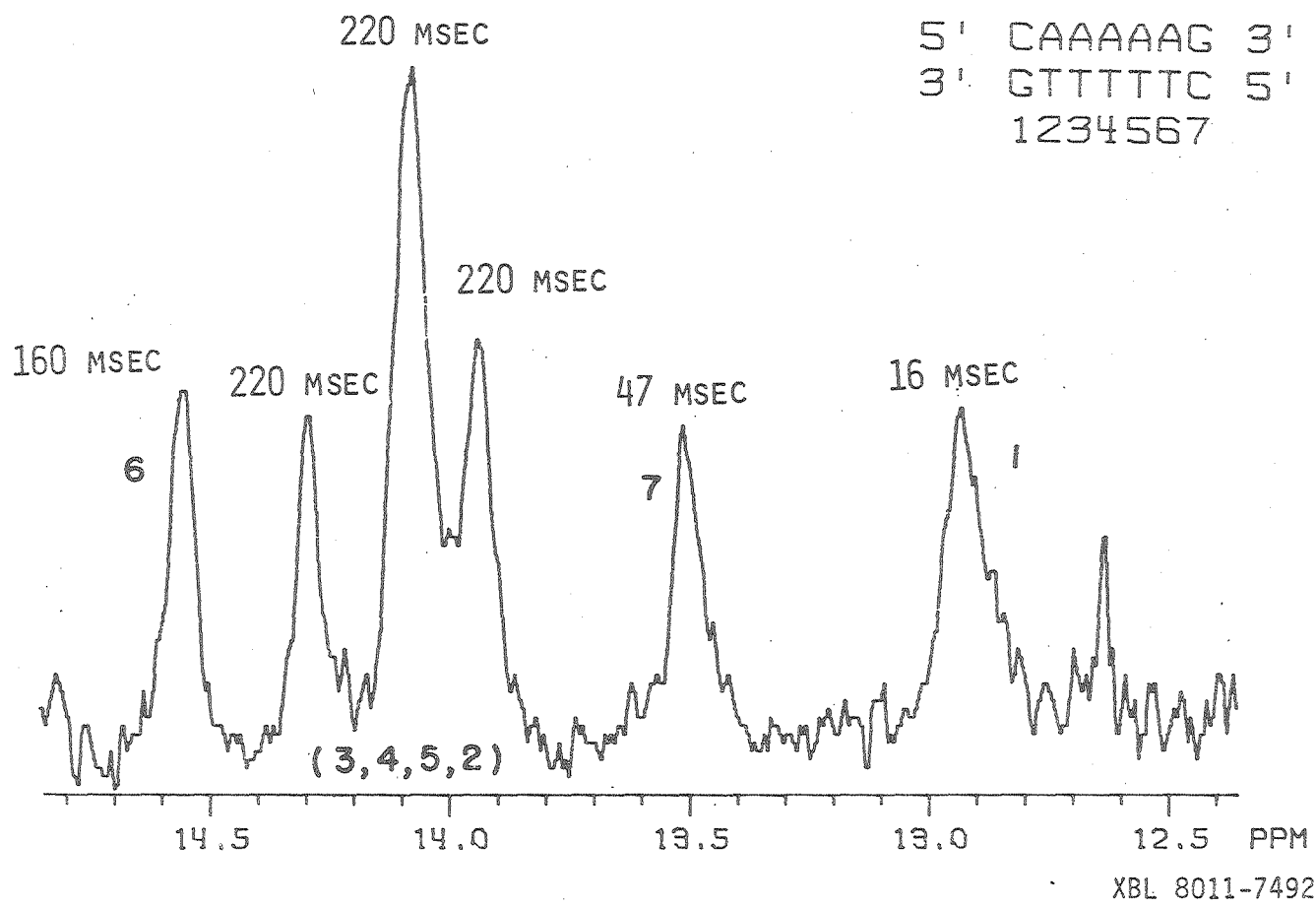
TABLE X

TEMPERATURE DEPENDENCE OF LIFETIMES IN dCA_5G + dCT_5G (msec)

Peak

Temperature	12.93 C·G(#1)	14.3 (Interior A·T)
3°C	—	∿300
(# of points)		(1)
5°C	16	220
(# of points)	(5)	(6)
7°C	13	260
(# of points)	(1)	(1)
10°C	7	205
(# of points)	(2)	(2)
16°C	—	∿88
(# of points)		(1)

D)   Lifetimes of the Imino Protons for the Hybrid Helix at 5°C

The lifetimes of the imino protons of the $dCT_5G + rCA_5G$ helix at 5°C are given in Table XI. There are fewer points than for the deoxy helix, so the errors on the lifetimes are on the order of 25%, except for the peaks at 13.4 and 13.5 ppm where the errors are slightly larger. These two peaks overlap slightly (see Figure 2.7) and, even though they have much different relaxation rates, it is still difficult to separate the contributions of the individual rates. The two peaks at 13.8 and 13.9 ppm relax with the same rate and were analyzed together.

4.   DISCUSSION

The relaxation rates of the imino protons after saturation has been studied in several oligonucleotides.[62,63] There may be many processes involved in the relaxation of these protons. For example longitudinal relaxation will contribute to the rate as well as chemical exchange rates between unperturbed water molecules. Saturation recovery experiments cannot distinguish between these relaxation mechanisms. Other relaxation processes involving magnetic cross-relaxation mechanisms may also be important. For example, nuclear Overhauser effects between the imino protons and other oligomer protons or water protons can contribute to relaxation.[66] Johnston and Redfield have studied these effects on the relaxation of imino protons in tRNA, and saw two types of

TABLE XI

LIFETIMES OF IMINO PROTONS IN rCA_5G + dCT_5G

DOUBLE HELIX AT 5°C (msec)

Peak	12.25	13.5	13.4	13.8	14.0	14.6
360 Mhz (# of points)	~22 (1)	9 (1)	63 (1)	–	–	–
270 MHz (# of points)	–	~18	48	107	100	35
Average of lifetimes at 270 and 360 MHz	22	~14	56	107	100	44

behavior.[62,63] At higher temperatures the relaxation
seemed to be exchange dominated. This was deduced by the
temperature dependence of the relaxation times and also the
fact that no isotope effect was seen on the rates in the
high temperature range. In going from 5 to 60% D_2O one
would expect a large change in the efficiency of magnetic
dipolar cross relaxation mechanism involving exchangeable
resonances, because the efficiency of H-H dipolar relaxation
is much larger than H-D relaxation. Johnston and Redfield
saw a sizable isotope effect at low temperatures in the
tRNA and concluded that in this range the relaxation was
mainly due to dipolar relaxation mechanisms.[63] At higher
temperatures, with faster rates, they saw little isotope
effect, and also observed temperature dependences of the
rates, from which they concluded that exchange was domi-
nating the relaxation mechanism.

The interior A·T protons on this helix have lifetimes
of 220 msec at 5°C (see Figure 3.7). There is no measurable
temperature dependence of the lifetime from 3 - 10°C for
the interior A·T at 14.3 ppm, as seen in Table X. It is not
until 16°C that this lifetime changes appreciably, where it
has a value of $\sim$ 90 msec. At this point exchange is probably
a more important relaxation process than the dipolar relaxation.
At temperatures below 10°C the measured lifetimes (220 msec)
are not due to chemical exchange but other faster processes.

Thus the exchange lifetimes and lifetimes for opening of the helix are greater than 220 msec below 10°C. The terminal base pairs on the helix have much shorter lifetimes and show some temperature dependence, so these protons are probably in the exchange limiting range.

An interesting result seen in this oligonucleotide helix is the large difference in the lifetimes of the two terminal C·G base pairs. The C·G #1 imino proton has a lifetime of 16 msec, while C·G #7's lifetime is 47 msec, as seen in Figure 3.7. This effect is presumably due to the differences in the energy of breaking the H-bonding structure for the two ends of the helix. Different stacking energies for these two terminal base pairs are most likely the major contributions to the different opening rates.

For the hybrid helix dCT_5G + rCA_5G the lifetimes of the imino protons are much shorter than the lifetimes in the deoxy helix at 5°C, as shown in comparison of Table IX and XI. The rates in this helix are more likely to be exchange rate dominated even for the interior A·T base pairs because of the lower stability of the hybrid helix.[44] This difference in rates is probably a reflection of the faster exchange rates in the hybrid helix. There are again differences in the lifetimes of the two terminal C·G imino protons, although not as large as in the deoxy helix. The C·G #1 imino proton has a lifetime of 22 msec while the C·G #7 has a lifetime of 14 msec. The interior A·T protons have lifetimes in the range of 100 msec.

A)   Are These Helices in the Open Limited Region?

An assumption that exchange of the imino protons was open limited was made in the derivation used for analysis of the saturation recovery experiments. The validity of that assumption is based on other experimental work performed on the exchange of imino protons under similar conditions.[19,53-55] The assumption states that $1/\tau_{cw} \gg 1/\tau_{cl}$ (see equations 1 and 2) and implies that everytime the helix opens to the coil state, the protons exchange with water. Here $1/\tau_{cw} = k_{cw}$[catalyst] where exchange is a base-catalyzed reaction, and the catalyst in our buffer is HPO_4^{2-}. The HPO_2^{2-} concentration was 11 mM under our conditions. The rate constant k_{cw} for HPO_4^{2-} has been measured in the oligo-nucleotide system dATGCAT to be 2×10^6 $M^{-1}sec^{-1}$ at 5°C, so $1/\tau_{cw} = 2.2 \times 10^4$ sec^{-1} in our system. We now want to compare this to $1/\tau_{cl}$ where $1/\tau_{cl} = k_{cl}$[single strand], and k_{cl} for oligonucleotides has been measured by temperature jump methods on other oligonucleotides to be $\sim 10^6$ $M^{-1}sec^{-1}$ at this temperature.[19,20] $1/\tau_{cl}$ will then be less than 10^2 in our experiment, so in this case $1/\tau_{cw} \gg 1/\tau_{cl}$, and our analysis is valid. This will be true for the interior protons which will exchange only when the whole helix goes from double to single strand.

This is the same result found by Hilbers and Patel for dATGCAT,[54-55] where the interior C·G base pairs exchange only when the whole double strand goes to single strand. The A·T imino protons were found to have much faster exchange rates than the double to single strand rate. Their system was modeled by the three states shown in Figure 3.8. The A·T imino protons can exchange by going through state B or C; but only by going to the single strand can the interior C·G imino proton exchange. The end base pairs thus open and close at much faster rates than the double to single strand rates, and this behavior is termed fraying on the ends of the helix. Kallenbach et al. observed very similar results in the helix dAAAGCTTT.[19]

In our helices dCA_5G + dCT_5G and rCA_5G + dCT_5G we also observe fraying on the ends of the helix, with this being manifested as shorter lifetimes of the terminal base pair imino protons relative to the interior protons in the helices. Our analysis assumes that even on the end base pairs, the exchange is open limited. This means that every time a base pair opens, the imino proton exchanges. The available evidence cannot show that this assumption is true, but we think that it is more likely than in the case of dATGCAT or AAAGCTTT because of the more stable C·G base pairs on the ends of our oligonucleotide helices. Evidence that opening was not the rate limiting step for exchange of the A·T imino protons in dATGCAT and dAAAGCTTT was mainly from the chemical

Figure 3.8. Proposed structures of dATGCAT in
double helix (from reference 73).

Scheme I.
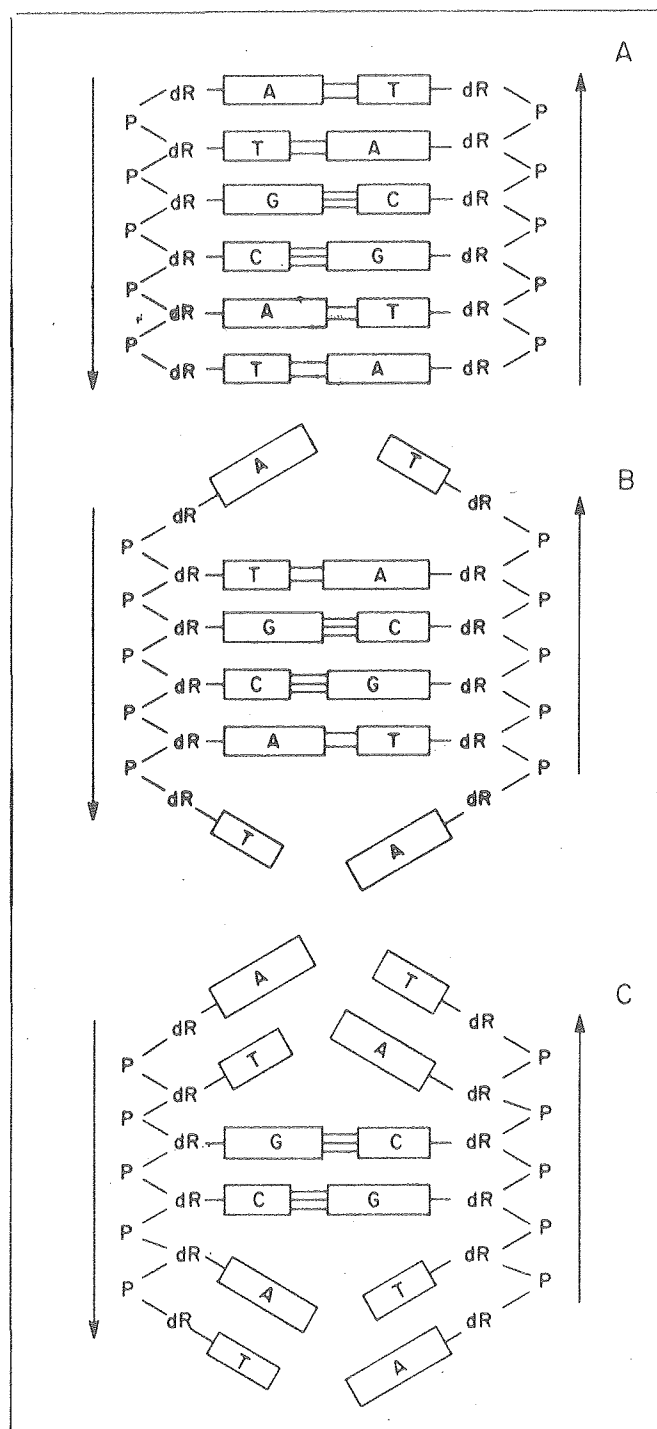
shift of the imino protons with temperature.[19,54,55] They
found fairly large chemical shift changes for the A·T base
pairs, up to 0.25 ppm for the terminal A·T imino proton in
dATGCAT, but little chemical shift changes for the internal
C·G imino protons. The chemical shift changes of the A·T
base pairs are from the closed and open state being in
fast exchange. Therefore the shift of the imino resonance
with temperature is from changes in the populations of the
two states with temperature, and not due to exchange with
H_2O. In our helices we see very little chemical shift
changes of the imino protons with temperature. Figures
2.9 and 2.17 show that there are almost no chemical shift
changes of the terminal, or interior, base paired imino protons
in the dCA_5G + dCT_5G helix or the rCA_5G + dCT_5G helix, until
the temperature where the resonances are very broad. So in
our systems the assumption of open limited exchange is
much more likely than in oligonucleotides with A·T base
pairs on the ends. Since there are no chemical shift
changes of the imino protons until they are extremely broad
in these helices, the analysis used by Patel and Hilbers
in dATGCAT is not applicable.[54] Thus the only reasonable
interpretation of the data that can be made is the assumption
of open limited exchange for all the imino protons.

5)   CONCLUSIONS

Studies on the exchange rates of the imino protons
of dCA_5G + dCT_5G and rCA_5G + dCT_5G were done by proton mag-
netic resonance. For the deoxy helix the results showed that
the terminal base pairs have much faster exchange rates, and
open much more often than the internal base pairs. The two
terminal C·G base pairs in this helix also have different
exchange rates, indicative of a sequence dependence for these
exchange rates. One also expects that the rate of opening
of the terminal base pair in a helix is essentially independent
of the length of the helix. So that a C·G base pair on the
end of the helix $\frac{\text{CAAAAAA}}{\text{GTTTTTT}}$ would open at the same rate even if
this sequence were added to the end of a much longer more
stable polynucleotide helix. The stability of the rest
of the helix is not the rate determining factor in exchange
on the ends, but only the sequence of the neighboring base
pairs.

The interior protons of the dCA_5G + dCT_5G show lifetimes
at 5°C which are most likely due to other relaxation pro-
cesses besides exchange with water. What these lifetimes
do provide is a lower limit on the lifetime of the helical
state, with this lifetime being greater than 220 msec at
5°C.

For the hybrid helix rCA_5G + dCT_5G the measured life-
times of the terminal base pairs are again much shorter than
those of the interior base paired imino protons, and also show
a slight sequence dependence. The lifetimes of the interior
A·T imino protons are a factor of 2 shorter than the interior

A·T protons in the deoxy helix at 5°C. This is indicative
of a lower stability of the hybrid helix compared to the
deoxy helix. Whether this shorter lifetime for opening of the
hybrid helix compared to the deoxy helix is a property of
this particular sequence of nucleic acid, or is general for
all sequences, is a question still to be answered.

PART II

CHAPTER IV

1.   INTRODUCTION

Ethidium (Et.) is a planar aromatic cation (shown in Figure 4.1) known to intercalate into DNA and RNA.[68]   It has been shown to be a frameshift mutagen in the Ames test.[11] Spectroscopic studies of ethidium (and other intercalating drugs) binding to nucleic acids have recently been reviewed.[39,69] Krugh et al. have extensively studied the physical pro- perties of ethidium binding to oligonucleotides by NMR, circular dichroism (CD), UV-visible absorption, and fluorescence methods.[72,77]   Their studies on dinucleoside monophosphates with ethidium have shown the formation of mini-helices, with ethidium intercalated between the two base pairs. X-ray studies   have provided detailed structures of ethidium in complexes with iodo rCpG and iodo rUpA.[70,71] A sequence dependence for ethidium binding has been found where ethidium preferentially binds to pyrimidine (3' - 5') purine sites compared to purine (3' - 5') pyrimidine sites.[72]

Proton magnetic resonance studies on dinucleoside mono- phosphates with ethidium[73] and a similar analog propidium[74] have shown that the same mixed sugar pucker seen in the crystal complexes also exists in solution. The sugar

Figure 4.1.   Structure of ethidium bromide.

Ethidium Bromide

XBL 782-7422

puckers found in solution are 3' <u>endo</u> for the 5' residue and 2' <u>endo</u> for the 3' residue in the molecule. This is indicative of at least partial similarity between the crystal and solution structures.

Lee and Tinoco have studied complexes of rCpG, rCpUpG, and rGpUpG + rCpC with ethidium by proton NMR.[73] These systems represent intercalation of ethidium into a perfect helix (rCpG), a helix with a bulged uracil on both strands (rCpUpG), and a helix with bulge on only one strand, (rGpUpG + rCpC). The proposed structures for these complexes are schematically shown in Figure 4.2. Bulged base structures may be important in the mechanism of frameshift mutagenesis by ethidium. Specifically ethidium may intercalate in transient bulges formed during replication, repair, or recombination of DNA.[73]

In this chapter we will investigate the thermodynamics of ethidium binding to several different dinucleoside monophosphates (rCpG, rUpA, and dCpG), a trinucleoside diphosphate which can form a bulge on both strands (rCpUpG), and a mixture of a trinucleoside and a dinucleoside (rGpUpG + rCpC) which can form a bulged structure on one strand. We will try to answer questions about the properties governing the sequence specificity of ethidium, and the strength of ethidium binding to perfect helices compared to those with bulges.

Figure 4.2.   Proposed structures for ethidium

binding to oligonucleotides (from reference

73).

CpG

CpUpG

GpUpG + CpC
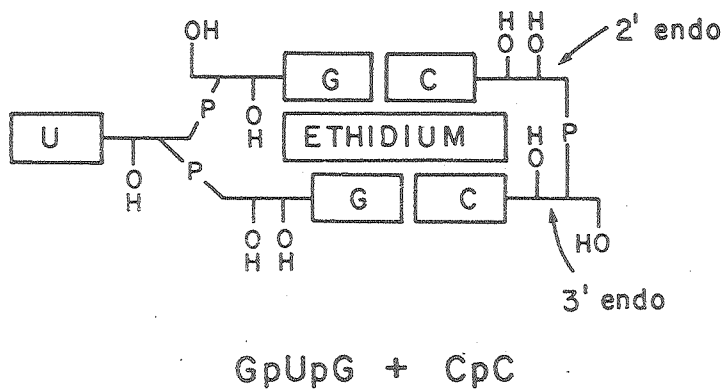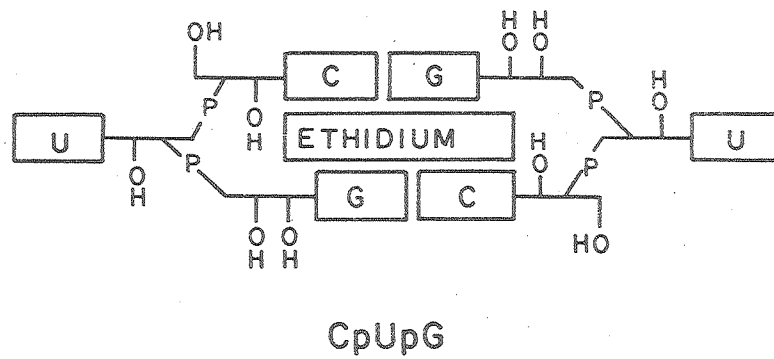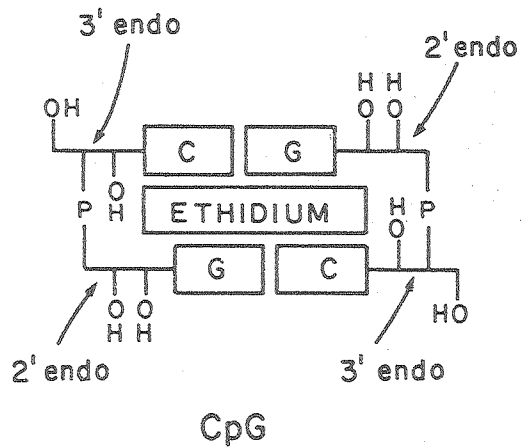
2. OPTICAL STUDIES EXPERIMENTAL

A) Materials

The ribo- dinucleoside 3'-5' monophosphates were purchased from Sigma. The deoxyribo- dinucleoside 3'-5' monophosphates were purchased from Collaborative Research. Ethidium bromide was obtained from Sigma; the trimers rGpUpG and rCpUpG were bought from Boehringer Mannheim, however the majority of the rCpUpG used in this study was enzymatically synthesized with polynucleotide phosphorylase using standard procedures.[24] The E. coli DNA used in this study was obtained from Worthington.

B) Methods

Visible absorption studies were done on a Cary 118 spectrometer, with an external bath (Haake model F) used for temperature regulation to an accuracy of ± 0.5°C. Melting studies were done on a Beckman DU spectrophotometer and a Gilford Model 2000 recorder, which measures temperature to ± 0.5°C. Circular dichroism spectra were measured on a Model 60 Cary spectropolarimeter equipped with a 6001 CD attachment. Equilibrium sedimentation studies were done on a Model E analytical ultracentrifuge, with an A_nF rotor.

All samples contained 8.0 mM Na_2HPO_4, 20 mM NaH_2PO_4, 0.18 M NaCl, 0.1 mM Na_2EDTA, pH = 7.0 unless otherwise noted. Centrifugation of the samples helped eliminate dust

particles, and was performed before most of the optical experiments. Extinction coefficients used for the dimers were from the CRC handbook.[29] The extinction cofficients of the trimers were calculated with the assumption of only nearest neighbor interaction, using the extinction coeffecients of the dinucleoside monophosphates and mononucleotides. The extinction coefficient of ethidium was taken as 5.45×10^3 at 480 nm.[86] The extinction coefficient of E. coli DNA was taken as 6.4×10^3 at 260 nm.[87] All these extinction co-efficients are for 25°C.

The low salt experiments performed on E. coli DNA were done after exhaustive dialysis of the DNA against a solution of double distilled water with 0.6 mM NaOH added to adjust the pH of the water to 7.0. Thus the dialysate had a sodium ion concentration of 0.6 mM, but the DNA solution's sodium ion concntration was not known since the number of sodium counter ions bound to the DNA was not taken into account. The concentration of DNA, per phosphate, was around 0.5 mM so the actual sodium ion concentration in the DNA solution was probably less than 1.5 mM.

The ethidium concentration in most of the optical experiments was around 0.05 mM. The oligonucleotide concentrations ranged from 0.1 - 5 mM depending upon the experiment. Samples were prepared by added given amounts of ethidium and oligonucleotides from stock solutions, so the total concentrations of ethidium and nucleotide in each sample were known.

3.   RESULTS

A)   Determination of Equilibrium Constants of Ethidium

Binding to Oligonucleotides

Equilibrium constants were calculated using the large

change in the visible absorption spectrum of ethidium upon

binding to nucleic acids.[75]   The shift in the visible

absorption is seen in Figure 4.3, which shows ethidium

binding to the dimer rCpG at 1°C. The largest change in the

Figure 4.3. Binding of ethidium at different

concentrations of rCpG. Ethidium concentration

was constant at 0.12 mM. All solutions were

run in standard buffer. The curves are:

a) free ethidium.

b) [rCpG] = 0.22 mM.

c) [rCpG] = 0.33 mM.

d) [rCpG] = 3.0 mM.

BINDING OF ETHIDIUM BROMIDE TO CpG   1°C
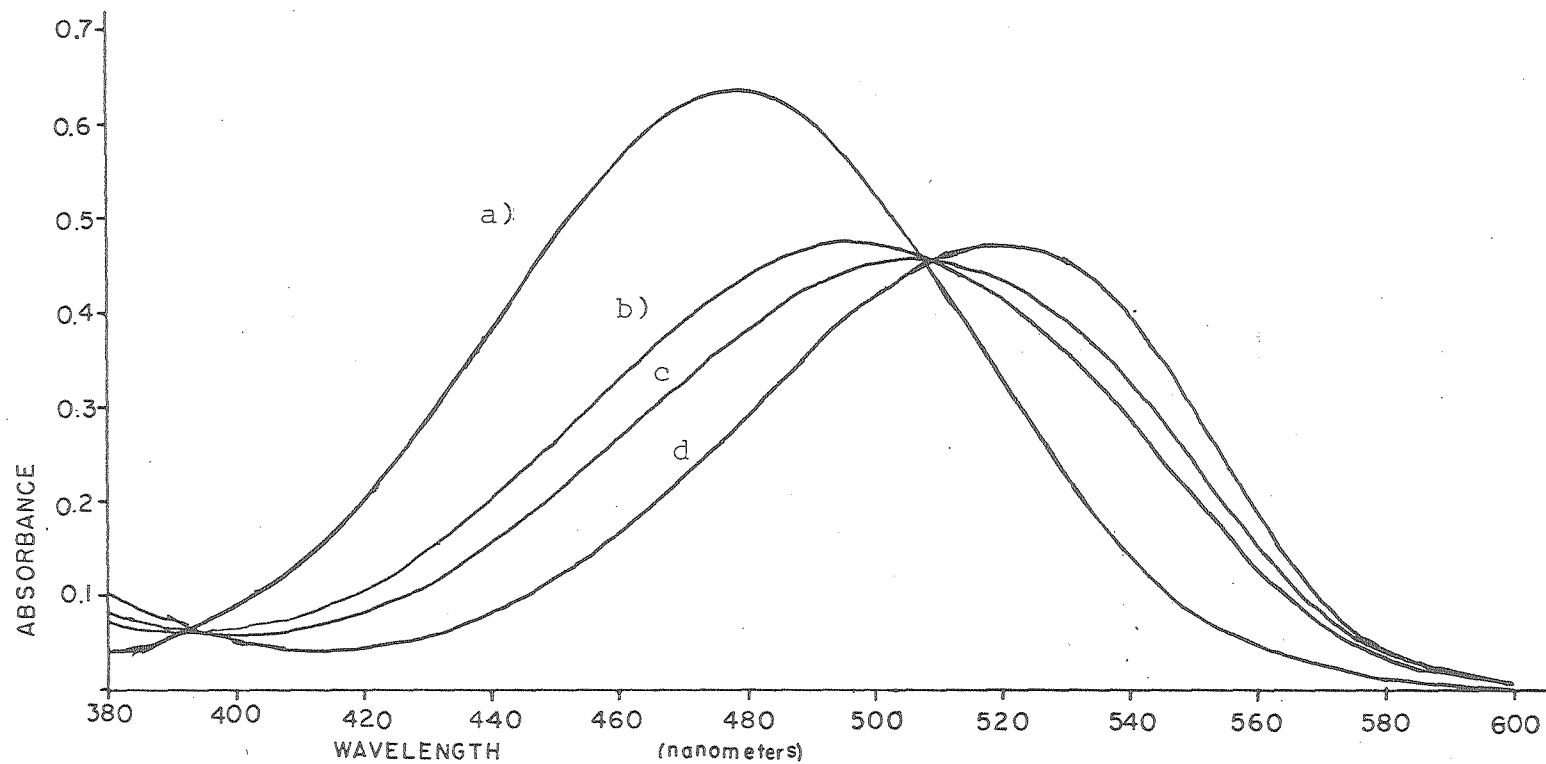
XBL 782-7366

absorbance is at 465 nm and was the wavelength used in these calculations. The equilibrium constant for a 2 to 1 complex can be written as follows (the determination of the stoichiometry will be discussed in a later section)

$$\text{Nuc}_a + \text{Nuc}_b + \text{Et.} \rightleftharpoons \text{complex} \qquad (1)$$
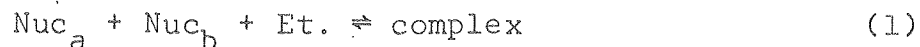
$$(2) \qquad K = \frac{[C_{complex}]}{[C_{Nuc_a o} - C_{complex}][C_{Nuc_b o} - C_{complex}][C_{Et o} - C_{complex}]}$$

where $C_{complex}$ is the concentration of the complex in solution and $C_{Nuc_a o}$, $C_{Nuc_b o}$ and $C_{Et o}$ are the total concentrations of nucleotide a, nucleotide b, and ethidium respectively, in solution. The analysis of the absorption data was done by two methods. One method used by Blake and Peacocke involves obtaining the spectrum of the dye in the complex.[76] This is done by holding the concentration of the dye constant and titrating with nucleic acid until all the dye is bound; with this spectrum and the spectrum of the free dye it is possible to obtain the concentrations of the free and bound dye. This analysis assumes that there are only two states for the dye in the system, either free in solution or bound to nucleic acid. It also assumes that the nucleic acid does not absorb at this wavelength. The method requires fairly high equilibrium constants in order to obtain a spectrum of the fully bound. If the total concentrations of the nucleic

acid and dye in solution are known then the equilibrium constant for dye binding can be calculated. Let

$$C_{complex} = \alpha C_{Et^o} \qquad (3)$$

$$\alpha = \frac{A_f - A}{A_f - A_b}$$

where A_f, and A_b are the absorbances of the free and bound dye respectively, A is the absorbance of an intermediate state where α, the fraction of ethidium in the complex, is being calculated. Table XII shows the calculations of the equilibrium constant for rCpG + ethidium at 0°C using this method.

The other method of analysis involves using a Benesi-Hildebrand type analysis. We can write

$$C_{complex} = \frac{A - \varepsilon_f C_{Et.^o} \ell}{(\varepsilon_b - \varepsilon_f) \ell} \qquad (4)$$

where A is the measured absorbance of the solution (normalized to 1 cm), $C_{Et.^o}$ the total concentration of ethidium, ℓ the pathlength of the cell in cm, ε_f the extinction coefficient of free ethidium at 465 nm, and ε_b the extinction coefficient of the ethidium in the complex. Substituting equation (4) into equation (2) and rearranging with the assumptions that $Nuc_{a^o} = Nuc_{b^o}$ and $Nuc^o = Nuc_{a^o} + Nuc_{b^o}$ we obtain (which is the form of the equation for self-complementary oligonucleotides)

TABLE XII

EQUILIBRIUM CONSTANTS FOR ETHIDIUM BINDING TO rCpG 0°C

CALCULATED USING PEACOCKE-TYPE ANALYSIS

$A_b = 0.074$ A_f 0.219 $\lambda = 465$ nm $\alpha = (A_f - A)/(A_f - A_b)$

[Nuc] (mM)	α	K (M^{-2})
1.3×10^{-4}	0.47	1.0×10^8
2.0×10^{-4}	0.67	9.3×10^7
2.7×10^{-4}	0.80	8.5×10^7
4.0×10^{-4}	0.91	8.6×10^7

average K = 9.1×10^7 (M^{-2})

$$\frac{C_{Et^\circ}}{(A - \varepsilon_f C_{et^\circ}\ell)} = \frac{1}{(C_{Nuc^\circ} - 2C_{complex})^2(\varepsilon_b - \varepsilon_f)K}$$

$$+ \frac{1}{(\varepsilon_b - \varepsilon_f)} \tag{5}$$

A plot of $C_{Et^\circ}/(A - \varepsilon_f C_{Et^\circ}\ell)$ versus $1/(C_{Nuc^\circ} - 2C_{complex})^2$ yields K and $(\varepsilon_b - \varepsilon_f)$ immediately. However, the quantity $(C_{Nuc^\circ} - 2C_{complex})$ is not known, but only the total concentration of the nucleotide C_{Nuc°. Assuming that the concentration of complex was small compared to the total concentration of added nucleotide, the first fitting to equation (5) had $C_{complex}$ set equal to zero. The resulting equilibrium constant was then used to find the value for $C_{complex}$ by substitution into equation (2). Refitting of the data in equation (5) with this value of $C_{complex}$ included gave a new estimate of the equilibrium constant. This iteration was done until convergence of the equilibrium constant occurred to within 1%. Figures 4.4a and 4.4b show ethidium binding to several dimers using this analysis. The equilibrium constants derived from these data will be given in a later section. Both the Peacocke and Benesi-Hildebrand methods gave equivalent results in our systems.

Figure 4.4.

      a) Benesi-Hildebrand type plot for rCpG

         at 0 and 5°C.

      b) Benesi-Hildebrand type plot for dCpG

         at 0 and 5°C.

      c) Melting of ethidium with rCpG, for

         several concentration of ethidium and rCpG.

         The T_m for each concentration is at

         relative absorbance equal to 0.5.

a)

XBL 8011-7477

168

b)

XBL 8011-7476

c)
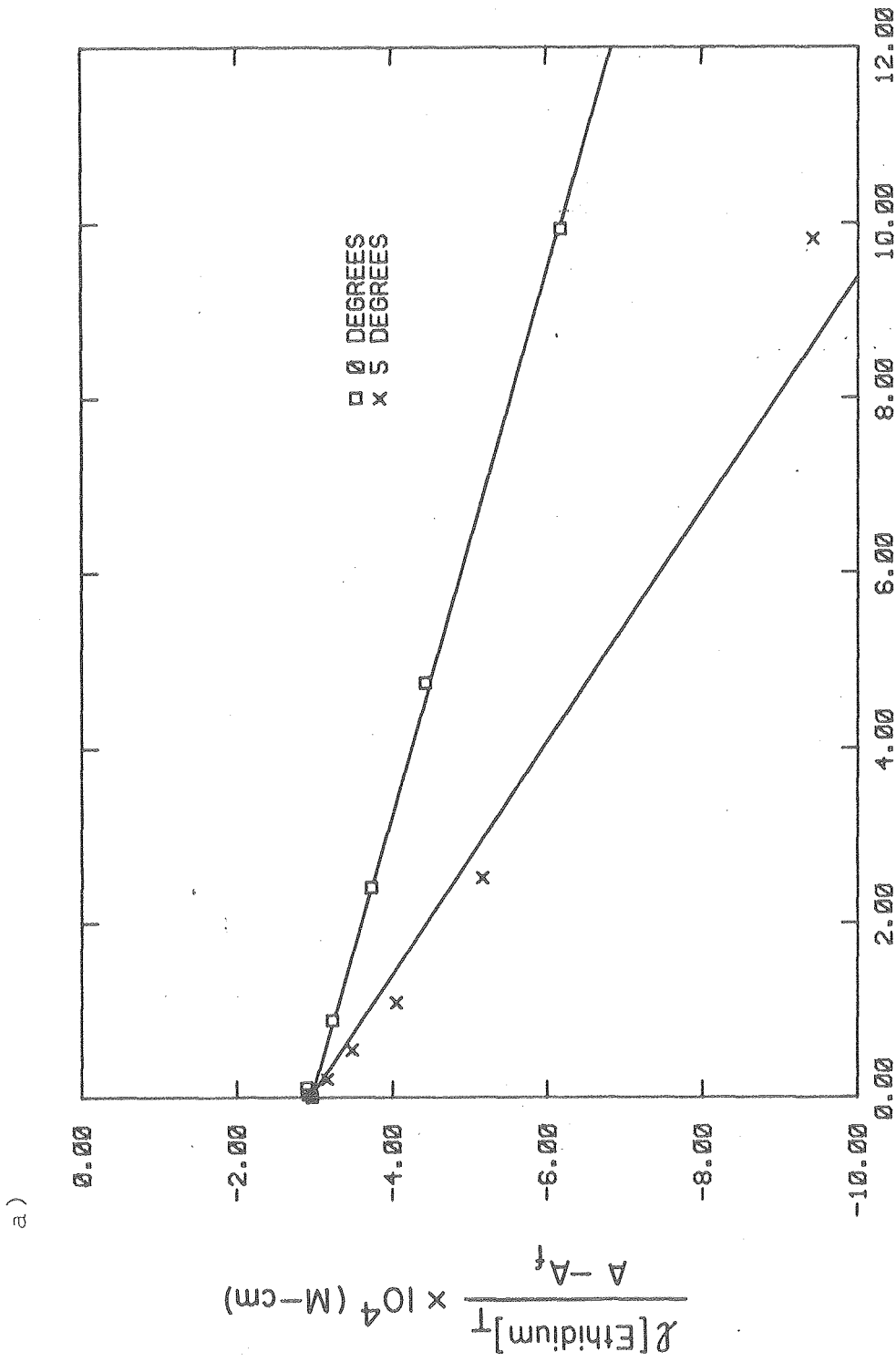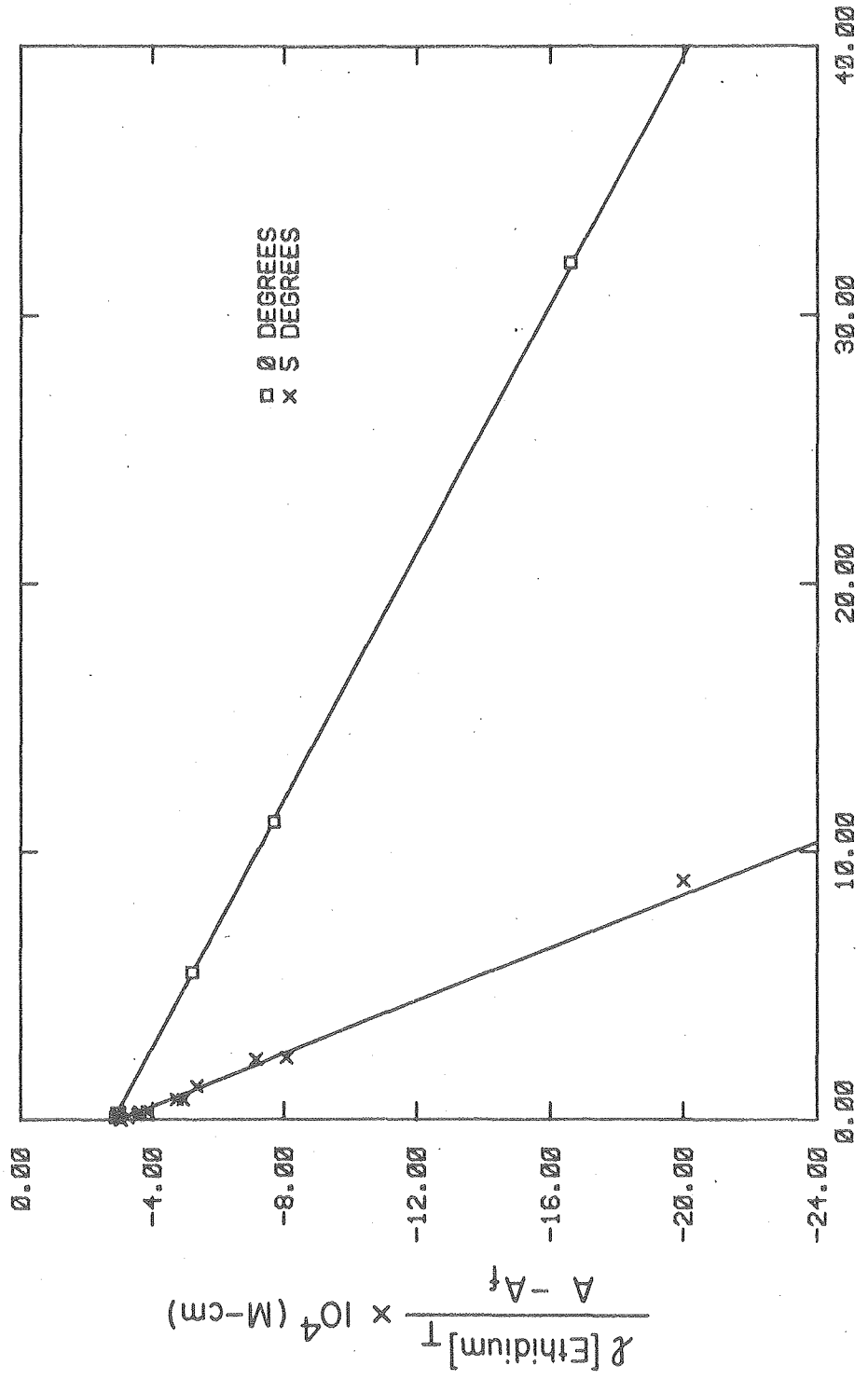
MELTING OF ETHIDIUM WITH CPG
RELATIVE ABSORBANCE VS TEMPERATURE

	CONC DIMER	CONC DYE
$	0.800E-03	0.200E-03
+	0.200E-02	0.500E-03
*	0.280E-02	0.700E-03
>	0.440E-02	0.110E-02
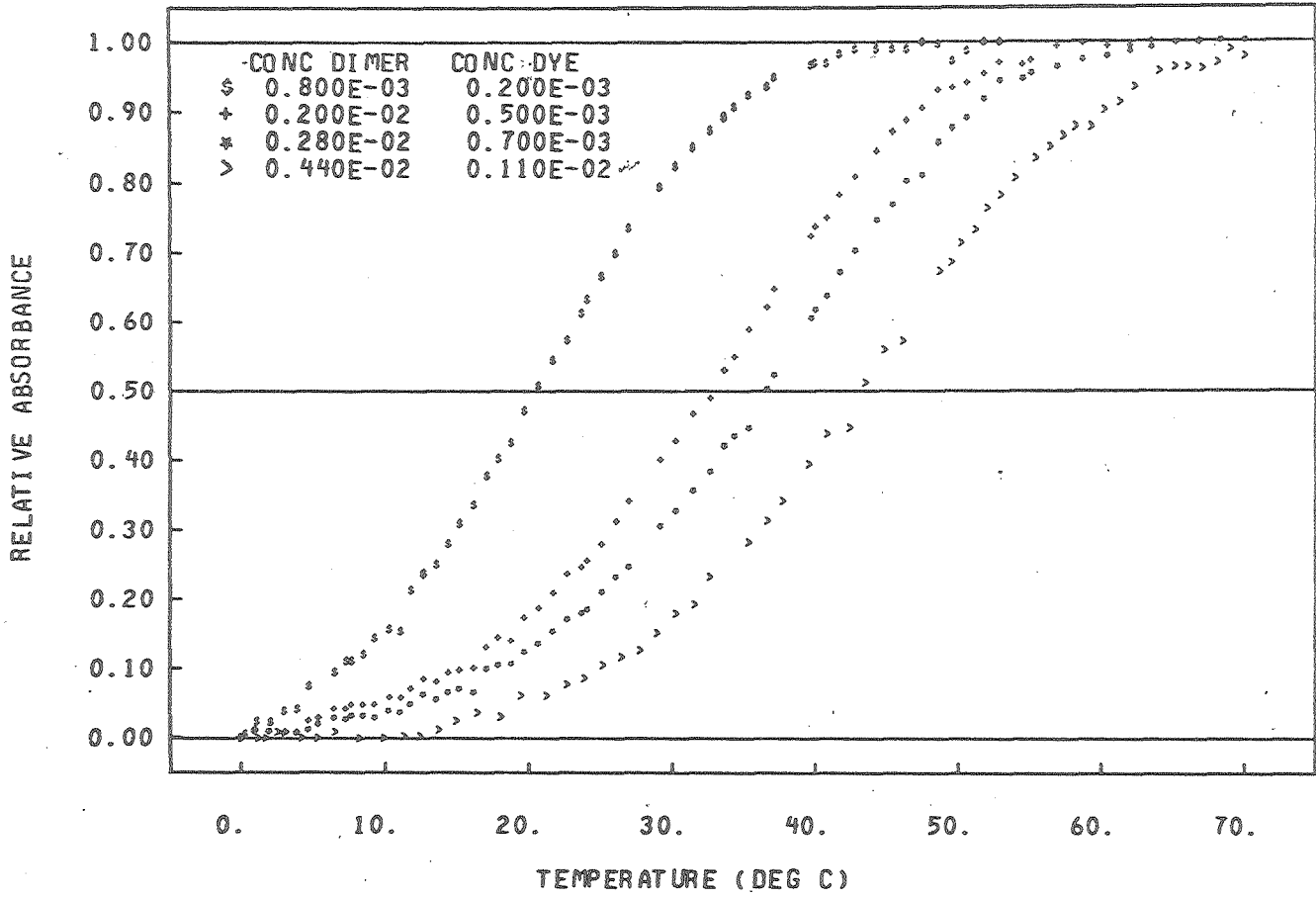
XBL 796-10029

This procedure worked well in our systems because the concentration of nucleotides was always well in excess of the ethidium concentration (usually 4 to 100 times the ethidium concentration). This also helped insure a 2:1 complex as opposed to the 2:2 complex seen in crystal structures of dimers with ethidium.[70,71]

B)   Stoichiometry of the Complex

Krugh found complexes of dinucleotides and ethidium had stoichiometries of 2:1 dimer:ethidium under conditions similar to those in this work.[72,77] Our evidence for a 2:1 complex stems from the inability to fit the absorbance data of ethidium to other stoichiometries. There are good isosbestic points in the visible spectra of ethidium titrated with dinucleotides, which indicates there are only two states for the ethidium, free in solution, and bound in a complex. A Benesi-Hildebrand equation similar to (5) can be derived for a 1:1 complex of dimer with ethidium. The data do not fit a 1:1 complex, shown by the nonlinearity of the data fit using the 1:1 equation. A 2:2 complex was also ruled out in the concentration range used in this study. Inability of the data to fit a 2:2 stoichiometry was shown by assuming a Peacocke-type analysis for that equilibrium. The spectrum of the fully bound ethidium can be found by going

to very high nucleotide concentrations. The amount of ethidium
in the complex for an intermendiate state (where the ethidium
is parially bound and partially free) is found from equation
(3). Knowing the concentration of the complex and the total
concentrations of ethidium and oligonucleotide, it is possible
to calculate the equilibrium constant. Each intermediate
point in the titration curve will give a value for the
equilibrium constant. These equilibrium constants should
be the same over the whole titration curve. A large variation
in the calculated equilibrium constant implies that the
assumed stiochiometry is incorrect. Table XIII shows the
equilibrium constants calculated for a 2:2 and a 2:1 complex
for the titration of ethidium with rCpG at 0°C. The equili-
brium constants for the 2:1 complex differ by about 10%
over the titration, whereas this difference is over three
orders of magnitude for the 2:2 complex. Clearly, the
stiochiometry is 2:1 and not 2:2 for the complexes in the
concentration range we are working.

C) Equilibrium Constants for Ethidium Binding to Oligo-
. nucleotides

Equilibrium constants for ethidium binding in a 2:1
complex were found for the following self-complementary
oligonucleotides: rCpG, dCpG, rUpA, and rCpUpG. An upper
limit on the equilibrium constant of rGpUpG + rCpC was
also found. The equilibrium constants at 0°C are given

TABLE XIII

FIT OF DATA TO 2:1 AND 2:2 NUCLEOTIDE:ETHIDIUM COMPLEXES

rCpG at 0°C

$A_b = 0.074$ $A_f = 0.219$ $\lambda = 465$ $\alpha = (A_f - A)/(A_f - A_b)$

[Nuc] (mM)	α	calculated K for 2:1 complex (M^{-2})	calculated K for 2:2 complex (M^{-3})
1.3×10^{-4}	0.47	1.0×10^8	5×10^{14}
2.0×10^{-4}	0.67	9.3×10^7	7×10^{12}
2.7×10^{-4}	0.80	8.5×10^7	1×10^{12}
4.0×10^{-4}	0.91	8.6×10^7	3×10^{11}

below:

Nucleotide	Equilibrium Constant at 0°C (M^{-2})
rCpG	$100\pm20 \times 10^6$
dCpG	$8\pm2 \times 10^6$
rUpA	$1\pm0.3 \times 10^6$
rCpUpG	$1\pm0.3 \times 10^6$
rGpUpG + rCpC	$<10^5$

The errors in the equilibrium constants were obtained from errors in calculating the slope of the Benesi-Hildebrand type plots (see equation 5; Figures 4.4a and 4.4b show examples of these plots). Equilibrium constants at 5°C were obtained on several of these systems and are shown below:

Nucleotide	Equilibrium Constant at 5°C (M^{-2})
rCpG	$42\pm15 \times 10^6$
dCpG	$1.5\pm0.2 \times 10^6$

D) Binding of Ethidium to Single Strands

To find the strength of binding of ethidium to a single strand nucleotide in a 1:1 complex, the equilibrium constants for ethidium and rUpG or rCpA were measured. rUpG (or rCpA) is not selfcomplementary so it cannot form base pairs with itself in solution; this also rules out 2:1 dimer:ethidium complexes in solution. The equilibrium constant for the single strands were measured in the same manner as with the selfcomplementary nucleotides. An

equation similar to equation (5) was derived for 1 to 1
binding. The equilibrium constants obtained at 0°C are:

Nucleotide	K at 0°C (M^{-1})
rUpG	130 ± 30
rCpA	300 ± 100

These numbers are small compared to the binding of
ethidium in the 2:1 complexes; thus single strand binding
can be neglected in these systems.

E)   Determination of the Enthalpy for Ethidium Binding to
     Oligonucleotides

$\Delta H°$ values for ethidium binding to these oligonucleotides
were obtained from melting curves using the analysis of
Martin et al.[24] By monitoring the absorbance of the ethidium
at 465 nm it is possible to follow the amount of ethidium
bound with temperature throughout the melt. Typical melting
curves are shown in Figure 4.4c, for several concentrations
of rCpG with ethidium. The ratio of total nucleotide to
ethidium was held constant at 4:1 in all these experiments.
The melting temperature of the ethidium, the T_m, is the
point where half the ethidium is bound in the complex and
half is free in solution. Equation (2) can then be used to
calculate the equilibrium constant at this temperature.
The slope of a plot of ln(K) versus $1/T_m$ is then $-\Delta H°/R$, which
gives the enthalpy for complex formation.

Another method for calculating $\Delta H°$ is from the slope of the melting curve $(d\alpha/dT)$ at the T_m, the formula derived for the case of 4:1 nucleotide:ethidium is[24]

$$\Delta H° = -\frac{16}{3} R(T_m)^2 \left(\frac{d\alpha}{dT}\right)_{T_m} \tag{6}$$

where α is the fraction of ethidium in the complex.

The $\Delta H°$'s were calculated by both methods for these systems, and are given below along with the calculated $\Delta S°$ values:

Nucleotide	$\Delta H°$ $(d\alpha/dT)$ (kcal/mole)	$\Delta H°$ $(\ln(K)$ vs $1/T_m)$ (kcal/mole)	$\Delta S°$ (e.u.)
rCpG	-33	-32	-84
dCpG	-27	-29	-69
rCpUpG	-29		-79

F) Equilibrium Sedimentation Studies

Equilibrium sedimentation was done to determine whether aggregates exist in solution. What we were testing was to see if there was any aggregation of the 2:1 complexes with each other. This will be an important consideration in the studies of the induced CD of ethidium with dimers described later. Samples were run at 5°C and reached equilibrium after 24 hours. The weight average molecular weight of the complex was calculated using the following equation:[78]

$$M_{complex} = \frac{1}{2} M_{NaCl} \; Z(\frac{1 - \bar{V}_{NaCl}\rho}{1 - \bar{V}_{complex}\rho})$$

$$+ \; Z[\frac{2RT \; \frac{\partial \; \ln(C)}{\partial r^2}}{(1 - \bar{V}_{complex})\omega^2}] \tag{7}$$

where Z is the charge on the complex, $\bar{V}_{complex}$ and $\bar{V}_{NaCl}$ are

the partial specific volumes of the complex and sodium

chloride respectively, ρ is the density of the buffer solution,

C is the concentration of the complex at distance r from the

axis of rotation, and ω is the angular velocity of the rotor.

$\bar{V}$ for the complex was calculated by assuming it is the weight

average of the component partial specific volumes. Thus

for a complex of 2 CpG:1 ethidium, $\bar{V}$ is

$$\bar{V}_{complex} = \frac{2M_{CpG}\bar{V}_{CpG} + M_{Et}\bar{V}_{Et}}{2M_{CpG} + M_{Et}} \tag{8}$$

The partial specific volumes of the components, rCpG and

ethidium were obtained by sedimentation on the isolated

species.

Integration and rearrangement of equation (7) gives a

linear equation where a plot of ln(C) versus r^2 has a slope

from which $M_{complex}$ can be calculted. Table XIV shows the

conditions for the equilibrium sedimentation and gives the

measured partial specific volumes of the component species.

The molecular weight of the complex was measured at a

concentration where all of the ethidium was bound in a 2:1

complex, and under similar conditions to those used in the

TABLE XIV

CONDITIONS AND RESULTS OF EQUILIBRIUM SEDIMENTATION

Samples were run in standard buffer with

ρ = 1.0094 gm/cc

$\bar{V}_{NaCl}$ = 0.3 cc/gm

T = 278°K

speed = 42000 rpm

Partial Specific Volumes

rCpG⁻Na⁺   0.58 cc/gm 2.5×10^{-5} M
measured from sedimentation run on rCpG solution

Et.⁺Cl⁻   0.75 cc/gm
measured from sedimentation run on 0.1 mM Ethidium solution

2:1rCpG:Et   0.62 cc/gm
complex
calculated from equation (8)

$M_{complex}$ = 1,800 gm/mole

calculated using equation (7) on solution of 2.5 mM rCpG
0.1 mM ethidium.

rest of the optical studies. Figure 4.5 shows the plot of $\ln(C)$ versus r^2 for the rCpG ethidium complex. The measured molecular weight of the complex was 1,800 gm/mole. This result shows that aggregates do not exist in solution to any appreciable extent since the molecular weight of a 2:1 complex would be 1,600, in good agreement with the measured value. Although the sedimentation equilibrium results cannot rule out a 2:2 complex, the earlier discussion on the stoichiometry showed that a 2:2 complex was not possible in our system.

G) Induced CD of Ethidium upon Binding to Oligonucleotides

The induced CD of ethidium was measured when bound to the following oligonucleotides: rCpG, dCpG, and rUpA. The CD from 290 to 420 nm is shown in Figure 4.6 for these three dimers. The epsilon left - epsilon right ($\Delta\varepsilon_b$) shown in Figure 4.6 is per ethidium bound. The spectra were measured under the same conditions (and often on the same solutions) as those used in the equilibrium constant determinations. The $\Delta\varepsilon_b$ values were calculated from the relation

$$\theta° = 32.98(\Delta A) = 32.98(C_{complex}\Delta\varepsilon_b\ell)$$

where $\theta°$ is the measured ellipticity in degrees, $C_{complex}$ is the concentration of complex (calculated using the K's given earlier) and ℓ is the pathlength of the cell in cm.

Figure 4.5.   ln(A) <u>versus</u> r^2 plot for 2.5 mM rCpG

and 0.1 mM ethidium.   This is equivalent to

ln(C) <u>vs.</u> r^2 since A $\propto$ C.

XBL 8011-7474
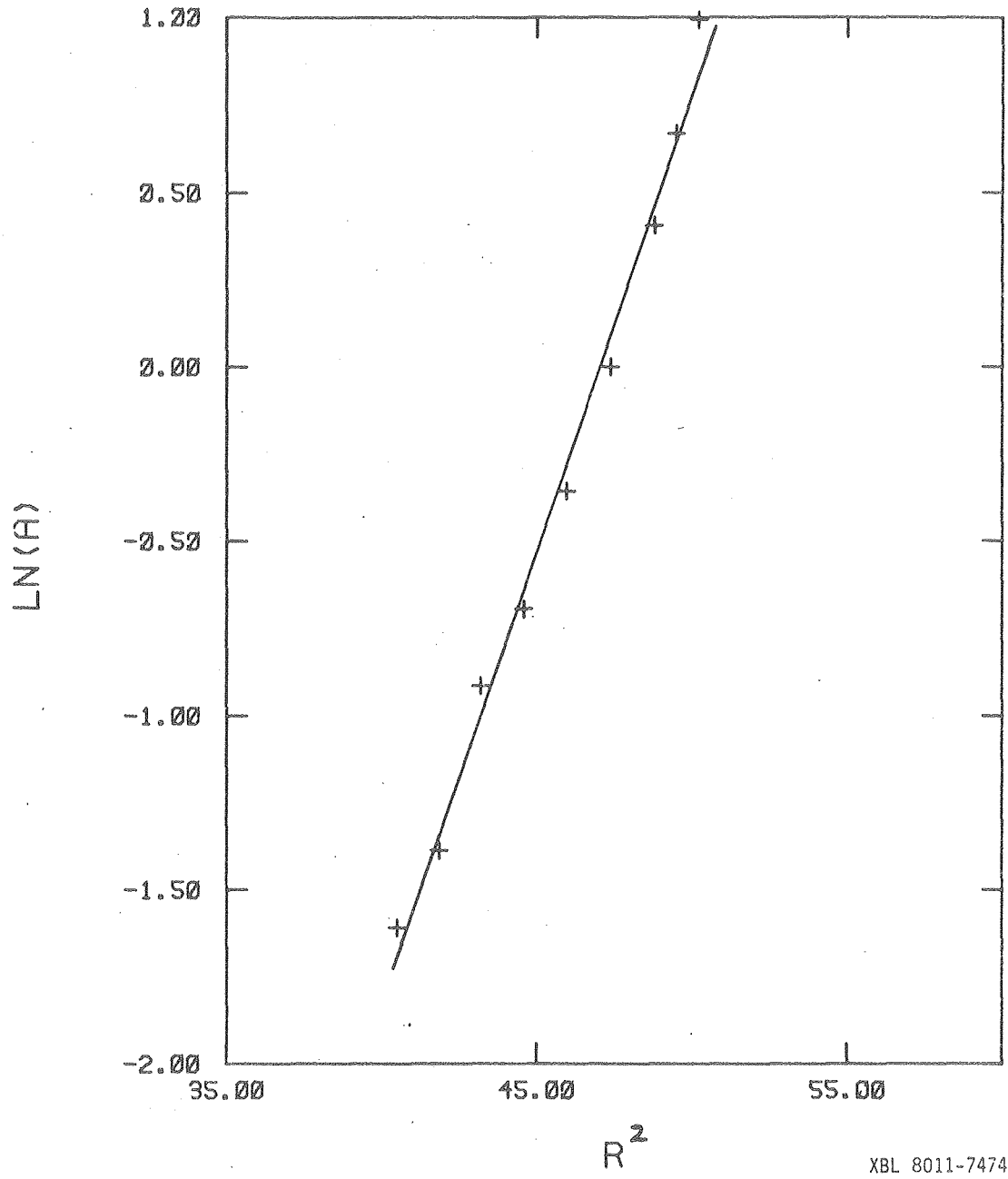
Figure 4.6. Induced CD of ethidium when bound to

rUpA, rCpG, or dCpG.

INDUCED CD OF ETHIDIUM BROMIDE WITH DIMERS

△ △ RIBO UPA
+ + RIBO CPG
◇ ◇ DEOXY CPG

WAVELENGTH (NM)

EPSILON LEFT - EPSILON RIGHT

XBL 795-9565

183
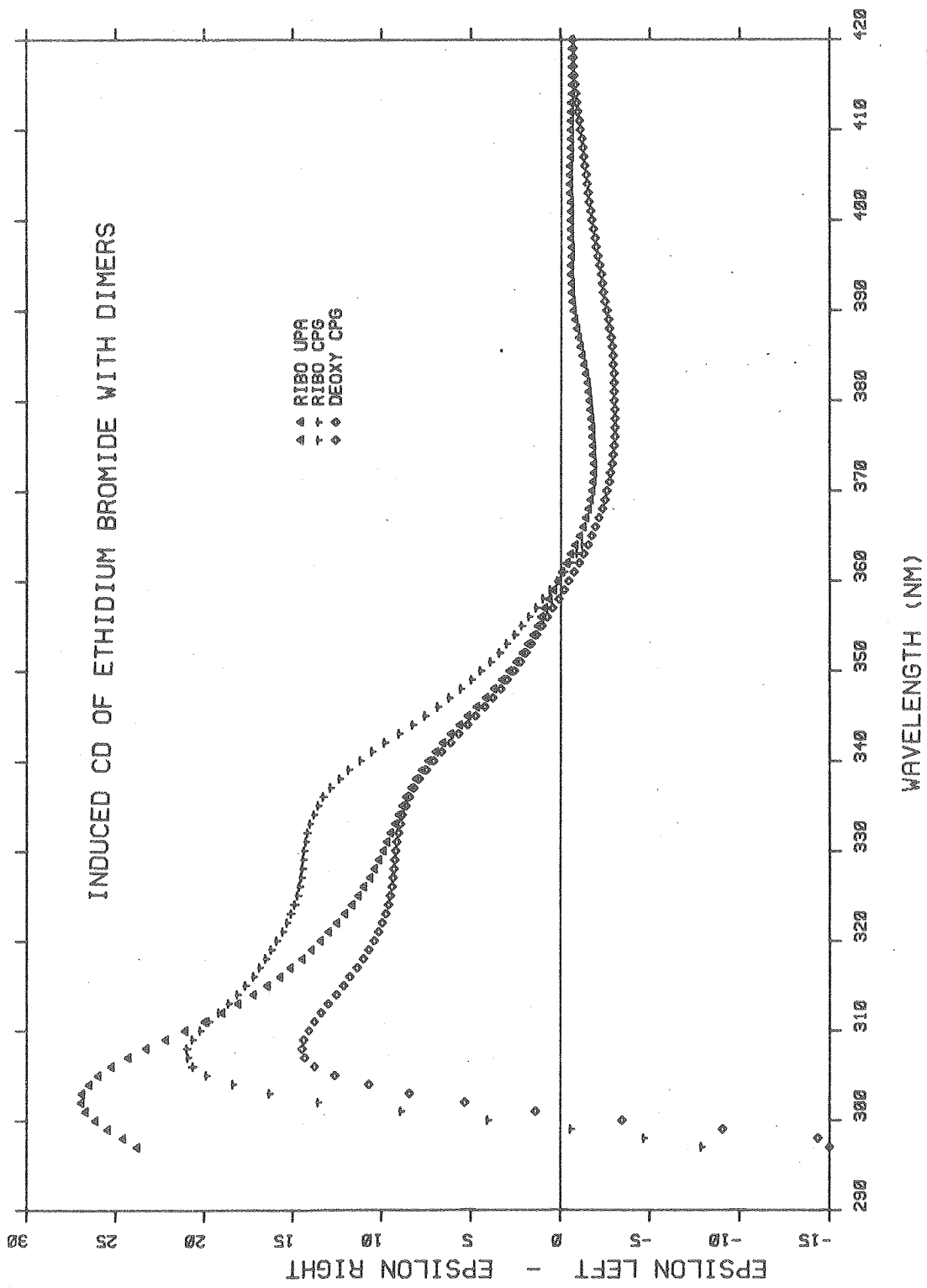
The maximum in the CD of ethidium is around 307 nm, and the $\Delta\varepsilon_{b307}$'s for the three dimer-ethidium complexes are slightly different, with rUpA being the largest and dCpG the smallest (see Figure 4.6). For a given dimer the calculated $\Delta\varepsilon_{b307}$ is fairly constant throughout the titration curve as seen in Table XV. This will be important when comparing the induced CD obtained from ethidium-dimer complexes with those from ethidium-DNA complexes.

Figure 4.7 shows the induced CD of ethidium upon binding to oligonucleotides with a bulge on one strand (rGpUpG + rCpC), and with bulges on both strands (rCpUpG). This data was taken and kindly provided by Ms. Barbara Dengler. The conditions are slightly different than those used in this study (no buffer or salt was added, pH = 7.0, and the ratio was 2:1 nucleotides:ethidium) so the equilibrium constants obtained earlier are probably not valid here. The epsilon left - epsilon right in Figure 4.7 is not per ethidium bound and therefore not comparable with that in Figure 4.6. The shapes of the induced CD for rGpUpG + rCpC + Et. and rCpUpG + Et. are very similar to those of the dinucleosides with ethidium shown in Figure 4.6. This indicates that the property of the oligonucleotides which causes the induced CD is present in complexes with bulges as well as those with perfect helices.

TABLE XV

MAGNITUDE OF THE INDUCED CD OF ETHIDIUM AT 307 nm DURING

TITRATION CURVE

rCpA 0°C

dCpG 0°C

[rCpG] mM	α	$\Delta\epsilon_b$ 307 M^{-1} cm^{-1}		[dCpG] mM	α	$\Delta\epsilon_{b307}$ $M^{-1} cm^{-1}$
0.13	0.47	28		0.35	0.49	12.6
0.20	0.67	24		0.5	0.67	13.2
0.27	0.80	24		0.70	0.79	11.5
0.4	0.91	22.5		1.0	0.89	15.2
1.0	0.99	23.5		2.0	0.98	14.4
2.0	1.00	23.3		3.0	0.99	11.8

Figure 4.7. Induced CD of ethidium when bound
to rCpUpG, rGpUpG + rCpC, rGpUpG, or rUpG.

CD OF ETBR + NUCLEOTIDES, T=0 DEGREES

WAVELENGTH (NANOMETERS)

EPSILON LEFT - EPSILON RIGHT

———— GUG + CC + ETBR
— — — CUG + ETBR
- - - - GUG + ETBR
.... UG + ETBR
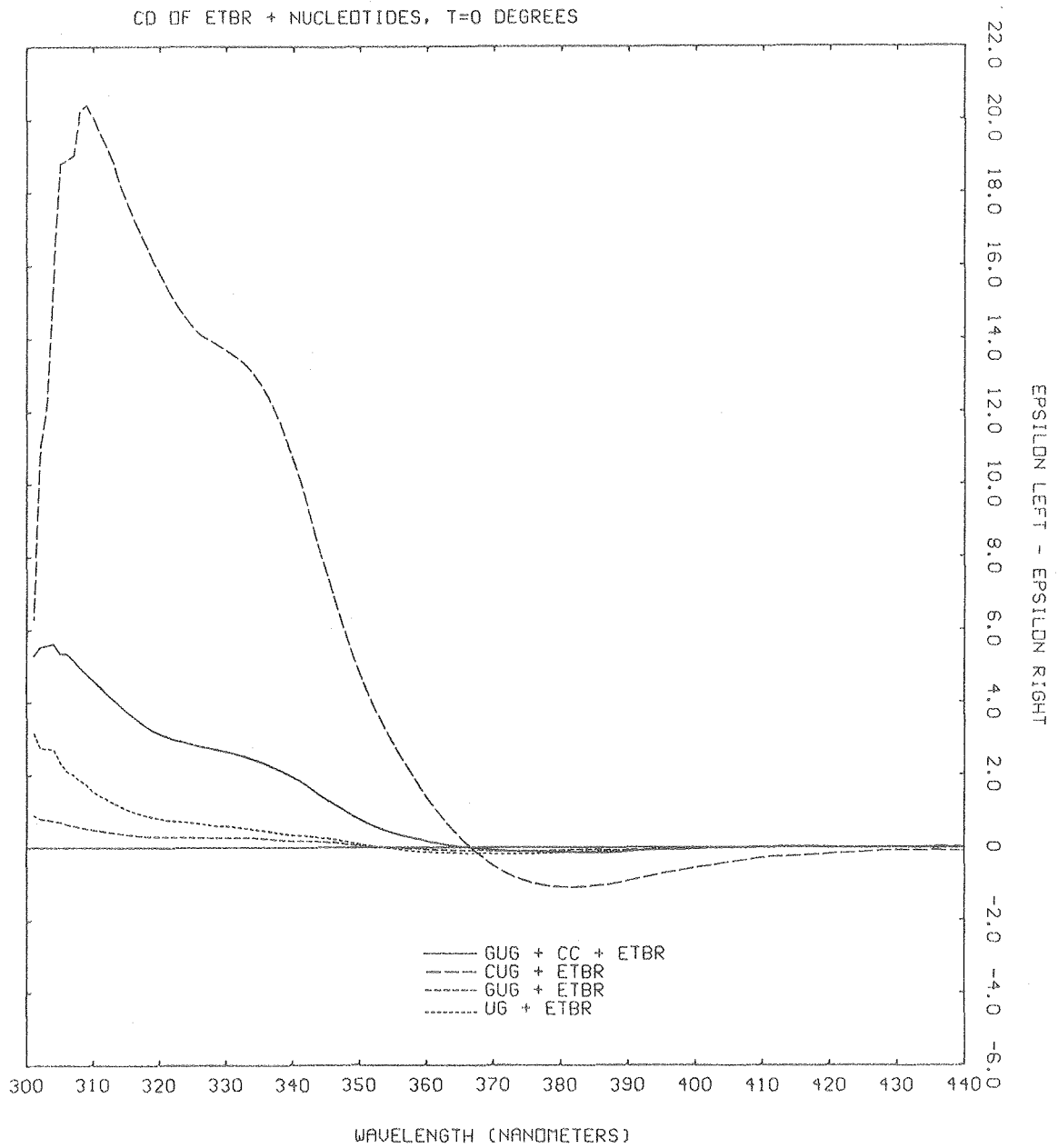
XBL 784-8169

H)   Induced CD of Ethidium upon Binding to E. coli DNA

The CD of ethidium upon binding to DNA has been thoroughly studied in the past.[79,80] The magnitude of the CD per ethidium bound at 307 nm ($\Delta\varepsilon_{b307}$) changes with r, the amount of ethidium bound per phosphate, in the same manner for many different types of DNA.[80] The reason for this change is not known but proposed mechanisms will be discussed later. In order to study this phenomenon we tried to perturb the system in such a manner that, for a set value of r, we obtain a change in the $\Delta\varepsilon_{b307}$ for the ethidium. An experiment such as this was done by Aktipis and Kindelis but they found no effect on the change of the value of $\Delta\varepsilon_{b307}$ with r when the salt concentration was changed from 40 mM to 5 M NaCl.[81] Thus, higher salt concentrations do not seem to affect the behavior of the induced CD. Here we chose to lower the salt concentration to see how this affected the induced CD of ethidium when bound to DNA. Figure 4.8 shows the CD of ethidium when bound to DNA under different conditions, and also compares these with the spectrum of ethidium when bound to the dimer rCpG. The two curves for the 50 - 500 mM Na^{+} salt range show the variation in $\Delta\varepsilon_{b307}$ with r. From comparing the 0.6 mM and 50 - 500 mM Na^{+} curves with the same values of r, we see that the magnitude of $\Delta\varepsilon_{b307}$ is much larger for the low salt curve. This means that by changing the amount of salt in solution, we have changed the value of

Figure 4.8. Induced CD of ethidium binding to
rCpG or E. coli DNA. The amount of ethidium
bound per phosphate, r, was obtained by
looking at the visible absorption of the
ethidium and from knowing the total amount
of DNA in the sample. The ethidium was essen-
tially all bound in these samples with DNA.
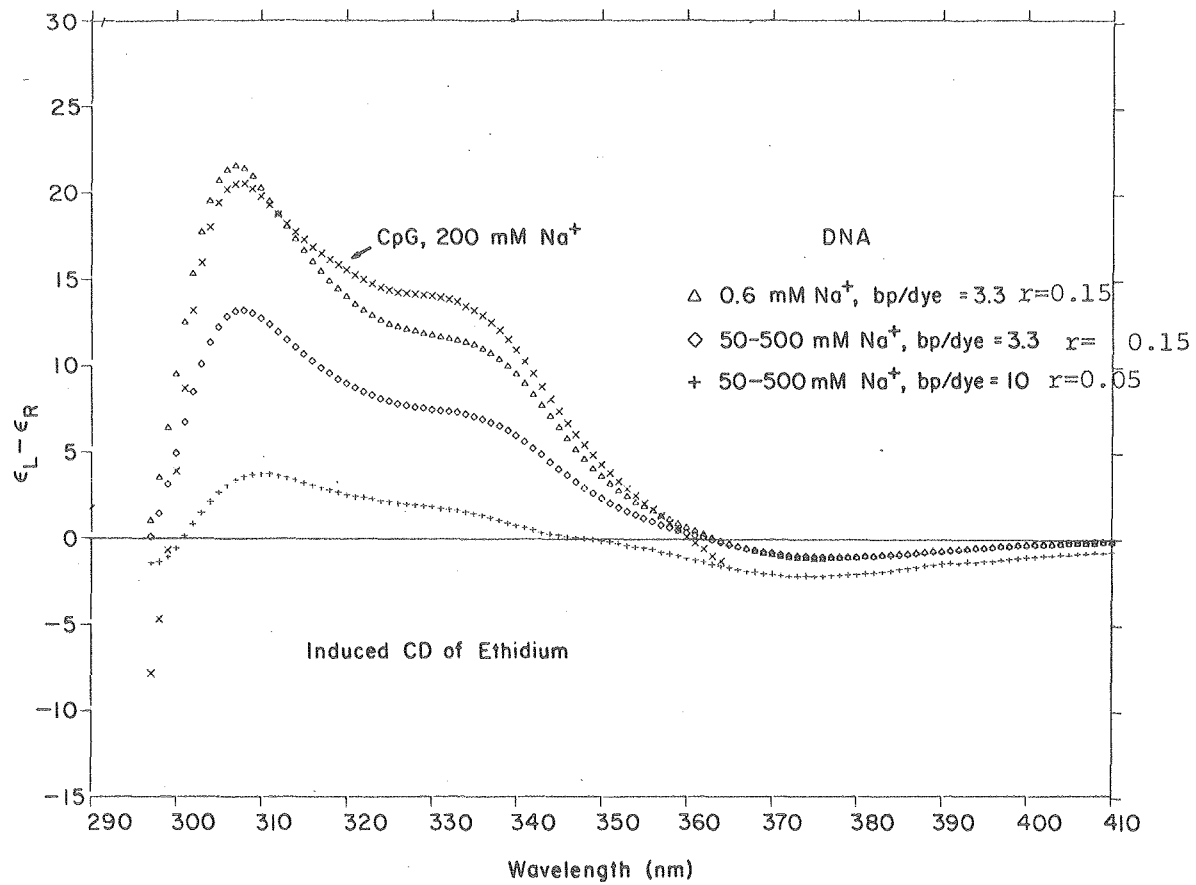
XBL 793-8897

$\Delta \varepsilon_{b307}$ without changing r. Therefore the amount of ethidium bound per phosphate (r) is not the only important parameter in the magnitude of the induced CD of ethidium when bound to DNA.

Comparison of the CD spectra of E. coli DNA without ethidium in 50 mM and 0.6 mM sodium ion, shows changes in the magnitude and shapes of the two curves. There was approximately a 15% decrease in the measured ellipticity at 257 nm in going from the 50 mM to 0.6 mM sodium ion. This difference is probably due to changes in the conformation of the DNA, which may be an important factor in the behavior of the induced CD of ethidium when bound to DNA.

4.   DISCUSSION AND CONCLUSIONS

A)   Thermodynamics of Ethidium Binding to Oligonucleotides

Ethidium has been studied in complexes with dinucleoside monophosphates,[72,77] and dinucleotide diphosphates,[82] by spectroscopic methods. These studies found that minihelices of two dimers per one ethidium were formed in solution. They also found that many of the properties of ethidium when bound in these dimer complexes were similar to those when ethidium intercalates in DNA. A sequence dependence for ethidium binding was found where ethidium prefers to bind to pyrimidine (3'-5') purine sites compared to purine (3'-5') pyrimidine sites.[72]

In this study we were able to measure the equilibrium constants and $\Delta H°$ values for ethidium binding in a complex which has a stoichiometry of two oligonucleotides and one ethidium. The equilibrium constants at 0°C were measured with the strength of the complex being

$$rCpG > dCpG > rCpUpG \approx rUpA > rGpUpG + rCpC.$$

There is a sequence dependence of the binding, with the rCpG complex having a much higher equilibrium constant than the rUpA. At least part of this difference is due to the lower stability of the A·U base pairs compared to the C·G base pairs. We also saw an order of magnitude higher K for binding of ethidium to the ribose dimer CpG compared to the deoxyribose dimer CpG. This difference may reflect the lower stability of deoxy C·G base pairs compared to ribose C·G base pairs.

A complex of ethidium with oligonucleotides which can form a bulge on one strand (rGpUpG + rCpC) was found to have a much smaller equilibrium constant than the rCpUpG-ethidium complex, which can form bulges on both strands. The rCpUpG complex is still much less stable than the perfect helix rCpG. All these oligonucleotides are too unstable to measure their equilibrium constants in the

absence of ethidium. Thus it is not possible to tell if the differences in the strength of the ethidium-oligonucleotide complexes are due to differences in the stability of the oligonucleotide helices themselves, or the strength of ethidium binding to that particular helix.

B)   Induced Circular Dichroism of Ethidium

Ethidium is not optically active and hence has no intrinsic CD. A large positive CD from 300 - 360 nm for ethidium has been observed upon binding to DNA.[79] For this wavelength range the magnitude of the CD per ethidium bound has been shown to increase dramatically with the amount of ethidium bound.[80,81] A maximum is reached at an r value of 0.25, which is the neighbor exclusion limit for dye binding to DNA. This means that the magnitude of the induced CD for an individual ethidium molecule is dependent on how many other ethidiums are also bound to the nucleic acid. Several mechanisms have been proposed for this induced CD of ethidium upon binding to the DNA.[79,73] One proposal involves a direct interaction between two or more ethidium molecules bound in neighboring sites. Exciton interactions between the transition moments of these ethidiums bound in close proximity, will give rise to a conservative CD for this band. The change in $\Delta\varepsilon_{b307}$ with r is just a reflection of the fact that more dye molecules are closer together at higher r values.

The second model states that increasing number of ethidium molecules alter the environment of other dye molecules bound nearby, by changing the local DNA conformation. Thus the change in the $\Delta\varepsilon_{b307}$ for ethidium with r would be due to changes in the conformation of the ethidium-DNA complex. For this model the induced CD could arise from the assymetry of the binding site, or from the exciton interactions between the ethidium and the aromatic base transition moments.[79]

To get a better understanding of the induced CD of ethidium we have studied its binding to oligonucleotides and to DNA (as seen in Figures 4.6 - 4.8). The $\Delta\varepsilon_{b307}$ for the rCpG complex is 24 ± 2.5 $M^{-1}cm^{-1}$, whereas Aktipis and Kindelis found this value to be 25, for calf thymus DNA at an r value of 0.25.[83] The earlier discussion on the dimer-ethidium complexes showed that they existed in solution as complexes of two dimers to one ethidium. The equilibrium sedimentation studies showed that there was no aggregation of these complexes, so the induced CD with the dimers arises from only one ethidium interacting with two dimers. The induced CD of the ethidium upon binding to dimers or DNA therefore cannot originate from dye-dye interactions.

As discussed earlier, the induced CD of ethidium may arise from base-dye interactions. Evidence against this mechanism comes from the similar induced CD of ethidium in

complexes of rUpA and rCpG. If the major cause of the CD
is from the coupling of the transition dipoles of the
ethidium and the bases, then we might expect quite
different spectra for these two dimers which have no bases
in common.

The induced CD may simply be a function of the con-
formation of the DNA around the ethidium binding site. We
cannot rule out this possibility, by making this hypothesis
our results indicate that the conformation of the ethidium-
dimer complexes would be similar to the conformation of
the ethidium when it is bound to DNA near the neighbor
exclusion limit.

The interaction of the amino groups on the ethidium
with the phosphates in the nucleic acids, may be an important
contribution to the induced CD of the ethidium. Molecular
orbital calculations on ethidium have shown that the major
contribution to the large red shift in the visible absorbance
of ethidium is the interaction of the ethidium with the
charged phosphates.[84] The induced CD of ethidium upon
binding to E. coli DNA changed by going to very low salt
(where the charge on the phosphates may be different than
at higher salt levels).[85] This indicates interaction of
ethidium with the charged phosphates may be important in the
induced CD of ethidium when bound to nucleic acids. These
questions and others are presently being pursued by Mr.
Kenneth Dahl, who I wish to thank for providing valuable advice
and help on this project.

APPENDIX I

NMR STUDY OF A DOUBLE HELIX WITH A MISMATCHED BASE

The imino proton region of the helix $dCA_5G + dCT_6G$ was observed from 1 - 15°C. These molecules can form a double helix with a bulged thymine on one strand. If the C·G base paris on both strands are formed, then we would expect to see their imino protons in the NMR spectrum. What was observed for this helix was a broad peak for all the A·T imino protons, and another very broad, much smaller, peak at higher field presumably due to C·G protons. This is illustrated in Figure I.1, which gives the spectra for the perfect helix $dCA_5G + dCT_5G$ and the mismatched helix $dCA_5G + dCT_6G$. The spectrum of the mismatched helix shows that both C·G base protons are not formed, and is indicative of dangling ends on this helix (the structure of a dangling end is shown above the spectrum in Figure I.1). Since the bulge did not seem to form, even at 1°C, we tried to stabilize that structure by changing the conditions in solution. The sample was run in a mixture of 1:2 methanol:H_2O (v/v) at -20°C. Essentially no change in the spectrum was observed. Other conditions attempted were, 1 M NaCl, 1°C; 1 M NaCl + 5 mM Mg^{2+} in H_2O, and 1 mM spermidine in our standard buffer at 1°C. In none of these experiments were we able to observe a spectrum which had two C·G imino protons, which indicates

Figure I.1 Comparison of the imino proton region
of a perfect helix, $dCT_5G + dCA_5G$, and a
helix which has a mismatched base on one
strand, $(dCA_5G + dCT_6G)$.

IMINO PROTONS

XBL 808-11278

that we were not getting a helix with a bulged thymine. The bulged structure must be energetically less favorable than the dangling end in this helix. Studies on helices which can form a bulge, but not a dangling end, will be attempted in the future.

APPENDIX II

COMPUTER PROGRAMS

Computer programs were written in Fortran on the Vax

system at the Laboratory of Chemical Biodynamics.

WIDTH2 calculates the lineshape of a two state system

with exchange between the two states. The input parameters

are the chemical shifts, the linewidths, and the lifetimes

of the two states. The program will then calculate the

chemical shift of the largest peak and its linewidth. It

will also plot the whole spectrum using a program called

PLOT (Mr. David Keller).

ITWIDT is a program similar to WIDTH2, but it also

finds the best fit for the experimental and calculated

chemical shift for a two state system. It does this by

varying the mean exchange lifetime of the system, for a

given population, until the best fit between the calculated

and experimental results are obtained.

ITWIDT

```
c       This program is similar to the WIDTH2 program and the documentation
c       for WIDTH2 explains most of the parameters needed here.  The
c       difference is that ITWIDT will vary the mean lifetime (tau) of
c       the two state system until the best fit between the experimental
c       and calculated chemical shift are found.  It does this for
c       a given population and where all the other parameters are fixed.
c       Thus it will increment the population of the two states, and
c       find the lifetime which gives the best fit between the experimental
c       and calculated chemical shift of the largest peak in the spectrum.
c
c
c
c
c
c


        COMMON V,DELTA,DELTAA,DELTAB,T2A,T2B,POPA,POPB,DMAX,TMAX,PI
        DIMENSION V(5000),TTAU(400)
        DOUBLE PRECISION DELTA(5000),TAU
111     CONTINUE
        TYPE *,'THE TEMPERATURE IS =  (I3)'
        READ 110, ITEMP
        TYPE *,'THE MINIMUM POPULATION OF STATE A IS        POPAMIN=  (F5.2)'
        READ 200,POPAMIN
        TYPE *,'THE MAXIMUM POPULATION OF STATE A IS        POPAMAX=  (F5.2)'
        READ 200, POPAMAX
        TYPE *,'THE INTERVAL FOR CALCULATING THE POPULATION = (F5.2)'
        READ 200, THEIN
        TYPE *,'THE CHEMICAL SHIFT OF A IS     DELTAA=  (F10.3) IN HZ'
        READ 300,DELTAA
        TYPE *,'THE CHEMICAL SHIFT OF B IS     DELTAB=  (F10.3) IN HZ'
        READ 300,DELTAB
        TYPE *,'THE EXPERIMENTAL CHEMICAL SHIFT IS = (F10.3) IN HZ'
        READ 300,EXMAX
        TYPE *,'LINEWIDTH OF STATE A IS EQUAL TO      (E12.5)'
        READ 100,T2A
        TYPE *,'LINEWIDTH OF STATE B IS EQUAL TO      (E12.5)'
        READ 100,T2B
        PI=3.141592
        T2=T2*PI
        DELTA(1)=(DELTAA + DELTAB)/2. - 200.
        ID=INT(DELTA(1))
        DELTA(1)=FLOAT(ID)
        DO 50 I=2,4000
        DELTA(I)=DELTA(I-1) + 0.1
50      CONTINUE
        POPA=POPAMIN - THEIN
        WRITE(2,510)ITEMP
        WRITE(2,700)DELTAA,DELTAB
        WRITE(2,710)EXMAX
        WRITE(2,800)T2A/PI
        WRITE(2,801)T2B/PI
        WRITE(2,860)
        DO 1100 J=1,(POPAMAX-POPAMIN)/THEIN +1
        POPA=POPA + THEIN
        POPB=1.-POPA
        TAUMAX=ABS(40./(2.*PI*(DELTAA - DELTAB)))
        TAUMIN=ABS(0.05/(2.*PI*(DELTAA - DELTAB)))
1150    CONTINUE
        SIN=ABS((LOG10(TAUMAX)-LOG10(TAUMIN))/20.)
        IF (TAUMAX .GT. TAUMIN ) THEN
                XY=TAUMIN
        ELSE
```

```
             XY=TAUMAX
          END IF
          TTAU(1)=LOG10(XY)
          DMAX1=1000.
          DMAX2=2000.
          TAU1=XY
          DO 1111 M=1,20
          TTAU(M +1)=TTAU(M) + SIN
          TAU=10.**TTAU(M)
          CALL GETMAX(TAU)
          X=ABS(DMAX-EXMAX)
          IF (X .LT. DMAX1) THEN
             DMAX2=DMAX1
             DMAX1=X
             TAU2=TAU1
             TAU1=TAU
             GO TO 1111
          END IF
          IF(X .LT. DMAX2) THEN
             DMAX2=X
             TAU2=TAU
          END IF
1111      CONTINUE
          X2=ABS(TAU1-TAU2)
          X3=ABS(0.01*TAU1)
          IF (X3 .GT.X2) GO TO 1090
1110      CONTINUE
          TAUMAX=TAU1
          TAUMIN=TAU2
          GO TO 1150
1090      CONTINUE
          TAU=TAU1
          CS=POPA*T2B +POPB*T2A
          DO 60 I=1,4000
          SP=TAU*(T2A*T2B - (PI*(DELTAA + DELTAB) -2.*PI*DELTA(I))**2 +
     2    (PI*(DELTAA - DELTAB))**2) + POPA*T2A + POPB*T2B
          SQ=TAU*(PI*(DELTAA + DELTAB) - 2.*PI*DELTA(I) - (POPA -
     2      POPB)*PI*(DELTAA - DELTAB))
          SR=(PI*(DELTAA+DELTAB)-2.*PI*DELTA(I))*(1.0+TAU*(T2B+T2A))
     2      + (POPA -POPB)*(DELTAA - DELTAB)*PI +
     3    TAU*PI*(DELTAA-DELTAB)*(T2B-T2A)
          V(I)=((1. + TAU*CS)*  SP + SQ*SR)/(SP**2 + SR*SR)
60        CONTINUE
          V(1)=0.
          DO 190 I=2,4000
          IF (V(I) .GT. TMAX) THEN
             TMAX=V(I)
             DMAX=DELTA(I)
          END IF
190       CONTINUE
          SNEARZ=1000.
          DO 210 I=1,4000
          IF (ABS(TMAX/2.-V(I)) .LT. SNEARZ) THEN
             HMAX=DELTA(I)
             SNEARZ=TMAX/2-V(I)
          END IF
210       CONTINUE
          EXCH=ABS(2.*PI*(DELTAA-DELTAB)*TAU)
          WIDTH=ABS((DMAX-HMAX)*2.)
          POPAMX=(DMAX -DELTAB)/(DELTAA-DELTAB)
          POPBMX= 1. -POPAMX
          WRITE(2,500)POPA,TAU,DMAX,WIDTH,POPAMX,EXCH
1100      CONTINUE
```

```
710      FORMAT('   THE EXPERIMENTAL CHEMICAL SHIFT IS = 'F10.3)
800      FORMAT('   INTRINSIC LINEWIDTH OF PEAK A IS EQUAL TO = 'E12.5)
801      FORMAT('   INTRINSIC LINEWIDTH OF PEAK B IS EQUAL TO = 'E12.5)
100      FORMAT(E12.5)
110      FORMAT(I3)
112      FORMAT(////////////)
200      FORMAT(F5.2)
300      FORMAT(F10.3)
500      FORMAT(10X,F5.2,T30,E10.2,T45,F7.1,13X,F7.1,18X,F5.2,T110,F8.2)
510      FORMAT('   THE TEMPERATRUE OF THIS  DATA SET IS 'I3)
700      FORMAT('   THE CHEMICAL SHIFT OF STATE A IS = ',F8.2,/
      2  '   THE CHEMICAL SHIFT OF STATE B IS = ',F8.2)
860      FORMAT(///,T10,'INPUT POPULATION',T30,'CALCULATED ',T45,
      2  'CALCUALTED',T65,'CALCULATED WIDTH',T85,'CACULATED POPULATION',
      3  T115,'EXCHANGE ',/,T12,'OF STATE A ',T35,'TAU',T50,
      4  'MAX',T88,'OF STATE A',T115,'PARAMETER'/)
         WRITE(2,112)
         TYPE *,'DO YOU WANT TO ENTER ANOTHER DATA SET? 1=YES,2=NO'
         READ 110,IN
         IF (IN .EQ. 1) GO TO 111
         END
C
C
C
C
C
         SUBROUTINE GETMAX(TAU)
         DIMENSION V(5000)
         DOUBLE PRECISION DELTA(5000)
         COMMON V,DELTA,DELTAA,DELTAB,T2A,T2B,POPA,POPB,DMAX,TMAX,PI
         CS=POPA*T2B +POPB*T2A
         DO 60 I=1,4000,10
         SP=TAU*(T2A*T2B - (PI*(DELTAA + DELTAB) -2.*PI*DELTA(I))**2 +
      2  (PI*(DELTAA - DELTAB))**2) + POPA*T2A + POPB*T2B
         SQ=TAU*(PI*(DELTAA + DELTAB) - 2.*PI*DELTA(I) - (POPA -
      2  POPB)*PI*(DELTAA - DELTAB))
         SR=(PI*(DELTAA + DELTAB)-2.*PI*DELTA(I))*(1.0+TAU*(T2B+T2A))
      2   + (POPA -POPB)*(DELTAA - DELTAB)*PI + TAU*PI*(DELTAA-DELTAB)
      3  * (T2B-T2A)
         V(I)=((1. + TAU*CS)*SP + SQ*SR)/(SP**2 + SR*SR)
60       CONTINUE
         TMAX=0.0
         DO 190 I=1,4000,10
         IF (V(I) .GT. TMAX) THEN
             TMAX=V(I)
             DMAX=DELTA(I)
         END IF
190      CONTINUE
         RETURN
         END
```

WIDTH2

```
c     This program calculates the line shape of nmr lines when there is
C     chemical exchange between two states.  The equation and theory
C     used are from HIGH RESOLUTION NUCLEAR MAGNETIC RESONANCE by Pople
C     Schneider, and Berstein, page 222.
C
C
C
C
C            The parameters which you must enter are the chemical shifts
C     of the two states, the population of the two states, the average
C     T2 of the two states(this derivation assumes that both T2's are
C     the same), and the lifetimes of the two states.
C            It then calculates the lineshapes of the peaks for an area
C     which is plus or minus 200 Hz of the average chemical shifts of
C     the two resonances.  Therefore if the chemical shifts of the two
C     states differ by much more than 350 Hz or so, this program should
C     be modified to account for this large area.  The program outputs
C     a file by the name FOR002.DAT;(and some file extension) which has
C     the intensity of the peak over the chemical shift range designated
C     One can then set up a plot file and plot the data if so desired.
C
C
C
C
C     The plot program is called PLOT
      DIMENSION V(5000)
      DOUBLE PRECISION DELTA(5000)
      TYPE *,'THE TEMPERATURE IS =   (I3)'
      READ 110, ITEMP
      TYPE *,'THE VALUE OF tauA IS =    (E12.5)'
      READ 100,TAUA
      TYPE *,'THE VALUE OF TAUB IS =   (E12.5)'
      READ 100,TAUB
      TYPE *,'THE POPULATION OF STATE A IS      POPA=  (F5.2)'
      READ 200,POPA
      TYPE *,'THE CHEMICAL SHIFT OF A IS    DELTAA=  (F10.3) IN HZ'
      READ 300,DELTAA
      TYPE *,'THE CHEMICAL SHIFT OF B IS    DELTAB=  (F10.3) IN HZ'
      READ 300,DELTAB
      TYPE *,'INTRINSIC LINEWIDTH OF PEAK A  IS EQUAL TO   (E12.5)'
      READ 100,T2A
      TYPE *,'INTRINSIC LINEWIDTH OF PEAK B IS EQUAL TO   (E12.5)'
      READ 100,T2B
      TAU=TAUA*TAUB/(TAUA+TAUB)
      PI=3.141592
      POPB=1.-POPA
      SUME=0.0
      T2A=PI*T2A
      T2B=PI*T2B
      DELTA(1)=(DELTAA + DELTAB)/2. - 200.
      ID=INT(DELTA(1))
      DELTA(1)=FLOAT(ID)
      DO 50 I=2,4000
      DELTA(I)=DELTA(I-1) + 0.10000
50    CONTINUE
      CS=POPA*T2B+POPB*T2A
      SUM=0.
      DO 60 I=1.4000
      SP=TAU*(T2A*T2B - (PI*(DELTAA + DELTAB) -2.*PI*DELTA(I))**2 +
     2(PI*(DELTAA - DELTAB))**2) + POPA*T2A +POPB*T2B
      SQ=TAU*(PI*(DELTAA + DELTAB) - 2.*PI*DELTA(I) - (POPA -
     2 POPB)*PI*(DELTAA - DELTAB))
      SR=(PI*(DELTAA + DELTAB) - 2.*PI*DELTA(I))* (1.0 + TAU*(T2A+T2B))
```

```
      2      + (POPA -POPB)*(DELTAA - DELTAB)*PI + TAU*PI*(DELTAA-DELTAB)*
      3     (T2B-T2A)
             V(I)=((1. + TAU*CS)*SP + SQ*SR)/(SP**2 + SR*SR)
60           CONTINUE
             DO 70 I=1,3999
             SUM=SUM + (V(I) + V(I+1))/2.*0.1
70           CONTINUE
             TK=SUM
             DO 80 I=1,4000
             V(I)=V(I)*100./SUM
80           CONTINUE
             WRITE(2,600) (DELTA(I),V(I), I=1,4000,10)
             WRITE(9,601) (DELTA(I),V(I), I=1,4000,10)
             DO 90 I=1,3999
             SUME=SUME + (V(I)+V(I+1))/2.*0.1
90           CONTINUE
             V(1)=0.
             DO 190 I=2,4000
             IF (V(I) .GT. TMAX) THEN
                TMAX=V(I)
                DMAX=DELTA(I)
                IM=I
             END IF
190          CONTINUE
             SNEARZ=1000.
             DO 210 I=IM,IM+500
             IF (ABS(TMAX/2.-V(I)) .LT. SNEARZ) THEN
                HMAX=DELTA(I)
                SNEARZ=ABS(TMAX/2-V(I))
             END IF
             IF (SNEARZ .LT. 0.01*TMAX) GO TO 2100
210          CONTINUE
2100         CONTINUE
             WIDTH= ABS((DMAX-HMAX)*2.)
             POPAMX=(DMAX - DELTAB)/(DELTAA-DELTAB)
             POPBMX= 1. -POPAMX
             WRITE(2,510)ITEMP
             WRITE(2,400)TAUA,TAUB
             WRITE(2,500)POPA,POPB
             WRITE(2,700)DELTAA,DELTAB
             WRITE(2,660)WIDTH, DMAX
             WRITE(2,670)POPAMX,POPBMX
             WRITE(2,800)T2A/PI
             WRITE(2,801)T2B/PI
             WRITE(9,510)ITEMP
             WRITE(9,400)TAUA,TAUB
             WRITE(9,500)POPA,POPB
             WRITE(9,700)DELTAA,DELTAB
             WRITE(9,660)WIDTH,DMAX
             WRITE(9,670)POPAMX,POPBMX
             WRITE(9,800)T2A/PI
             WRITE(9,801)T2B/PI
400          FORMAT(//' THE ABOVE DATA IS FOR THE FOLLOWING PARAMETERS'///
      2     ' The value of tauA is = 'E12.5/' The value of tauB is = '
      3     E12.5)
500          FORMAT(//' The population of state A is ='F5.2/
      2     ' The population of state B is ='F5.2)
700          FORMAT(//' The chemical shift of A is ='F10.3' Hz'/
      2     ' The chemical shift of B is ='F10.3' Hz')
800          FORMAT(' THE INTRINSIC LINEWIDTH OF STATE A IS EQUAL TO ='E12.5)
801          FORMAT(' THE INTRINSIC LINEWIDTH OF STATE B IS EQUAL TO ='E12.5)
601          FORMAT(1X,F10.5,F13.5)
600          FORMAT(410(6(1X,F6.1,3X,F5.2,4X),/))
```

```
100       FORMAT(E12.5)
110       FORMAT(I3)
200       FORMAT(F5.2)
300       FORMAT(F10.3)
660       FORMAT(///'  The width at half max of the largest peak is   'F6.2
      2   'Hz'/'  The chemical shift of the maximum of this peak is  '
      3   F6.1'Hz'  )
670       FORMAT(////'   If one assumes we are in fast exhcange and uses this
      2   chemical shift to calcualte the populations you get:'
      3   /'  The calculated population of state A is =   'F5.2
      4   /'  The calculated population of state B is =   'F5.2)
510       FORMAT('   THE TEMPERATRUE OF THIS  DATA SET IS  'I3)
          END
```

REFERENCES

1. Watson, J.D. and Crick, F.H.C. (1953) Nature 171, 964.

2. Arnott, S., Fuller, W., Hodgson, A. and Prutton, I. (1968) Nature 220, 561.

3. Arnott, S., Chandrasekaran, R. and Selsing, E. (1975), in Structure and Conformations of Nucleic Acids and Protein-Nucleic Acid Interactions (Sundaralingam, M. ED.) pp 577-796, University Park Press, Baltimore, MD.

4. Bloomfield, V.A., Crothers, D.M. and Tinoco, I., JR. (1974) Physical Chemistry of Nucleic Acids, pp 339-342, Harper and Row, New York.

5. Giessner-Prettre, C. and Pullman, B. (1970) J. Theor. Biol. 27, 87.

6. Robillard, G.T. and Reid, B.R. (1979) in Biological Applications of Magnetic Resonance (Shulman, R.G., Ed.) pp 45-112, Academic Press, New York.

7. Kearns, D.R. (1977) in Annual Review of Biophysics and Bioengineering (Mullins, L.F., Hagins, W.A., Stryer, L. and Newton, C. eds.), Vol. 6, pp 477-503, Academic Press, London.

8. Lee, C.H., Ezra, F.S., Kondo, N.S., Sarma, R.H. and Danyluk, S.S. (1976), Biochemistry 15, 3627.

9. Ezra, F.A., Lee, C.H., Kondo, N.S., Danyluk, S.S. and Sarma, R.H. (1977) Biochemistry 16, 1977.

10. Karplus, M. (1959) J. Chem. Phys. 30, 11.

11. McCann, J., Choi, E., Yamasaki, E. and Ames, B.N. (1975) Proc. Nat. Acad. Sci. 72, 5135.

12. Streisinger, G., Okada, Y., Emrich, J., Newton, J., Tsugita, A., Terzaghi, E. and Inouye, M. (1966) Cold Spring Harbor Symposium on Quantitative Biology 31, 77.

13. Arter, D.B., Walker, G.C., Uhlenbeck, O.C. and Schmidt, P.G. (1974) Biochem. Biophys. Res. Commun. 61, 1089.

14. Heller, M.J., Anthony, T.T., and Maciel, G.E. (1974) Biochemistry 13, 1623.

15. Borer, P.N., Kan, L.S., and Ts'o, P.O.P. (1975) Biochemistry 14, 4847.

16. Hughes, D.W., Bell, R.A., England, T.E. and Neilson, T. (1978) Can J. Chem. 56, 2243.

17. Cross, A.D. and Crothers, D.M. (1971) Biochemistry 10, 4015.

18. Patel, D.J. (1974) Biochemistry 13, 2396.

19. Kallenbach, N.R., Daniel, W.E., Jr. and Kaminker, M.A. (1976) Biochemistry 15, 1218.

20. Early, T.A., Kearns, D.R., Burd, J.F., Larson, J.E. and Wells, R.D. (1977) Biochemistry 16, 541.

21. Milman, G., Langridge, R., and Chamberlin, M.J. (1967) Proc. Natl. Acad. Sci. 57, 1804.

22. Selsing, E., Wells, R.D., Early, T.A. and Kearns, D.R. (1978) Nature 21, 249.

23. Geerdes, H.A.M. and Hilbers, C.W. (1977) Nucl. Acids Res. 4, 207.

24. Martin, F.H. and Tinoco, I., JR. (1980) Nucl. Acids Res. 8, 2295.

25. Martin, F.H., Uhlenbeck, O.C. and Doty, P. (1971) J. Mol. Biol. 57, 201.

26. Patel, D.J. (1979) Eur. J. Biochem. 96, 267.

27. Patel, D.J. (1975) Biochemistry 14, 3984.

28. Khorang, H.G. (1968) Pure Appl. Chem. 17, 349.

29. Handbook of Biochemistry Selected Data for Molecular Biology 3rd Edition, CRC Press, pp 586.

30. Redifled, A.G., Kunz, S.D. and Ralph, E.K. (1975) J. Magn. Reson. 19, 114.

31. Ts'o, P.O.P., Barrett, J.C., Kan, L.S. and Miller, P.S. (1973) Ann. N.Y. Acad. Sci. 222, 290.

32. Cheng, D.M. and Sarma, R.H. (1977) J. Am. Chem. Soc. 99, 7333.

33. Chiao, Y.C.C. and Krugh, T.R. (1977) Biochem. 16, 747.

34. Dwek, R.A. (1973) Nuclear Magnetic Resonance in Biochemistry pp 213-326, London, Oxford University Press.

35. Barry, C.D., North, A.C.T., Glasel, J.A., Williams, R.J.P. and Xavier, A.V. (1971) Nature 232, 236.

36. Chan, S.I., Nelson, J.H., (1969) J. Am. Chem. Soc. 91, 168.

37. Lee, C.H., Tinoco, I., Jr. (1977) Biochem. 16, 5403.

38. Kearns, D.R. and Shulman, R.G. (1974) Acc. Chem. Res. 7, 33.

39. Sarma, R.H. (1980) Nucleic Acid and Geometry and Dynamics Pergamon Press, New York.

40. Kan, L.S., Borer, P.N. and Ts'o, P.O.P. (1975) Biochemistry 14, 4864.

41. Arter, D.B. and Schmidt, P.G. (1976) Nucl. Acids Res. 3, 1437.

42. Lee, C.H. and Tinoco, I., Jr. (1980) Biophys. Chem. 11, 283.

43. Ts'o, P.O.P., Kondo, N.S., Schweizer, M.P. and Hollis, D.P. (1969), Biochemistry 8, 997.

44. Nelson, J.W., Martin, F.H., and Tinoco, I., Jr., in preparation.

45. Gutowsky, H.S., and Holm, C.H. (1956), J. Chem. Phys. 25, 1228.

46. Kaplan, J.I. and Fraenkel, G. (1980) NMR of Chemically Exchanging Systems, pp 74-80, Academic Press, New York.

47. Altona, C., and Sundaralingam, M. (1973) J. Am. Chem. Soc. 95, 2333.

48. Porschke, D., and Eigen, M. (1971) J. Mol. Biol. 62, 361.

49. Ravetch, J., Gralla, J. and Crothers, D.M. (1973) Nucl. Acids Res. 1, 109.

50. Arnott, S. and Hukins, D.W.L. (1973) J. Mol. Biol. 81, 93.

51. Shum, B.W.K. (1977), Ph.D. Thesis, Yale University.

52. Feeney, J., Batchelor, J.G., Albrand, J.P. and Roberts, G.C.K. (1979) J. Magn. Reson. 33, 519.

53. Hilbers, C.W. (1979) in Biological Applications of Magnetic Resonance (Shulman, R.G., Ed.) pp 1-44, Academic Press, New York.

54. Patel, D.J. and Hilbers, C.W. (1975) Biochemistry 14, 2651.

55. Hilbers, C.W. and Patel, D.J. (1975) Biochemistry 14, 2657.

56. Crothers, D.M., Cole, P.E., Hibers, C.W. and Shulman, R.G. (1974) J. Mol. Biol. 87, 63.

57. Englander, J.J., Kallenbach, N.R. and Englander, S.W. (1972) J. Mol. Biol. 63, 153.

58. Teitelbaum, H. and Englander, S.W. (1975) J. Mol. Biol. 92, 55.

59. Teitelbaum, H. and Englander, S.W. (1975) J. Mol. Biol. 92, 79.

60. Kallenbach, N.R. (1980) in Nucleic Acid Geometry and Dynamics (Sarma, R.H. Ed.), pp 231-255, Pergamon Press, New York.

61. Waelder, S., Lee, L., and Redfield, A.G. (1975) J. Am. Chem. Soc. 97, 2927.

62. Johnston, P.D. and Redfield, A.G. (1977) Nucl. Acids Res. 4, 3599.

63. Johnston, P.D. and Redfield, A.G. (1978) Nucl. Acids Res. 5, 3913.

64. Shih, W.C.W. (1979) Ph.D. Thesis, University of California, Berkeley.

65. McConnell, H.M. (1958) J. Chem. Phys. 28, 430.

66. Campbell, I.D., Dobson, C.M. and Ratcliffe, R.G. (1977) J. Magn. Reson. 27, 455.

67. Marshall, A.G., Marcus, T. and Sallos, J. (1979) J. of Magn. Reson. 35, 227.

68. LePecq, J.B. and Paoletti, (1967) J. Mol. Biol. 27, 87.

69. Krugh, T.R., Nuss, M.E. in Biological Applications of Magnetic Resonance (Shulman, R.G., Ed.) pp 113-177, Academic Press, New York.

70. Tsai, C.C., Jain, S.C. and Sobell, H.M. (1977) J. Mol. Biol. 114, 301.

71. Jain, S.C., Tsai, C.C. and Sobell, H.M. (1977) J. Mol. Biol. 114, 317.

72. Krugh, T.R. and Reinhardt, C.G. (1975) J. Mol. Biol. 97, 133.

73. Lee, C.H. and Tinoco, I., Jr. (1978) Nature 274, 609.

74. Patel, D.J. and Shen, C. (1978) Proc. Nat. Acad. Sci. 75, 2553.

75. Waring, M.J. (1968) Nature 219, 1320.

76. Blake, A. and Peacocke, A.R. (1968) Biopolymers 6, 1225.

77. Krugh, T.R., Wittlin, F.N., Cramer, S.P. (1975) Biopolymers 14, 197.

78. Tanford, C. (1961) Physical Chemistry of Macromolecules, Wiley, NY

79. Houssier, C., Hardy, B. and Fredericq, E. (1974) Biopolymers 13, 1141.

80. Dalgleish, D.G., Peacocke, A.R., Fey, G. and Harvey, C. (1971) Biopolymers 10, 1853.

81. Aktipis, S. and Martz, W.W. (1974) Biochemistry 13, 112.

82. Davanloo, P. and Crothers, D.M. (1976) Biochem. 15, 5299.

83. Aktipis, S. and Kindelis, A. (1973) Biochem. 12, 1213.

84. LeBret, M., and Chalvet, O. (1977) J. Molecular Structure 37, 299.

85. Manning, G.W. (1969) J. Chem. Phys. 51, 924.

86. Le Pecq, J.B. (197) Methods of Biochemical Analysis 20 41.

87. Felsenfeld, G. and Hirsham, S. (1965) J. Mol. Biol. 13, 407.